AD-A022 111

DETERMINING THE POTENTIAL OF RADIOFREQUENCY RESONANCE
ABSORPTION DETECTION OF EXPLOSIVES HIDDEN IN AIRLINE
BAGGAGE

William L. Rollwitz, et al

Southwest Research Institute

Prepared for:

Federal Aviation Administration

October 1975

NCJRS

MAR 1 6 1978

ACQUISITIONS

45666

BEST SELLERS

FROM NATIONAL TECHNICAL INFORMATION SERVICE

Product Liability Insurance: Assessment of Related Problems and Issues. Staff Study
PB-252 204/PAT 181 p PC$9.50/MF$3.00

Evaluation of Home Solar Heating System
UCRL-51 711/PAT 154 p PC$6.75/MF$3.00

Developing Noise Exposure Contours for General Aviation Airports
ADA-023 429/PAT 205 p PC$7.75/MF$3.00

Cooling Tower Environment, 1974. Proceedings of a Symposium Held at the University of Maryland Adult Education Center on Mar. 4-6, 1974
CONF-74 0302/PAT 648 p PC$13.60/MF$3.00

Biological Services Program. Fiscal Year 1975
PB-251 738/PAT 52 p PC$4.50/MF$3.00

An Atlas of Radiation Histopathology
TID-26-676/PAT 234 p PC$7.60/MF$3.00

Federal Funding of Civilian Research and Development. Vol. 1. Summary
PB-251 266/PAT 61 p PC$4.50/MF$3.00

Federal Funding of Civilian Research and Development. Vol. 2. Case Studies
PB-251 683/PAT 336 p PC$10.00/MF$3.00

Handbook on Aerosols
TID-26-608/PAT 141 p PC$6.00/MF$3.00

for the Assessment of Ocean Outfalls
ADA-023 514/PAT 34 p PC$4.00/MF$3.00

Guidelines for Documentation of Computer Programs and Automated Data Systems
PB-250 867/PAT 54 p PC$4.50/MF$3.00

NOx Abatement for Stationary Sources in Japan
PB-250 586/PAT 116 p PC$5.50/MF$3.00

U.S. Coal Resources and Reserves
PB-252 752/PAT 16 p PC$3.50/MF$3.00

Structured Programming Series. Vol. XI. Estimating Software Project Resource Requirements
ADA-016 416/PAT 70 p PC$4.50/MF$3.00

Assessment of a Single Family Residence Solar Heating System in a Suburban Development Setting
PB-246 141/PAT 244 p PC$8.00/MF$3.00

Technical and Economic Study of an Underground Mining, Rubblization, and in Situ Retorting System for Deep Oil Shale Deposits. Phase I Report
PB-249 344/PAT 223 p PC$7.75/MF$3.00

A Preliminary Forecast of Energy Consumption Through 1985
PB-251 445/PAT 69 p PC$4.50/MF$3.00

HOW TO ORDER

When you indicate the method of payment, please note if a purchase order is not accompanied by payment, you will be billed an addition $5.00 ship and bill charge. And please include the card expiration date when using American Express.

Normal delivery time takes three to five weeks. It is vital that you order by number

or your order will be manually filled, insuring a delay. You can opt for *airmail delivery* for a $2.00 charge per item. Just check the *Airmail Service* box. If you're really pressed for time, call the NTIS Rush Order Service. (703) 557-4700. For a $10.00 charge per item, your order will be airmailed within 48 hours. Or, you can pick up your order in the Washington Information Center & Bookstore or at our Springfield Operations Center within 24 hours for a $6.00 per item charge.

You may also place your order by telephone or TELEX. The order desk number is (703) 557-4650 and the TELEX number is 89-9405.

Whenever a foreign sales price is NOT specified in the listings, all foreign buyers must add the following charges to each order: $2.50 for each paper copy; $1.50 for each microfiche; and $10.00 for each Published Search.

Thank you for your interest in NTIS. We appreciate your order.

METHOD OF PAYMENT

☐ Charge my NTIS deposit account no._____

☐ Purchase order no._____

☐ Check enclosed for $_____

☐ Charge to my American Express Card account number

Card expiration date_____

Signature_____

☐ Airmail Services requested

Clip and mail to:

NTIS

National Technical Information Service
U.S. DEPARTMENT OF COMMERCE
Springfield, Va. 22161
(703) 557-4650 TELEX 89-9405

NAME_____

ADDRESS_____

CITY, STATE, ZIP_____

Item Number	Quantity		Unit Price*	Total Price*
	Paper Copy (PC)	Microfiche (MF)		

All Prices Subject to Change
11/76

Sub Total	
Additional Charge	
Enter Grand Total	

086093

DETERMINING THE POTENTIAL OF RADIOFREQUENCY RESONANCE ABSORPTION DETECTION OF EXPLOSIVES HIDDEN IN AIRLINE BAGGAGE

William L. Rollwitz

J. Derwin King

Stanley D. Shaw

October 1975

Final Report

Prepared for

1. Report No.	2. Government Accession No.	3. Recipient's Catalog No.
FAA-RD-76-29		

4. Title and Subtitle	5. Report Date
DETERMINING THE POTENTIAL OF RADIO-FREQUENCY RESONANCE ABSORPTION DETECTION OF EXPLOSIVES HIDDEN IN AIRLINE BAGGAGE.	October 1975
	6. Performing Organization Code
	8. Performing Organization Report No.

7. Author's)	
W. L. Rollwitz, J. D. King, S. D. Shaw	SwRI 15-4225

9. Performing Organization Name and Address	10. Work Unit No. (TRAIS)
Southwest Research Institute	
8500 Culebra Road, P.O. Drawer 28510	11. Contract or Grant No.
	DOT-FA-75WA-3635
San Antonio, Texas 78284	13. Type of Report and Period Covered

12. Sponsoring Agency Name and Address	
Federal Aviation Administration	Final Report
Development Section C, ALG-313 (NJH)	
800 Independence Avenue, S.W.	14. Sponsoring Agency Code
Washington, D.C. 20591	

15. Supplementary Notes

FAA Contract Manager: A. R. Beier

16. Abstract

The potential of the radiofrequency resonance absorption spectroscopy (RRAS) techniques for detecting specified quantities of specific explosives in checked airline luggage was investigated. The RRAS techniques considered in this study included nuclear magnetic resonance (NMR), electron spin resonance (ESR) and nuclear quadrupole resonance (NQR). It was found that all the explosives, except black powder, could be detected by NMR and that the NMR response from explosives could be separated from the response produced by other materials likely to be found in luggage. It was also found that black powder and smokeless powders could be detected by ESR but none of the other explosives produced an ESR response. NQR was found useful only for the detection of the RDX base explosive C-4 but even this material could be more sensitively detected by NMR. A magnet and detection coil through which baggage with cross sectional dimensions up to 14" x 24" could be passed for inspection was constructed and tested. The results were sufficient to demonstrate the basic feasibility of using NMR for detection of responses from materials in the large volumes required to inspect checked baggage, but limitations on the available laboratory equipment prevented positive detection of explosives or explosives simulants in this space. The detection sensitivity was such, with the available apparatus however, that an explosive simulant equivalent to two sticks of dynamite could be detected in a volume adequate for inspecting large attache cases. Increased RF power from the laboratory apparatus is needed to detect explosives in the larger volume. Tests with potentially interfering materials in the attache case showed no serious problems. Tests with ESR showed adequate sensitivity to detect one pound of black powder in an inspection region of adequate extent to accommodate checked luggage. From the foregoing evidence, it was concluded that the use of hydrogen NMR appears feasible for use in detecting all explosives of interest, except black powder. NMR apparatus with adequate characteristics to detect the required quantities of these explosives in the specified size of checked baggage also appears feasible. Detection of black powder also appears feasible by combining ESR with the NMR.

PRICES SUBJECT TO CHANGE

17. Key Words	18. Distribution Statement
Radiofrequency Resonance Absorption Spectroscopy, Nuclear Magnetic Resonance, Nuclear Quadrupole Resonance, Electron Spin Resonance, Magnetic Fields, Radiofrequency Fields, Explosives Detection	Document is available to the public through the National Technical Information Service, Springfield, Virginia 22161.

| 19. Security Classif. (of this report)	20. Security Classif. (of this page)
Unclassified	Unclassified

Form DOT F 1700.7 (8-72)   Reproduction of completed page authorized

METRIC CONVERSION FACTORS

Approximate Conversions to Metric Measures

Symbol	When You Know	Multiply by	To Find	Symbol
		LENGTH		
in	inches	*2.5	centimeters	cm
ft	feet	30	centimeters	cm
yd	yards	0.9	meters	m
mi	miles	1.6	kilometers	km
		AREA		
in^2	square inches	6.5	square centimeters	cm^2
ft^2	square feet	0.09	square meters	m^2
yd^2	square yards	0.8	square meters	m^2
mi^2	square miles	2.6	square kilometers	km^2
	acres	0.4	hectares	ha
		MASS (weight)		
oz	ounces	28	grams	g
lb	pounds	0.45	kilograms	kg
	short tons (2000 lb)	0.9	tonnes	t
		VOLUME		
tsp	teaspoons	5	milliliters	ml
Tbsp	tablespoons	15	milliliters	ml
fl oz	fluid ounces	30	milliliters	ml
c	cups	0.24	liters	l
pt	pints	0.47	liters	l
qt	quarts	0.95	liters	l
gal	gallons	3.8	liters	l
ft^3	cubic feet	0.03	cubic meters	m^3
yd^3	cubic yards	0.76	cubic meters	m^3
		TEMPERATURE (exact)		
°F	Fahrenheit temperature	5/9 (after subtracting 32)	Celsius temperature	°C

*1 in = 2.54 (exactly). For other exact conversions and more detailed tables, see NBS Misc. Publ. 286. Units of Weights and Measures, Price $2.25, SD Catalog No. C13.10.296.
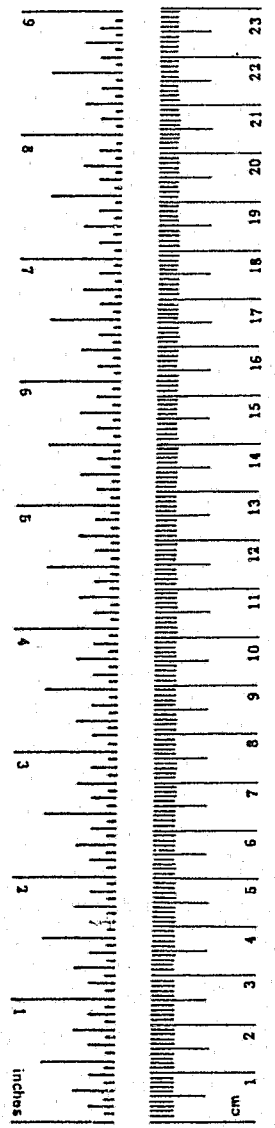
Approximate Conversions from Metric Measures

Symbol	When You Know	Multiply by	To Find	Symbol
		LENGTH		
mm	millimeters	0.04	inches	in
cm	centimeters	0.4	inches	in
m	meters	3.3	feet	ft
m	meters	1.1	yards	yd
km	kilometers	0.6	miles	mi
		AREA		
cm^2	square centimeters	0.16	square inches	in^2
m^2	square meters	1.2	square yards	yd^2
km^2	square kilometers	0.4	square miles	mi^2
ha	hectares (10,000 m^2)	2.5	acres	
		MASS (weight)		
g	grams	0.035	ounces	oz
kg	kilograms	2.2	pounds	lb
t	tonnes (1000 kg)	1.1	short tons	
		VOLUME		
ml	milliliters	0.03	fluid ounces	fl oz
l	liters	2.1	pints	pt
l	liters	1.06	quarts	qt
l	liters	0.26	gallons	gal
m^3	cubic meters	35	cubic feet	ft^3
m^3	cubic meters	1.3	cubic yards	yd^3
		TEMPERATURE (exact)		
°C	Celsius temperature	9/5 (then add 32)	Fahrenheit temperature	°F

°F	-40	0	32 40	80	98.6 120	160	200 212 °F
°C	-40	-20	0 20	37 40	60	80	100 °C

TABLE OF CONTENTS

TABLE OF CONTENTS (Cont'd)

LIST OF ILLUSTRATIONS

LIST OF ILLUSTRATIONS (Cont'd)

LIST OF ILLUSTRATIONS (Cont'd)

I. INTRODUCTION

The objective of the work reported herein has been to obtain evidence from which conclusions may be drawn as to the potential of the techniques of radiofrequency resonance absorption spectroscopy (RRAS) in detecting specified quantities of specific explosives in checked airline luggage. The program has included an investigation of the applicability to this problem of the three RRAS techniques: (a) nuclear magnetic resonance (NMR), (b) electron spin magnetic resonance (ESR), and (c) nuclear quadrupolar resonance (NQR).

The types of explosives and quantities specified to be detected are as follows:

Dynamite	8 sticks each, 1-1/8" dia x 8" long
Smokeless powder	4 pounds
Black powder	4 pounds
Plastic Explosive	2.5 pounds

The dynamites to be detected are those types using nitroglycerine. The plastic explosive included two types: type C-4 with an RDX base and plasticized PETN or Detasheet. The maximum size of the airline luggage to be considered was specified as being 14 inches (35.6 cm) by 24 inches (61 cm) by 30 inches (76 cm).

The program included an investigation to determine the basic detectability of each explosive by each of the three RRAS techniques. From this study the utility of each method in the detection of each explosive of interest has been established and data was obtained on the characteristics of the response produced by the materials. This study was primarily experimental in nature and data was obtained from small samples of the explosives which could be accommodated and handled in the laboratory. The work was supplemented by data available from the literature to aid in establishing the validity of the results where experimental evidence was either impractical or inconclusive. In addition, the feasibility of providing a sensitive detection volume of adequate size to accommodate the luggage of interest was also established by experimental apparatus assembled during the program. The effect of interfering materials was also considered and investigated to a limited extent.

During the program, it was found that all the explosives of interest, with the exception of black powder, provided a strong hydrogen

NMR response. The unique characteristics of the NMR response produced by most of the explosives is such that an excellent possibility exists for separating the signal obtained from these materials from that produced by other materials which would commonly be found in aircraft luggage.

While the possibilities for detecting black powder by NMR do not appear to be very high, it was found that this material exhibited a very strong ESR response. The smokeless powders were also found to have useful ESR characteristics though the amplitude of the response was much weaker than that from the black powder. The other explosives did not provide a detectable ESR characteristic.

From the results of the study conducted during this program, only RDX appears to be detectable by the pure NQR technique. Even in the case of RDX, detection of the nitrogen-14 pure NQR response was found to be much more difficult than was detection of the hydrogen NMR response from the same material. Evidence of the existence of a pure NQR was not found experimentally in the other explosive materials and a survey of pertinent literature tended to confirm the fact that detectable NQR responses would not be obtained.

Based on the encouraging results obtained with both NMR and ESR, program efforts were then directed toward establishing that both these RRAS techniques were capable of providing adequate sensitivity to detect the quantities of explosives of interest in an inspection region of adequate size to accommodate luggage of the specified dimensions. In the case of ESR, detection of black powder under these conditions was successfully demonstrated using a system assembled from conventional laboratory apparatus and a magnet which was available at SwRI. This system operated at a frequency near 950 MHz. Demonstration of NMR under these conditions required the fabrication of a special electromagnet and an RF sample coil to provide an inspection volume: (1) of adequate extent to accommodate the luggage and (2) of adequate characteristics to provide sensitive detection capabilities. When used with power sources available at SwRI these proved to be suitable for demonstrating the possibilities of detecting an NMR response from certain materials in the inspection volume. The quantity of materials which could be detected were comparable to that specified for the explosives of interest. Detection of the explosives (and other materials having a very short T_2) in this full size volume was not possible due to limitations on the peak RF power and in the recovery time of the apparatus available in the SwRI laboratory. The results were sufficient, however, to demonstrate the basic feasibility of providing a detection volume of adequate extent and characteristics to permit NMR detection of materials

in checked baggage. In addition, the results provide guidelines from which specifications have been derived for the apparatus to be used with the magnet and coil to permit explosives to be successfully detected in the full size inspection volume. The electromagnet was also used with a smaller coil to further demonstrate the available detection capabilities. This 6 in. (15.2 cm) high by 14 in. (35.5 cm) wide coil is such that an attache case may be passed through for inspection. Using this coil on an attache case, sensitivity was such that an explosive simulant equivalent to two sticks of dynamite could be detected with the available laboratory apparatus. This assembly was also used to evaluate, to a limited extent, the effects on the NMR response of various items that may be commonly carried in luggage. No serious problems were encountered in this regard.

As a result of the findings of the program, the use of NMR to detect all explosives of interest, except black powder, in the specified size luggage appears feasible. Similarly, the use of ESR to detect black powder appears feasible. Demonstration of the full NMR capability requires that apparatus of expanded capabilities in available power and recovery time be available for use with the magnet and the sample coil. Attainment of such expanded capabilities appears to be within the range of practicality. In addition, instrumentation means to recognize the response from explosives and discriminate against the response from other materials commonly found in luggage needs to be developed. The basis for such discrimination appears to be largely available from the findings of the present program.

Details of the apparatus, the investigations and the findings using NMR and ESR techniques are described in the following sections of this report. Similar information relative to NQR is contained in Volume 2 of this report which is bound separately and classified Confidential. The basis for the classification is the relationship of the work to that performed under U.S. Army Contract No. DAAK02-72-C-0467 and DAAK02-74-C-0056 and the relevant security requirements of these contracts. An analysis of the results obtained with all the RRAS techniques is included in subsequent sections of Volume 1 of the report along with the conclusions and recommendations derived from this study.

II.   TECHNICAL DISCUSSION

The three RRAS techniques which have been used are NMR, ESR and NQR. Each of these is a form of resonance absorption spectroscopy. General and theoretical discussions of these techniques are available in the literature. Further general information on these methods and discussions of specific application to explosives detection are included in Appendix A at the end of this report. In the following sections the technical discussions pertinent to the detection of explosives in airline luggage by RRAS techniques are given. This brief technique description is followed by descriptions of the apparatus used for experimentation and the experimental results.

A.   Nuclear Magnetic Resonance Studies

On the basis of previous work at SwRI, it appeared likely that nuclear magnetic resonance (NMR) techniques could be used to detect all of the explosives of interest with the possible exception of black powder and that this material could most likely be detected by electron spin resonance (ESR) techniques. This previous work had demonstrated the detection of certain explosives in letters and mines, and had provided data which indicated that the transient NMR method would provide the best detection sensitivity. On the basis of these previous findings, the transient NMR detection method was selected for use in the studies conducted during the present program. The pertinent aspects of this detection method are described in the following section.

1.   Transient NMR Detection Method

For NMR detection the material to be studied is placed in a static magnetic field, H_o, and the interaction of the nuclei of interest with an applied radiofrequency magnetic field, H_1, is detected. With the transient NMR detection method, the radiofrequency field is applied in single or multiple short bursts. The intensity of the biasing magnetic field, H_o, is chosen to be such that the nuclear species to be detected is resonant at the frequency of the RF energy. For hydrogen nuclei, this frequency, f_o, (in Hertz) is related to the field intensity, H_o, (in Gauss) by

$$f_o = 4257.6 \, H_o \qquad\qquad (1)$$

As an example, for resonance (and most sensitive detection) of hydrogen nuclei at a frequency of 2.5 MHz, the magnetic field must be at 587.19 Gauss.

When the burst of RF energy is properly applied and the magnetic field is at the proper value, the nuclei rotate (or precess) in a plane perpendicular to the direction of the applied RF field. The amount of the rotation is dependent upon the energy content of the burst of RF and for convenience the amount of energy is usually rated in terms of the affect on the angular precession of the nuclei which they induce. Thus, a 90° pulse is one which contains enough energy to cause a precession through an angle of 90°. The energy, and consequently the angle of rotation, θ, is linearly proportional to the product of the strength of the RF field, H_1, in Gauss, and the pulse width, t_w, in seconds. For hydrogen nuclei this is given by the relation

$$4,257.6 \times 2\pi\, H_1 t_w = \theta \tag{2}$$

where θ is expressed in radians and is $\pi/2$ for a 90° pulse and π for a 180° pulse. The energy content of the pulse bursts is very important to achieving optimum detection sensitivity. For a 90° pulse the product of H_1 and t_w is such that

$$H_1 t_w = 58.7 \times 10^{-6} \tag{3}$$

For good detection sensitivity, the intensity, H_1, of the RF pulse must be such that

$$4,257.6 \times H_1 \geq \frac{1}{T_2^*} \tag{4}$$

where T_2^* is the observed relaxation time of the hydrogen nuclei to be detected. This includes both the spin-spin relaxation time, T_2, for the hydrogen nuclei in the sample and the effects of inhomogeneity in the bias magnetic field ΔH_0. For the conditions encountered with hydrogen nuclei in explosives, a T_2^* value of about 40 microseconds is typical in a homogeneous field. As the field homogeneity becomes poorer the value of T_2^* decreases and a larger value of H_1 becomes necessary.

For the case where $T_2^* = 40$ microseconds and using Equation (4) the minimum value of H_1 is 5.87 Gauss. The width of a 90° pulse for an H_1 of 5.87 Gauss is, from Equation (3),

$$t_w = 10 \times 10^{-6} \text{ sec.}$$

In a static field of poorer homogeneity, a shorter pulse burst of higher intensity would provide more optimum detection sensitivity. Thus the useful pulse widths may range from 1.0 to 10.0 microseconds with corresponding values of H_1 ranging from 58.7 to 5.87 Gauss.

5

When a solenoid coil is used, the peak power required to generate an RF magnetic field of intensity, H_1, over volume, V, inside the coil is

$$P_{RF} = \frac{H_1{}^2 f V}{9Q} \quad \text{(watts)} \qquad (5)$$

where H_1 is the RF field in Gauss, Q is the quality factor of the coil producing the RF field, f is the operating frequency (in megahertz) from Equation (1), and V is the volume available in the coil in cubic centimeters. The maximum value of Q which may be used is dependent upon the bandwidth and rise time requirements and it becomes smaller as the pulse burst lengths, t_w, are reduced.
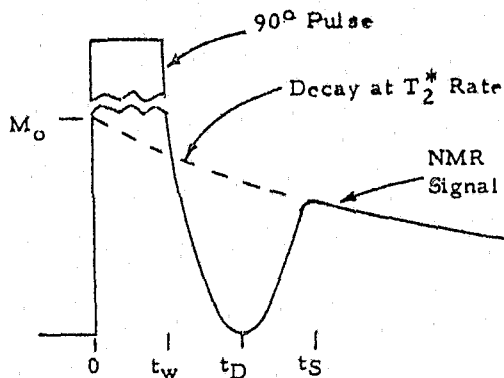
To accommodate luggage of the maximum specified size, an inspection volume 14 inches (35.6 cm) by 24 inches (61 cm) by 30 inches (76 cm) or 10,080 cubic inches (1.65×10^5 cm^3) is required. For simultaneous inspection of this entire volume for explosives an appropriate level of H_1 must be present throughout this region. Producing such a large field over this volume requires RF bursts of very high peak power. For example, when H_1 is 5.87 Gauss, the peak power required, when the Q is 10, is
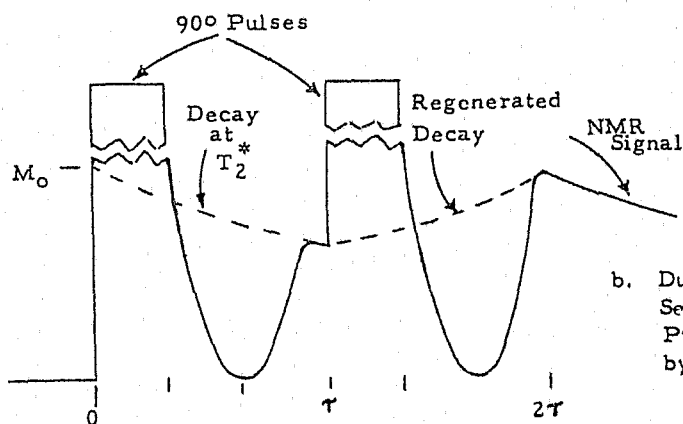
$$(P_{RF})_H = 158,000 \text{ watts.}$$

Where higher values of H_1 are necessary, the peak power requirements increase rapidly not only due to the influence of square of the H_1 term in the equation, but also due to the effect caused by the lower Q which must be used with shorter pulse burst lengths. In practice the RF peak power needed may range from 158,000 watts to more than 10 megawatts. The average power, however, is less than 10 watts in almost all cases.

Experience has shown that the RF pulses can be used singly, in pairs and in repeated series of up to 6 or 8 pulses. To date, however, most of the explosives detection work has used one of the following three pulse configurations: (a) a single 90° pulse, (b) a dual 90° pulse, and (c) a dual 90°-180° pulse sequence. These three pulse configurations and the transient NMR signals that they produce are given in Figure 1.
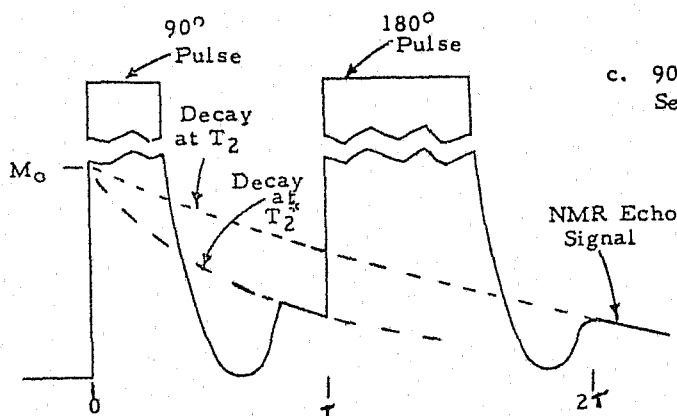
The single 90° pulse is drawn in Figure 1a. As soon as the RF is applied, the value of the nuclear magnetization starts to decay at the T_2^* rate because it is being rotated by the RF energy and is not in equilibrium. The 90° pulse decays by time t_D. The detection
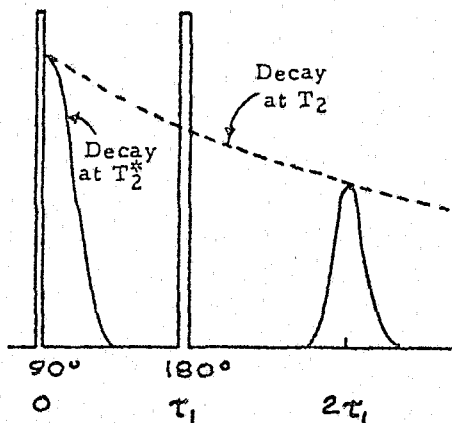
6

90° Pulse

Decay at T_2^* Rate

M_o

NMR Signal

0   t_w t_D t_S

a. Single 90° Pulse.

90° Pulses

Decay at T_2^*

Regenerated Decay

NMR Signal

M_o

0   τ 2τ

b. Dual 90° Pulse Sequence with Second Pulse Shifted in Phase by 90°.

3530

90° Pulse

180° Pulse

Decay at T_2

Decay at T_2^*

M_o

NMR Echo Signal

0   τ 2τ

c. 90°-180° Double Pulse Sequence with $T_2^* < T_2$.

Decay at T_2

Decay at T_2^*

90°   180°

0   τ_1 $2\tau_1$

d. 90°-180° Double-Pulse Sequence with $T_2^* \lll T_2$.

FIGURE 1.   PULSE SEQUENCES USED WITH THE TRANSIENT NMR METHOD

7

system then begins to recover from the effects of the high power pulse burst and the received signal through the system increases until it intersects the decay curve at time t_S in Figure 1a.

The dual 90° pulse sequence is drawn in Figure 1b. The second 90° pulse is delayed from the first by the time τ and is shifted in phase relative to the first pulse by 90°. The second 90° pulse, phase shifted by 90°, brings out a larger NMR signal than does the single 90° pulse. In the solid materials like explosives, the second 90° pulse regenerates the decay (gives an echo) as shown in Figure 1b when the second pulse is applied before the end of the T_2^* decay.

The 90°-180° double-pulse sequence is given in Figure 1c. The decay that is found for the magnetization M_0 is T_2 rather than T_2^*, where T_2 is longer than T_2^*. As shown in Figure 1c, the signal does not regenerate as it does in Figure 1b and when the pulses are close together, the NMR echo signal is not symmetrical. The case when T_2 is much, much longer than T_2^* is drawn in Figure 1d. In most cases, the 90°-phase shifted 90° pulse sequence of Figure 1b provides the best signal/noise ratios with the explosives. The experimental apparatus used to make transient NMR measurements on the explosives of interest will now be considered.

2.   Apparatus for Small Sample Transient
      NMR Measurements

In the interest of safety and to permit use of proven instrumentation available at SwRI, the initial transient NMR measurements on explosives were made with small samples. The small samples were adequate for determining the transient NMR characteristics of the materials and allow the measurements to be made in small sample coils, and from Equation (5), with relatively small peak powers. The equipment used to perform these measurements was composed of assemblies available in the Instrumentation Research Division of SwRI as a result of previous developments. A block diagram of the transient NMR apparatus used for these measurements is shown in Figure 2.

The program selector establishes the pulse sequence which is used. In making the measurements the single 90° pulse technique illustrated in Figure 1a as well as the 90°-90° (phase = 90°) dual-pulse sequence of Figure 1b were used. The 90° pulses were 5 microseconds wide and for the dual pulse sequence, the second followed the start of the first by 14 microseconds. Thus, from Figure 1b,

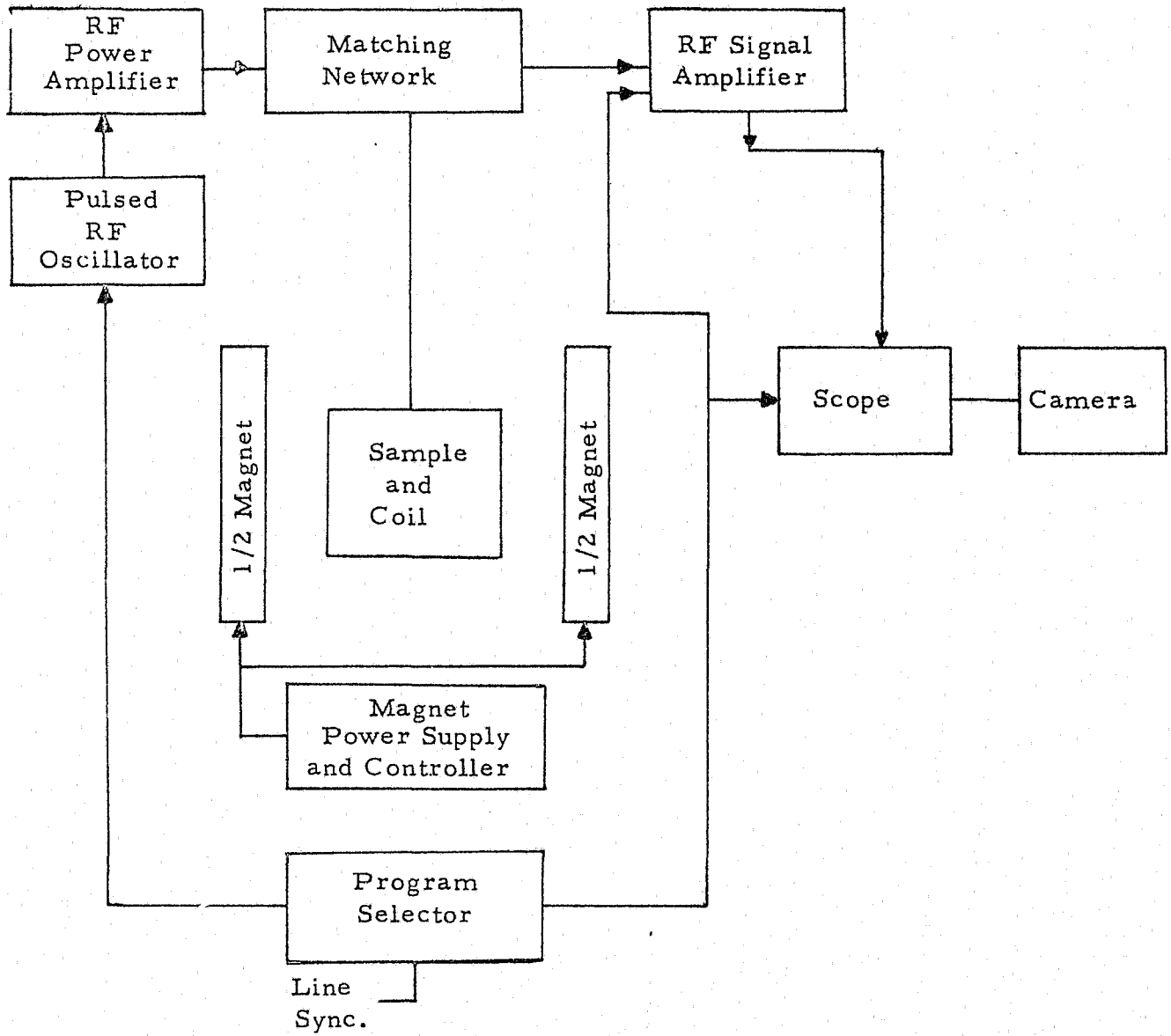FIGURE 2. BLOCK DIAGRAM OF THE SMALL SAMPLE HYDROGEN
TRANSIENT NMR APPARATUS

$$t_w = 5 \text{ microseconds}$$
$$\tau = 14 \text{ microseconds.}$$

A photograph of the dual 90° pulse sequence displayed on an oscilloscope is shown in Figure 3a. The detected signal resulting from the use of this dual 90° pulse sequence is displayed in Figure 3b. This particular signal was obtained from hexamethylenetetramine (HMT) which has certain characteristics which permit it to be used as an NMR simulant for some explosives. One of these characteristics is a long spin lattice relaxation time constant, T_1, and another is a relatively short spin-spin relaxation constant, T_2. The dual trace as shown in Figure 3b is a result of allowing two different times for polarization to occur prior to the transmitted pulse sequence. The larger signal results from a polarization time of sixty seconds, while the smaller signal was produced by allowing a shorter polarization time of around ten seconds. This difference is caused by the large value of T_1 of 30 seconds for HMT. The detected signal level increases exponentially as a function of t/T_1 and reaches 95% of the maximum value at $t = \gamma T_1$. In this case, t, is the time the sample is allowed to remain in the magnetic field prior to the transmitter bursts or the time allowed for polarization to occur.

The pulses out of the program selector control the pulsed RF oscillator. The output of the pulsed oscillator are pulses or bursts of radiofrequency voltage at a frequency of 2.5 megahertz. The burst duration is the same width as the width of the input pulses. These RF pulses are amplified by the RF Power Amplifier and applied to the sample coil through the matching network. The pulses out of the RF power amplifier are those shown in Figure 3a. The peak power available from the power amplifier used for these tests is about 10 kw. The pulses of RF cause a transient NMR signal to be emitted from the sample. This signal induces an RF voltage in the sample coil which, after amplification and detection, has the form shown in Figures 1b and 3b. This is usually displayed on the "Scope" in Figure 2.

The sample coil used for the tests has an inside diameter of 1 inch. The magnet used to supply the H_0 field has a gap width of 4 inches and a pole-piece diameter of 19 inches. This magnet produces an inhomogeneity across the 1-inch ID coil which is equivalent to a relaxation time, T_m, of 3×10^{-3} seconds. Where

$$T_m = \frac{1}{\gamma \Delta H} \qquad (6)$$

10
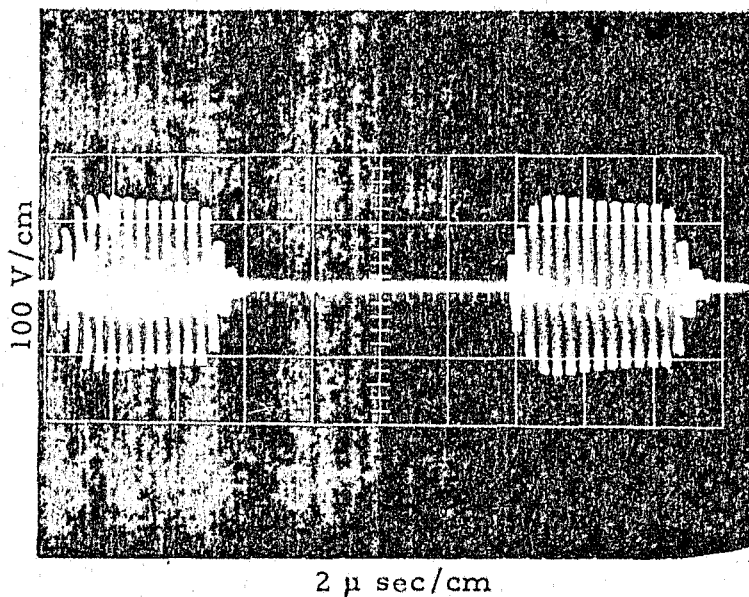
a. Dual-Pulse Sequence
   Voltage Across 60
   Ohm Load.

2 μ sec/cm

3531
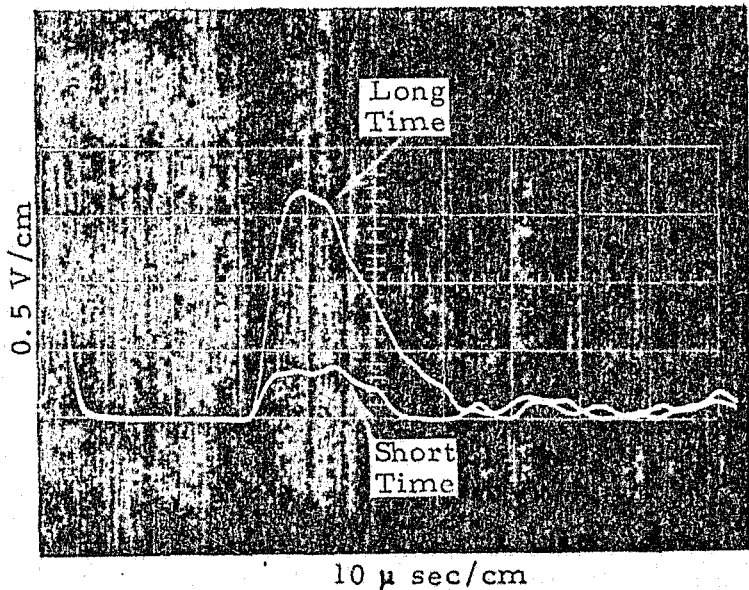
b. Transient NMR Signal With
   Dual 90°-90° (Phase = 90°)
   Pulse Sequence Using HMT
   as a Sample at Long and
   Short Polarization times.

10 μ sec/cm

FIGURE 3. PHOTOGRAPHS OF (a) THE 90°-90° (PHASE = 90°) DUAL PULSE
          SEQUENCE, AND (b) THE RESULTANT SIGNAL FROM HMT AT
          TWO POLARIZATION TIMES

11

Since the relaxation time T_2 for the explosives is from 10 to 50 micro-seconds, then the decay, T_2^*, of the transient NMR signal in the large magnet is controlled by the sample characteristics rather than the magnet characteristics. For example, the signal in Figure 3b has a T_2^* of 15 microseconds. The value of T_2 is calculated from the following equation

$$\frac{1}{T_2} = \frac{1}{T_2^*} - \frac{1}{T_m} = \frac{1}{15 \times 10^{-6}} - \frac{1}{3 \times 10^{-3}} \quad (7)$$

The inhomogeneity of the magnet causes an error of only 0.5 percent if the value of T_2 is calculated directly from the curve in Figure 3b. If the value of T_2 were 150×10^{-6} seconds, the error caused by the inhomogeneity would still be only 5 percent. Therefore, the uncorrected values of T_2^* taken directly from the transient NMR signals of the explosives can be used as the value of T_2 for the explosives to an accuracy which is more than adequate for most purposes.

The equipments as assembled for the small sample transient NMR measurements are shown in the photograph reproduced as Figure 4. The equipment rack on the left contains all of the components in Figure 2 except the magnet, the sample coil and the oscilloscope. The magnet is in the center of the picture and the sample coil is in the gap of this structure. The sample coil assembly is held in the gap by the white, foam plastic pad. The oscilloscope is to the right of the magnet.

3.   Apparatus for Full-Scale Tests

For the full-scale tests, that is, tests with a sampled volume of 14" x 24" x 30", the apparatus required may still be represented by the block diagram of Figure 2. However, the magnet, the magnet supply, the RF Power Amplifier, the detection coil and the matching network must have much greater capabilities than those required for the small sample tests. As shown previously, the RF power needed for the 14" x 24" x 30" sample volume ranges upward from 158,000 watts peak depending on the allowable time for a 90° pulse. For example, for the 5 microsecond wide, 90° pulses used with the small sample measurements, the full-scale tests will require peak pulse powers of 1.04 megawatts. This is based on using a coil, Q, of six which has been found to be about optimum for the small sample tests. In addition, the magnet must have a homogeneous field which extends throughout the 14" x 24" x 30" sample volume. These magnetic field and RF power requirements can be reduced by decreasing the size of
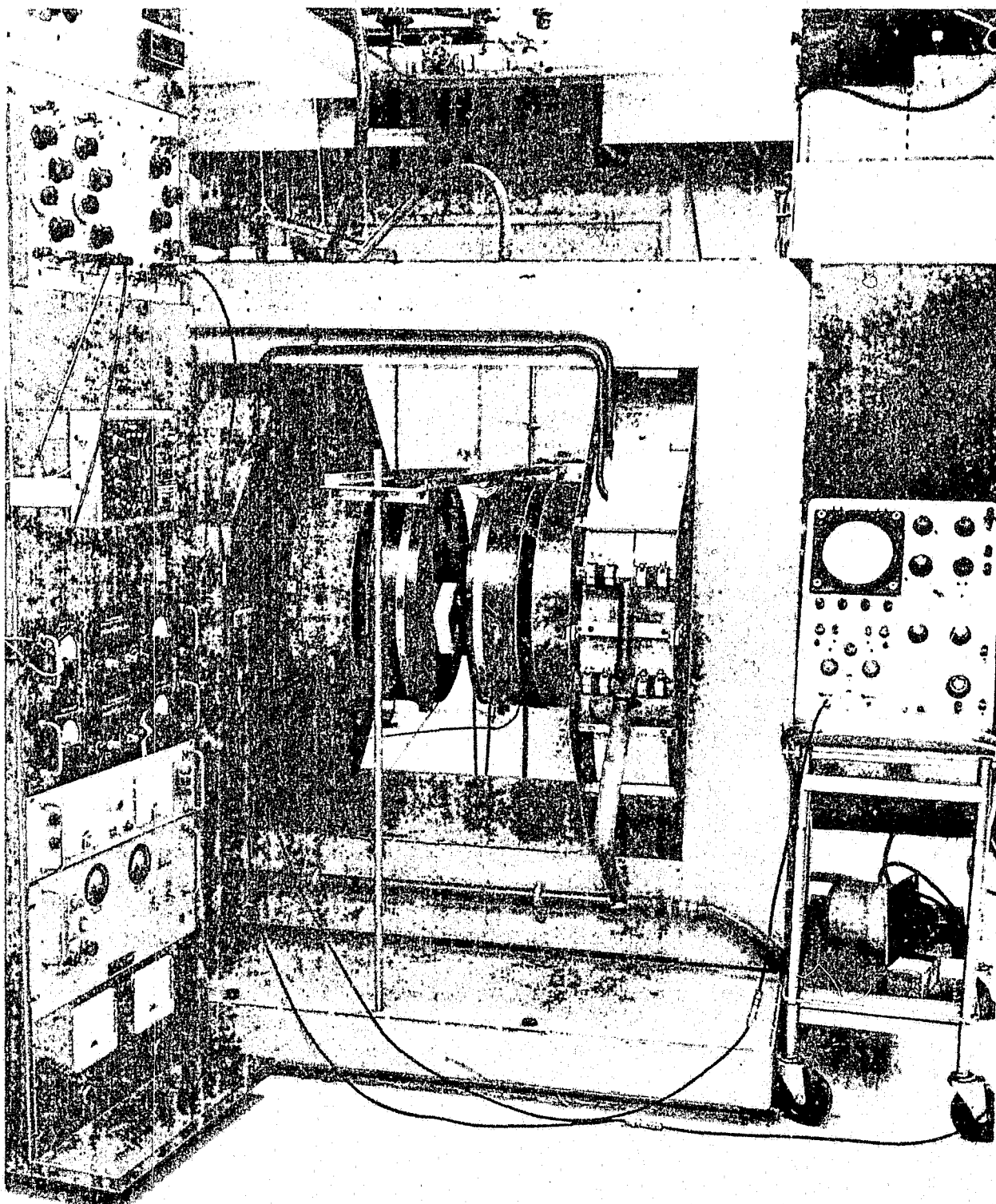
12

2419

FIGURE 4. SOUTHWEST RESEARCH INSTITUTE LABORATORY EQUIP-
MENT FOR ALL OF THE TRANSIENT NMR MODES AT
FREQUENCIES OF 3, 10 AND 30 MEGAHERTZ

13

the sample volume. This can be practically accomplished by reducing the length of the available inspection region. The capability to inspect the required size luggage can still be retained by arranging the structures such that the items to be inspected can pass through the sensitive inspection zone. This alternative increases the inspection time since large items will need to be examined at more than one point along their length. The savings that can accrue, in magnet size, weight and power requirements and in the RF power requirements, however, make this approach attractive. Both alternatives were considered during the program and the approach requiring a reduced volume was selected for implementation in experimental form. The experimental magnet as constructed and tested for these applications has a length of 24 inches, and an opening 17 inches high and 26 inches wide through which the baggage can be passed. The sample coil has an inside clearance of 14" x 24" and is 12" long. A 160,000 watt RF power amplifier which was available at SwRI from previous experimental work was used for most of the tests conducted with the foregoing structures. A higher power RF generator which was fabricated in breadboard form and evaluated during the program provided the capability to generate bursts of RF energy having a peak power of several megawatts; but, the characteristics of the bursts were such that the expected improvements in NMR detection range was not realized. The 160,000 KW peak power amplifier uses a conventional vacuum tube approach but the higher power generator was based on using a capacitor discharge technique which appeared to have advantages in simplicity and in ease of attaining much higher levels of peak power. The work with this generator technique is described in Appendix B. The magnet and the vacuum tube transmitter are described in the following paragraphs.

a.   The Magnetic Fields

In order to have a transient NMR signal, the sample must be subjected to both a steady bias magnetic field, H_O, and a radiofrequency magnetic field, H_1, at right angles to the direction of the bias field. It is usual to choose the z axis for the bias field direction and the x axis for the radiofrequency field. It is usual in the art of NMR instrumentation to consider a magnet constructed as shown in Figure 4. Such a magnet design, to give 600 and 800 Gauss in a volume 14" x 24" x 30" would weigh over 15 tons. Such a weight and the accompanying large size would make the device too large, too heavy and too costly to be useful. Because of previous work at Southwest Research Institute, however, a more promising design was available.

The experimental electromagnet developed for use in investigating the potential of NMR and ESR in detecting explosives

14

in airline luggage is shown in Figure 5. It consists of two coil combinations, each wound around a laminated iron core. These two coil and core assemblies are fitted between two laminated pole pieces, one below and one on top. The two coil combinations, one on each side, are in turn composed of four individual winding assemblies.

The main design feature of the magnet is that each coil combination produces a magnetic field which is North at the top and South at the bottom. The fields from these two coils cause the entire top pole piece to be at a constant magnetic potential relative to the bottom pole piece. With a constant magnetic potential difference between the top and bottom pole pieces, a nearly constant magnetic field, H_o, exists at every point in the gap which is 17" high, 26" wide and 24" deep. Any inhomogeneity in H_o will be caused by height differences in the gap, saturation effects in the pole pieces, differences in the magnetic properties of the pole pieces in different positions, differences in the ampere turns of the two coil combinations and by field spreading at the front and back edges of the gap.

To provide the capability to switch the magnetic field over a range of several hundred Gauss in a time on the order of 0.1 second, the cores for the coils and the pole pieces were constructed from thin strips of mild steel laminated together. The top and bottom pole pieces were each composed of 400 strips, each strip being 2.7" x 40" x 0.059" in size and made of hot rolled steel. The two coil cores were made from 42 sheets of hot rolled steel each 17" x 24" x 0.059".

The overall dimensions of each of the eight coils are 3-15/16" x 10" x 31-1/2" with an opening for the core which is 2-3/4" x 24-1/4". Each coil was wound with 20 layers of #5 plastic coated square aluminum wire laid down 20 turns per layer. With each coil having 400 turns, the left and right coil combinations each have 1600 turns. The 8 coils (4 on each side) are all connected in series so that the same current flows in each. The total DC resistance at room temperature (22°C) is 7.7 ohms. The inductance of the total magnet winding is 5.2 Henries. A current of 13.3 amperes produces the field of 587 Gauss required for the NMR hydrogen resonance frequency of 2.5 MHz. At room temperature this current results from 102 volts across the coil, giving a dissipation of 1357 watts.

The temperature of the coil rises very slowly after the current is turned on. Sheets of 1/8-inch thick aluminum were inserted below and above each coil to assist in the dissipation of heat from the windings. These cooling plates are readily visible in Figure 5. After a few hours after being excited, the coils reach their equilibrium

15
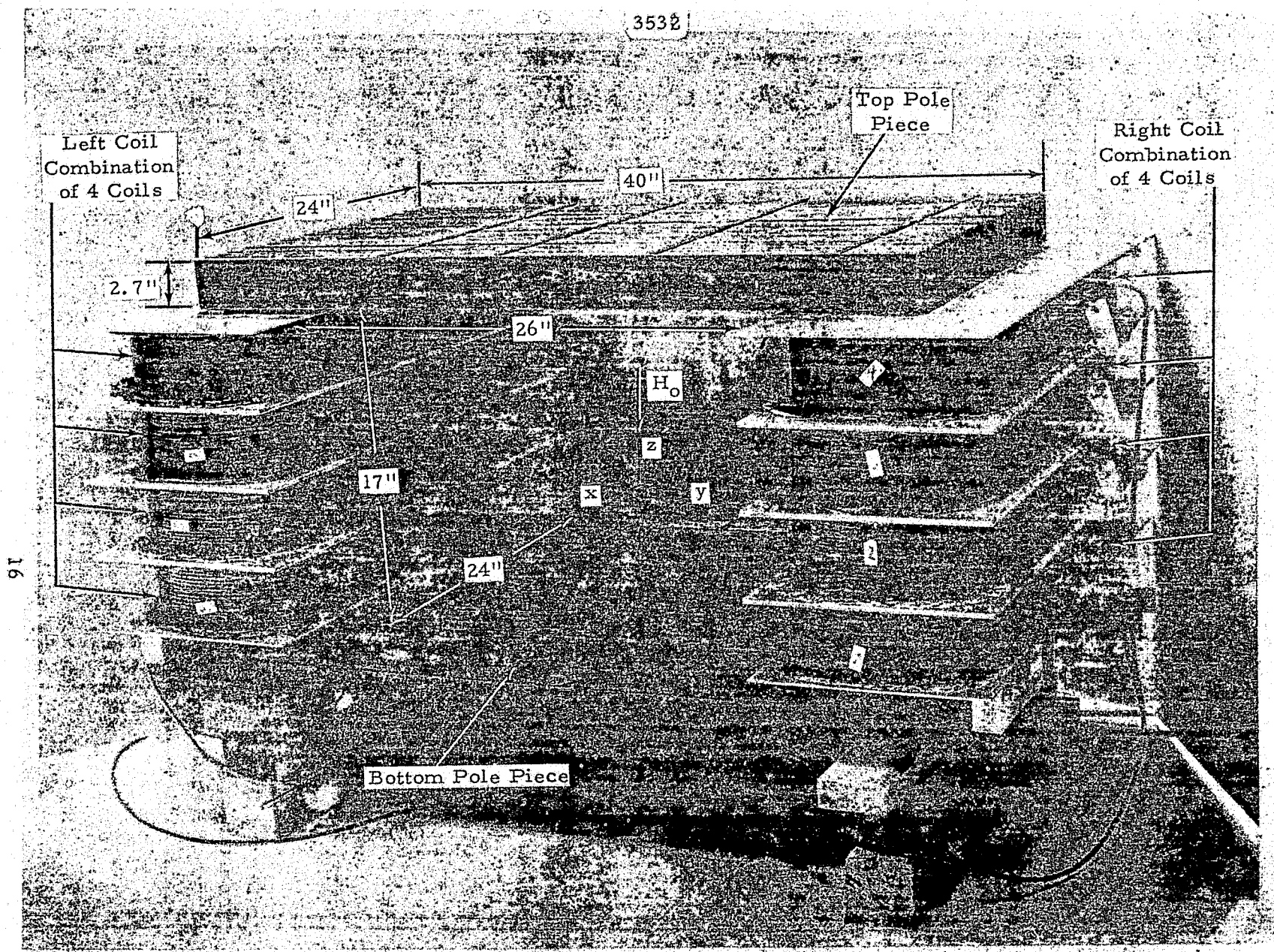
FIGURE 5. BIASING MAGNET FOR THE NMR DETECTION OF EXPLOSIVES IN LUGGAGE.
Effective Volume = 17" x 24" x 26"; Field Intensity, H_o = 600 Gauss.
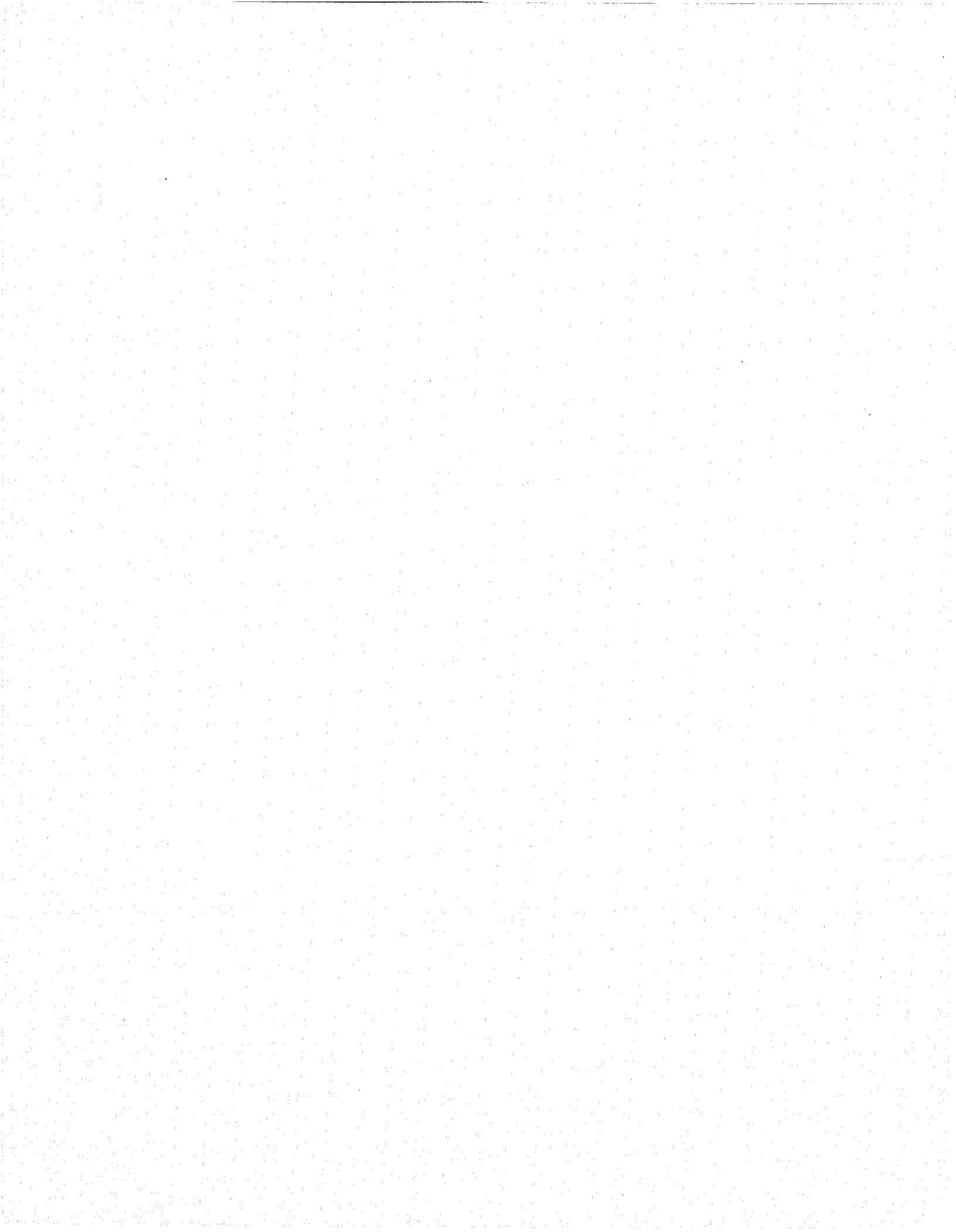
temperature. At this time, the resistance has increased to 8.65 ohms and the temperature of the cooling plates was measured to be 46°C. While noticeably warm, the temperature of the assembly appears to be well within tolerable limits.

The radiofrequency magnetic field, H_1, for the full-scale tests is produced by the radiofrequency coils shown in Figure 6. The coil is composed of two windings connected in parallel in such a manner that their magnetic fields are in series. Each coil is wound of No. 12 wire counterclockwise from the center of the bottom of the enclosed volume. One coil is wound counterclockwise toward the back and the other coil is wound counterclockwise toward the front. The outer ends of the two windings are connected together and to the shield ground. The inner ends of the windings are also connected together as can be seen in Figure 6 and used as the feed point. Each coil, front and back, has four turns spaced over a length of 4.5 inches. The inside dimensions of the coil are 14" x 24" x 9". The coil is surrounded by a 17" x 26" x 24" shield, made from double sided copper-clad fiberglass epoxy sheet. The parallel inductance value for the radiofrequency coil is 4.5 microhenries so that it resonates at 2.5 MHz with 910 picofarads.

The radiofrequency coil and its shield fit into the gap of the magnet. The complete NMR detection head assembly is shown in Figure 7.

The magnet (Figure 5) produces a field, H_0, in the sensitive volume which is 14" x 24" in cross section and about 9" long. When properly excited, the radiofrequency coil will produce a field, H_1, in this same volume which is in quadrature with H_0.

The magnet design in Figure 5 was chosen because it appeared to offer the potential of providing the required large volume of homogeneous magnetic field with a minimum of magnet weight. This has proven to be true since the magnet in Figure 5 weighs 2800 pounds in contrast to the 30,000 pounds that would have been required for a magnet of the design shown in Figure 4 to produce a field with similar inhomogeneity and intensity. To determine the field variation of the magnet in Figure 5, the field intensity was measured in five planes through the magnet volume, each parallel to each other and to the pole pieces. The first plane was just at the top of the bottom layer of windings of the radiofrequency coil or at a position 7 inches below the center of the magnet volume. The magnetic field in this first level or plane was measured at the corners of 4-inch squares. The magnetic field intensities at each of the above-described points in the first plane are given in Figure 8. The magnetic field intensities at each of the points
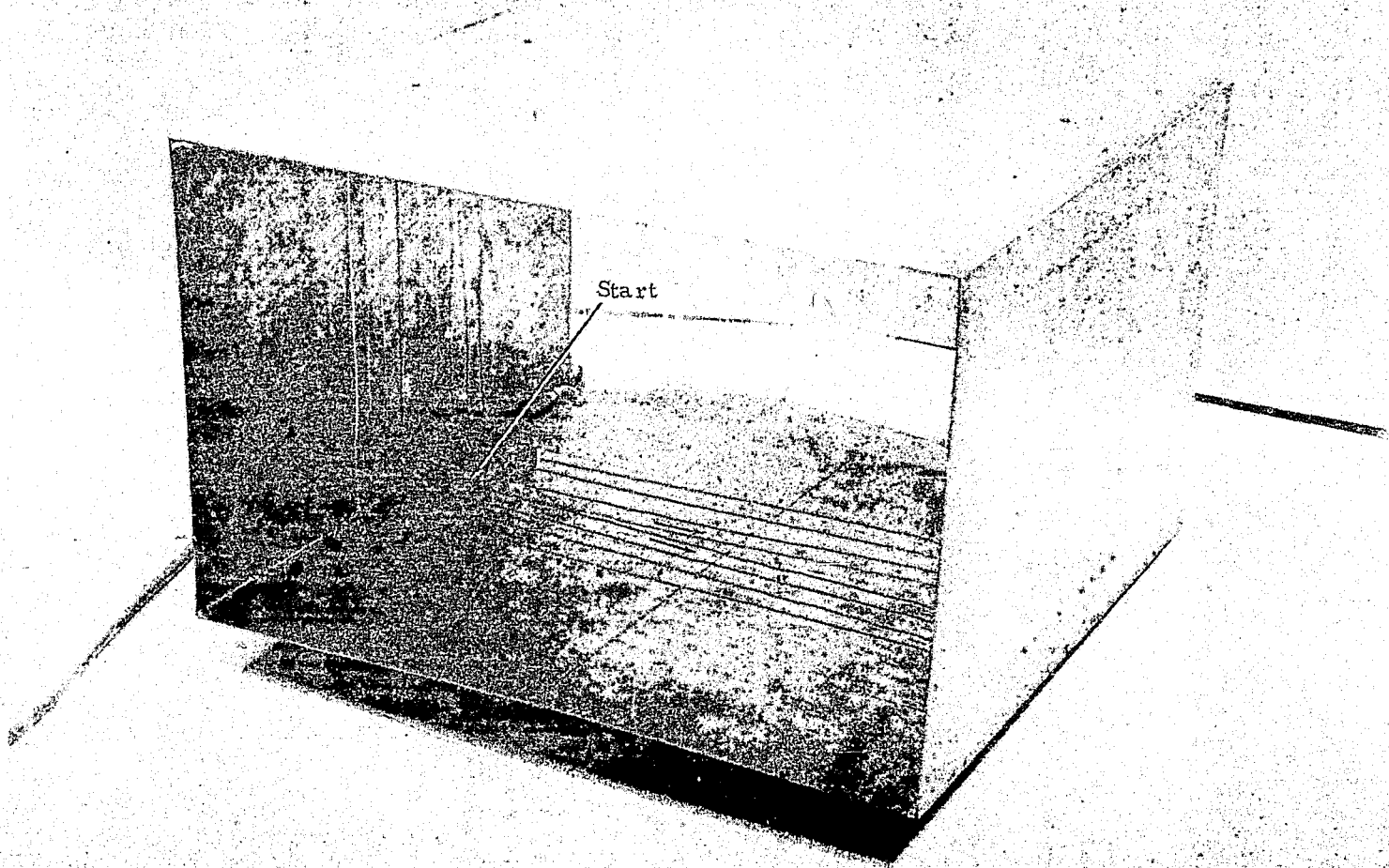
17

Start

FIGURE 6. RADIOFREQUENCY COIL TO PRODUCE THE RADIOFREQUENCY MAGNETIC FIELD
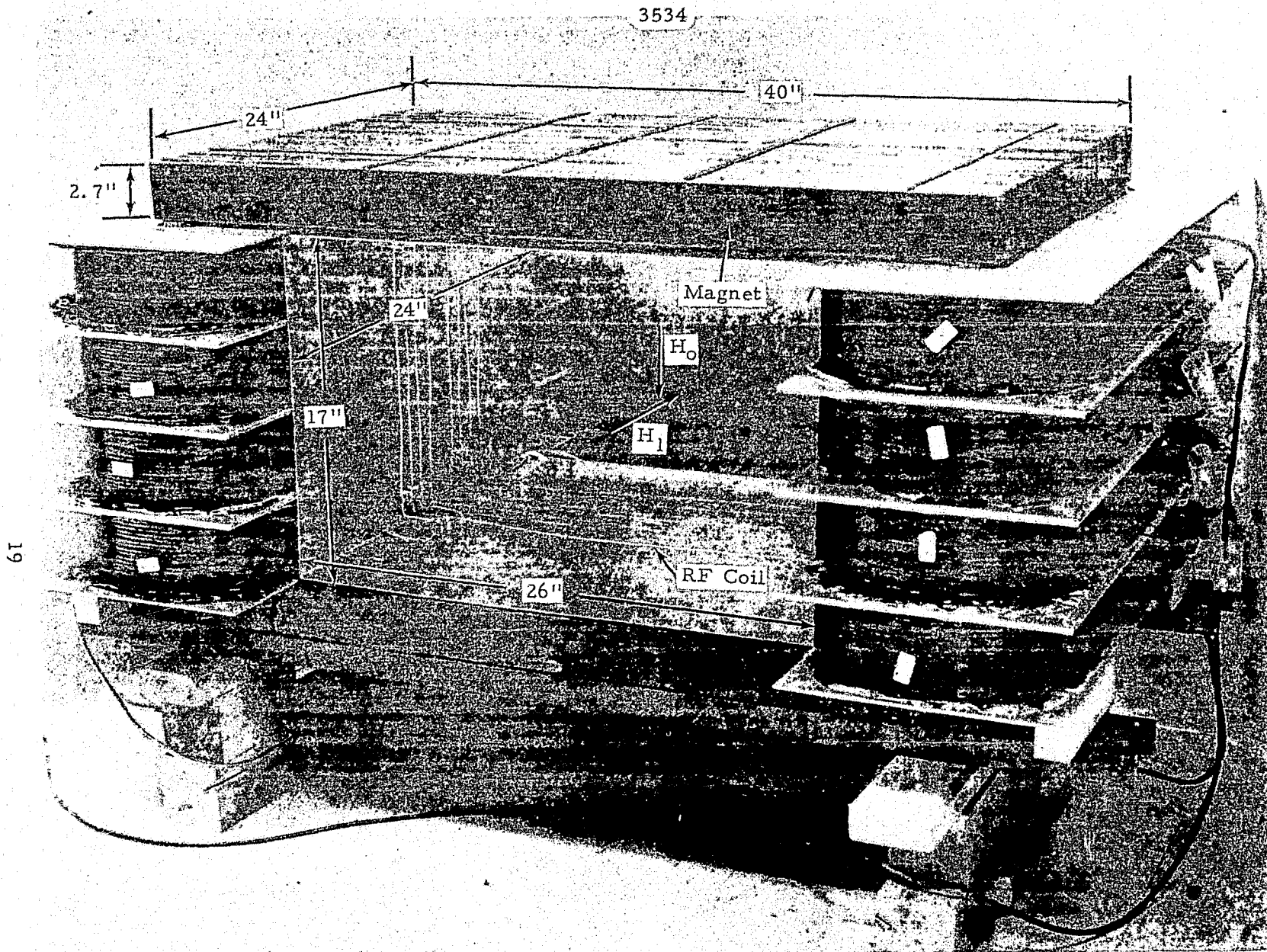FOR THE DETECTION OF EXPLOSIVES IN A VOLUME 14" x 24" x 24".

FIGURE 7. COMPLETE DETECTION HEAD FOR THE TRANSIENT NMR DETECTION OF EXPLOSIVES IN LUGGAGE. The magnet produces a field H_O and the RF coil produces a field H_1.
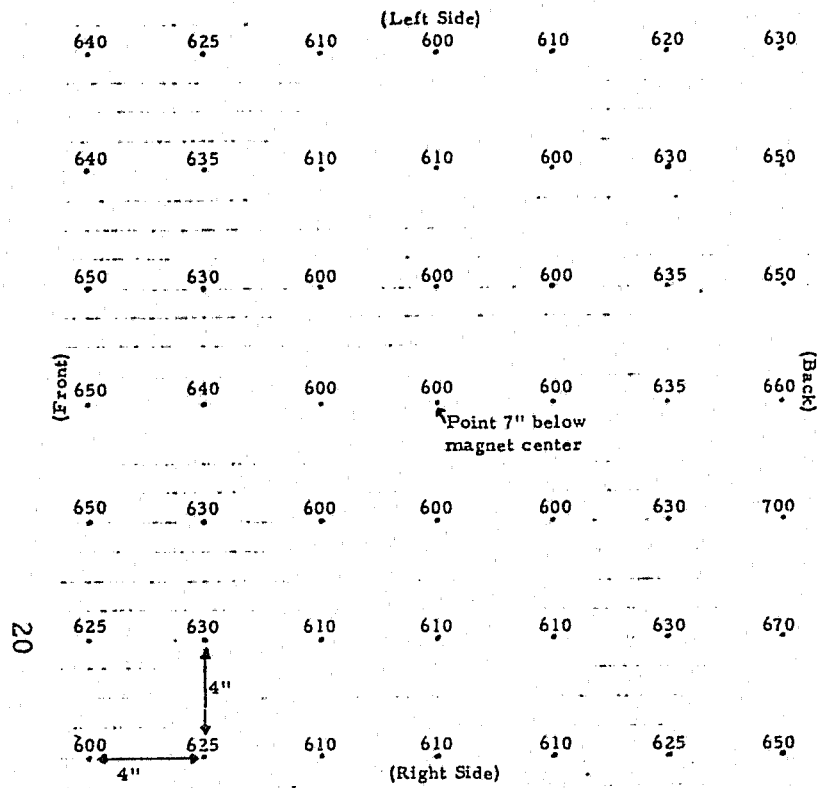
20

Figure 8 (Left)

(Left Side)

640	625	610	600	610	620	630
640	635	610	610	600	630	650
650	630	600	600	600	635	650
650	640	600	600	600	635	660
650	630	600	600	600	630	700
625	630	610	610	610	630	670
600	625	610	610	610	625	650

(Front) (Back)

↑Point 7" below magnet center

4"

4"

(Right Side)

FIGURE 8. GRAPH OF THE MAGNETIC FIELD INTENSITY AT THE CORNERS OF 4-INCH SQUARES OVER A PLANE 7 INCHES BELOW THE CENTER OF THE MAGNET IN FIGURE 5, OR THE FIRST PLANE.

Figure 9 (Right)

(Left Side)

480	590	600	600	600	590	520
480	580	600	600	600	590	500
490	580	595	600	595	585	510
500	580	595	600	595	590	510
480	580	595	600	595	585	510
490	580	600	600	600	590	510
490	590	600	600	600	590	510

(Front) (Back)

4"

4"

(Right Side)
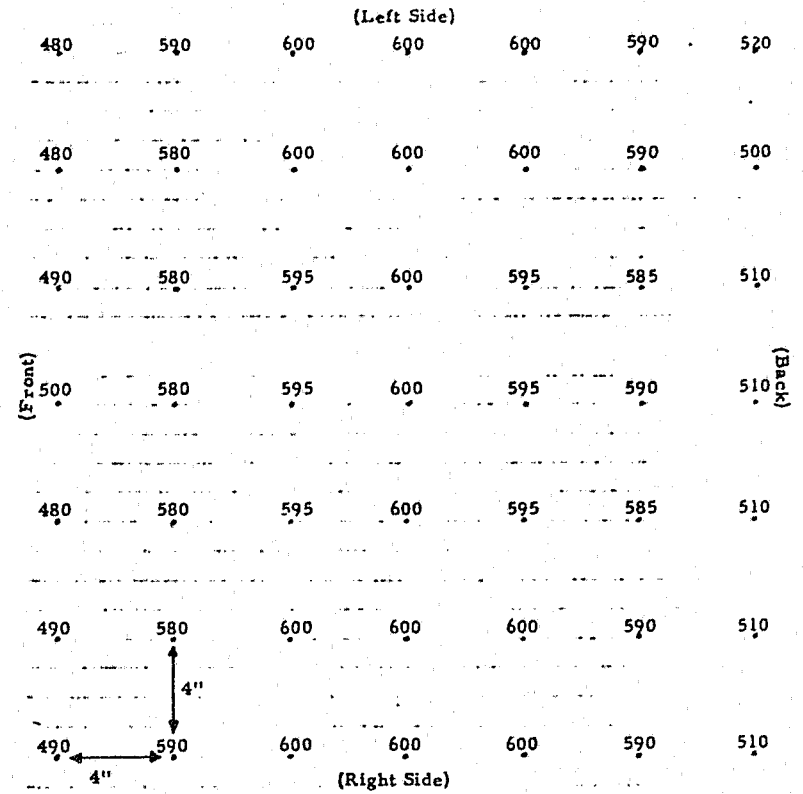
FIGURE 9. GRAPH OF THE MAGNETIC FIELD INTENSITY AT THE CORNERS OF 4-INCH SQUARES OVER A PLANE (the second plane) 4 INCHES BELOW THE CENTER OF THE MAGNET IN FIGURE 5.
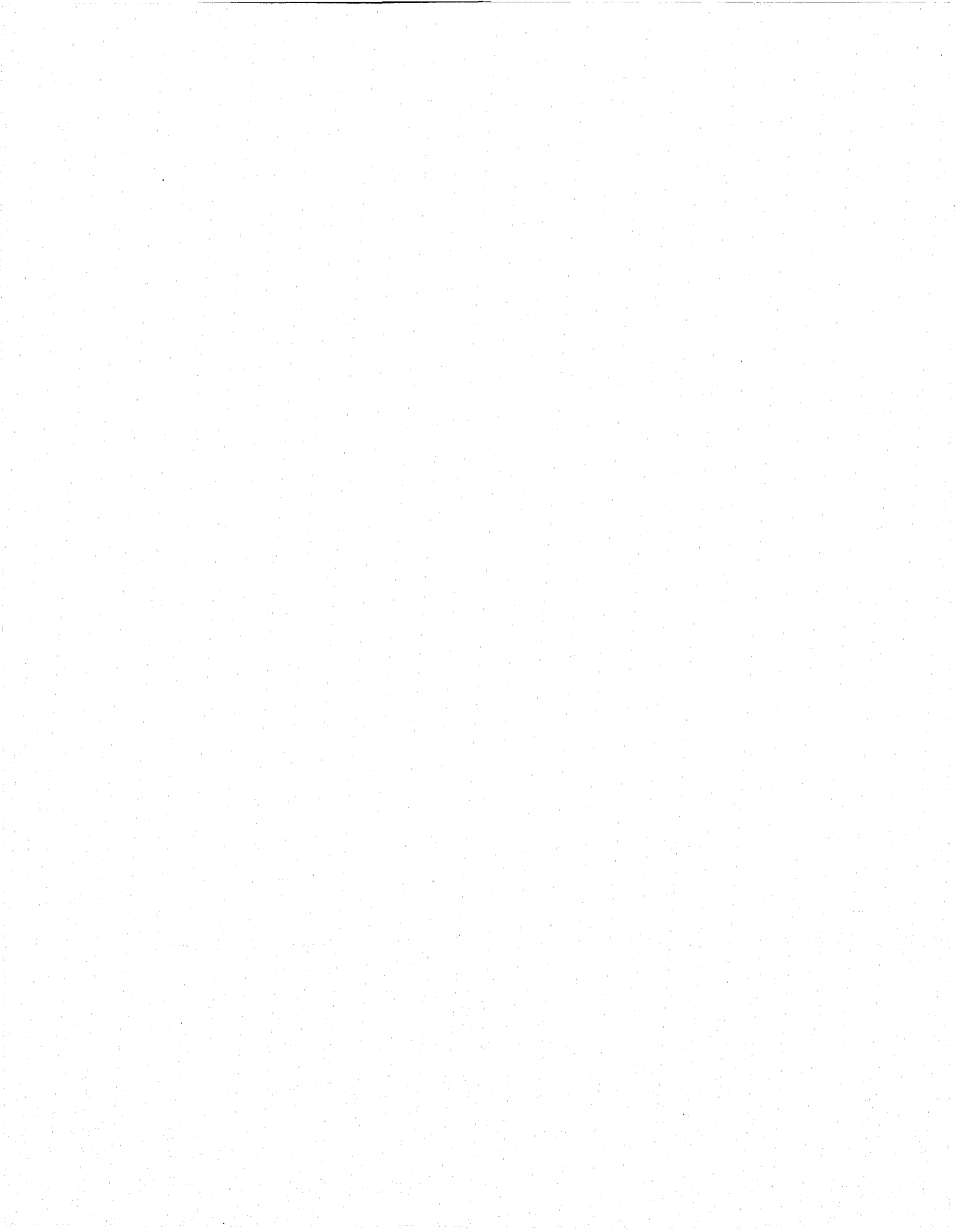
at the corners of 4-inch squares on a plane at a position 4 inches below the center of the magnet (the second plane) are given in Figure 9. The magnetic field at points in a plane through the center of the magnet (the third plane) are given in Figure 10. Similar plots for planes 4" and 7" above the center of the structure are shown in Figures 11 and 12, respectively. The intensities of the magnetic field along the x, y and z axes from the center in this third or median plane are graphed in Figure 13. From Figure 13, it can be concluded that the field through the center varies a maximum of (a) 10 Gauss from 12 inches to the right of center to 12 inches to the left of center, (b) 15 Gauss from 7 inches above the center to 7 inches below the center, and (c) 40 Gauss from 8 inches toward the back to 7 inches toward the front of the magnet. The foregoing means that over a volume 14 inches high, 24 inches wide and 12 inches thick, the magnetic field intensity varies no more than ± 20 Gauss out of 600 Gauss or ± 3.3 percent.

b. Electronics

The operational block diagram of the high-powered pulsed vacuum tube transmitter used in the large-scale NMR tests is shown in Figure 14. This transmitter was available from previous programs at SwRI and is capable of generating a 2.5 MHz RF output at peak power levels up to 165 KW when fed into a 50-ohm load. This is not as much as is required for explosive detection in the full-size sample volume but proved adequate for use in detection of other materials having a longer T_2.

The transmitter consists of a crystal oscillator, various TTL logic circuits, and a power amplifier having one transistor stage and three vacuum tube stages. It was designed to generate short bursts of radiofrequency energy, and to have rapid damping of the residual signal. Capability to generate doublet bursts of 90° pulses with the second pulse of each doublet being shifted 90° in phase relative to the first is incorporated in the design.

Design of the transmitter is relatively straight-forward except for some of the techniques made necessary by the relatively high (12 KV) plate potential used in the output stage and the necessity for keeping the circuits broadbanded to generate short, clean pulse bursts. Each of the amplifier stages is operated in a Class C mode with no plate or collector current being drawn in the absence of a signal applied to the input. The low-level stages provide the gating and frequency divider circuits required to generate short bursts of phase coherent RF signals.
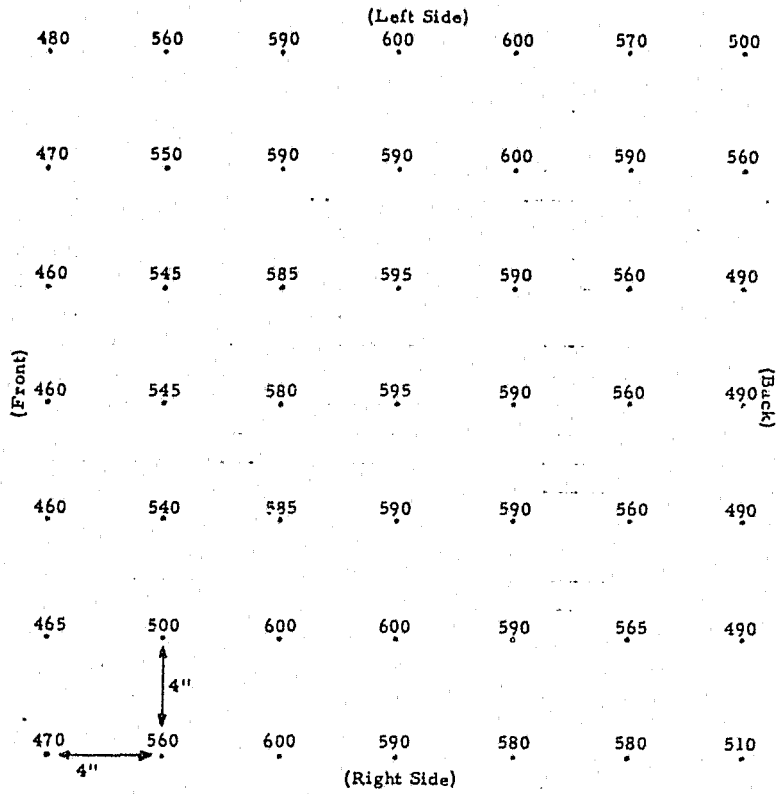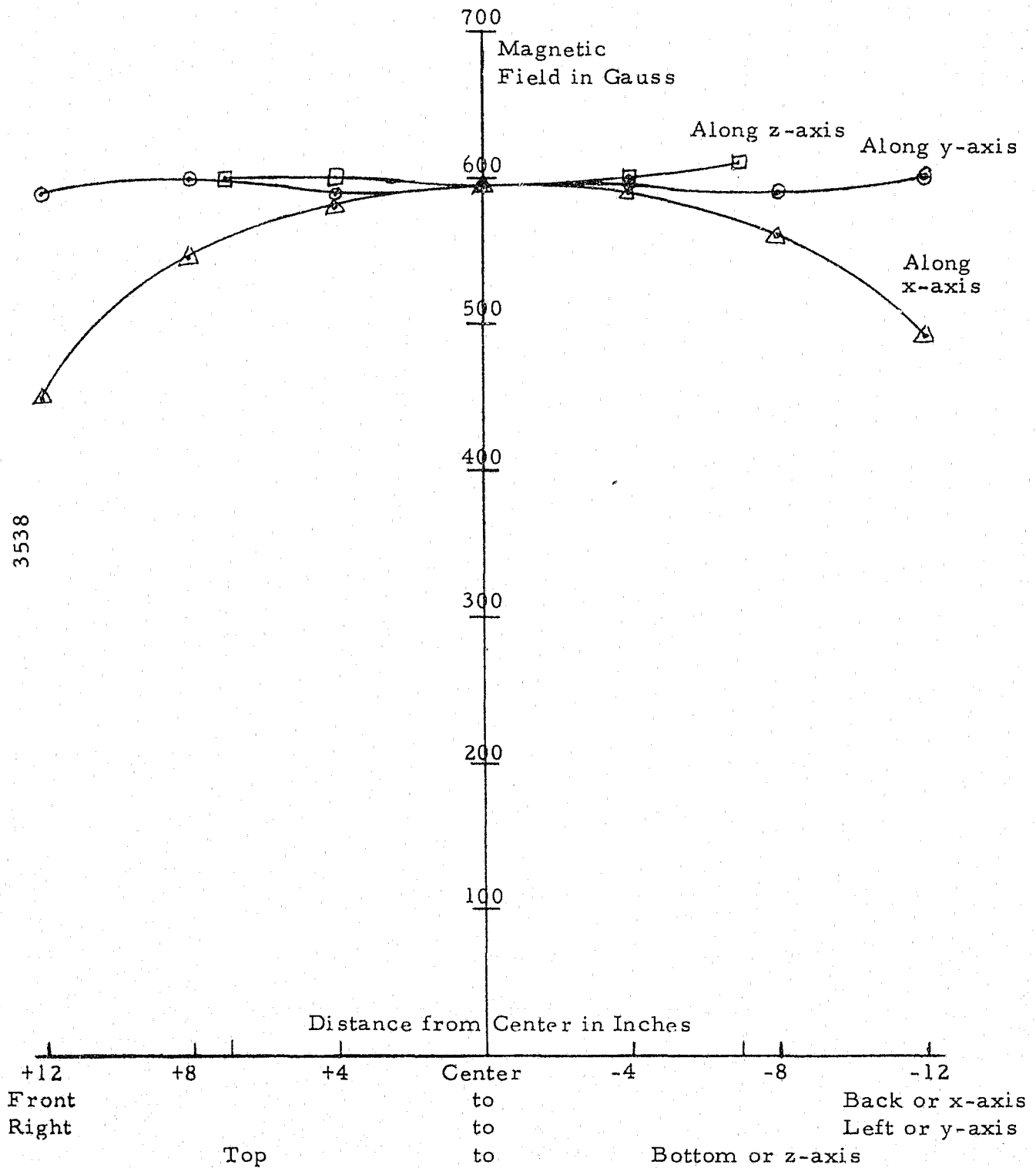
21

3536

(Left Side)

480	560	590	600	600	570	500
470	550	590	590	600	590	560
460	545	585	595	590	560	490
(Front) 460	545	580	595	590	560	490 (Back)
460	540	585	590	590	560	490
465	500	600	600	590	565	490
470	560	600	590	580	580	510

4"

4"

(Right Side)

FIGURE 10. GRAPH OF THE MAGNETIC FIELD INTENSITIES AT
THE CORNERS OF 4-INCH SQUARES OVER A PLANE
(the third plane) THROUGH THE CENTER OF THE
MAGNET IN FIGURE 5.

3537

Figure 11 (Left Side)

510	590	590	600	590	580	510
500	580	600	600	600	580	495
500	580	600	600	600	580	505
510	580	600	600	600	580	508
510	580	600	600	600	580	505
510	580	600	600	600	575	500
510	600	600	600	600	595	500

(Front) ... (Back) 4" 4" (Right Side)

FIGURE 11. GRAPH OF THE MAGNETIC FIELD INTENSITY AT THE CORNERS OF 4-INCH SQUARES OVER A PLANE (the fourth plane) THROUGH A POINT 4 INCHES ABOVE THE CENTER OF THE MAGNET IN FIGURE 5.

Figure 12 (Left Side)

650	640	600	600	600	620	700
670	650	620	610	610	650	730
670	660	610	610	610	650	750
680	650	615	610	610	690	700
680	660	610	610	610	700	700
680	650	620	600	620	630	700
670	640	600	600	600	620	700

(Front) ... (Back) 4" 4" (Right Side)

FIGURE 12. GRAPH OF THE MAGNETIC FIELD INTENSITY AT THE CORNERS OF 4-INCH SQUARES OVER A PLANE (the fifth plane) THROUGH A POINT 7 INCHES ABOVE THE CENTER OF THE MAGNET IN FIGURE 5.

23

FIGURE 13.   GRAPH OF THE MAGNETIC FIELD AS A FUNCTION OF
DISTANCE ALONG THE X, Y AND Z AXES FROM THE
CENTER OF THE MAGNET IN FIGURE 5.

24
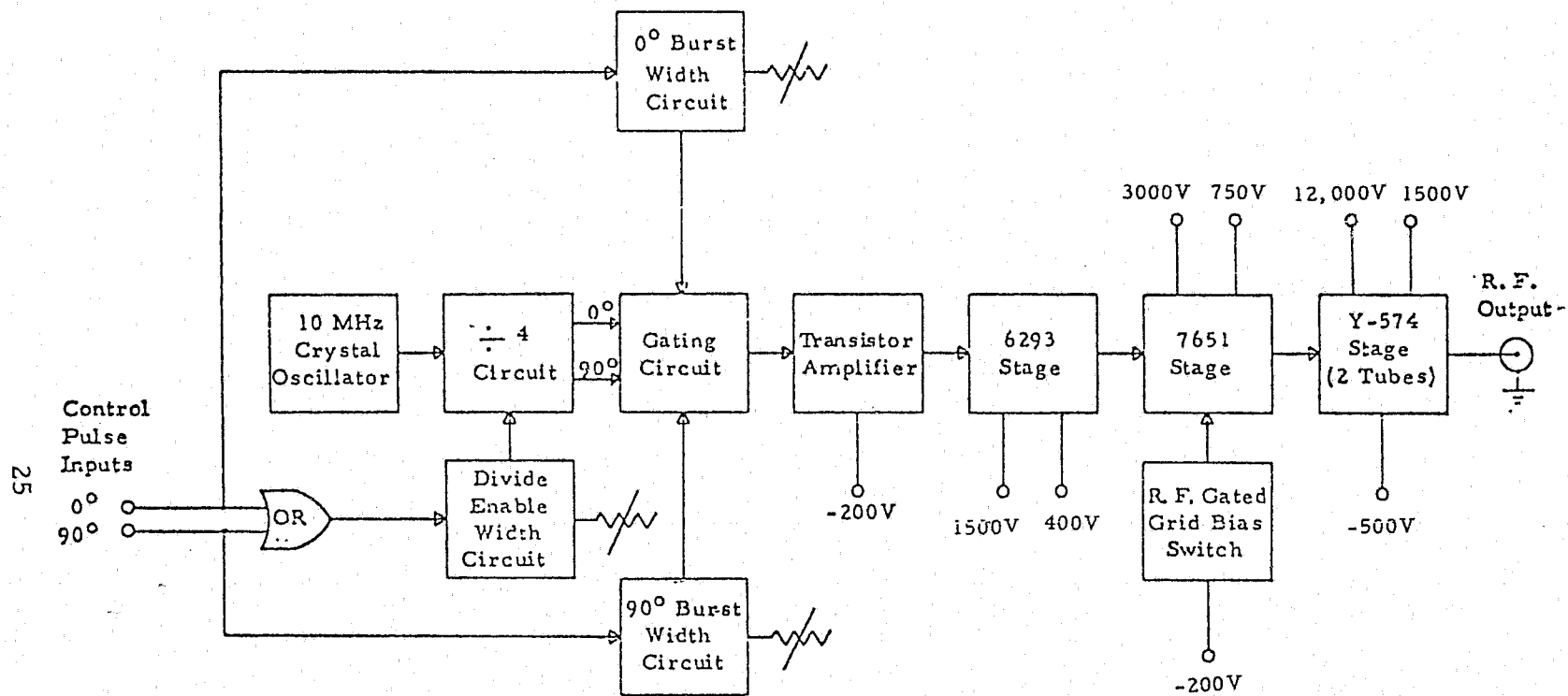
FIGURE 14. HIGH POWER PULSED TRANSMITTER

The first amplifier stage consists of a high-voltage PNP transistor and its associated biasing components. The output from this amplifier is connected directly to the grid of the 6293 vacuum tube without use of any tuned circuits. The low Q L-C plate circuit of the 6293 is transformer coupled to the grid of the 7651. Approximately 10 KW peak RF power is developed during the burst at the output of the 7651 stage. The plate circuit of the 7651 is a network which provides inductive coupling to the grid circuit of the output stage. The output stage is composed of two Eimac Y-574 vacuum tubes connected in parallel and operated in a conventional Class C. mode. A low Q resonant LC plate load circuit with a tapped inductor allows peak RF power outputs up to 165 KW to be coupled to an external load.

The transmitter output was connected through an appropriate matching circuit to the detection coil system shown in Figure 7. To perform the tests the magnet had to provide a field of 587 Gauss. For this field intensity a current of 13.3 amperes at 102.4 volts is needed when the magnet is cold. When the magnet is hot, a voltage of 115 volts is required. For some tests a field of around 800 Gauss was needed. This required a current of 18.1 amperes at a potential of 139 volts when the magnet is cold and 156.7 volts when it is hot. To perform the current regulation and field switching, a power supply which was available at SwRI as a result of previous programs was used. A block diagram of this unit is shown in Figure 15. The power supply is essentially a current regulated system in which the comparison amplifier feeds the difference between the control voltage and the voltage across the current sensing resistor to the feedback amplifier and thence to the series pass transistors. By this means, the voltage fed to the series pass transistors is adjusted to bring the voltage across the current sensing resistor equal to the control voltage within an error value which is the inverse of the open loop gain. The circuit may be switched from one current regulating level to another voltage by a signal fed into the comparison amplifier from the program selector. Thus, the current is both switched at the proper time and regulated at the proper value.

4.   Results of Small Sample Tests

The equipment described briefly in Section II. A. 2 was used to obtain the transient NMR signals from several explosives. Only a small amount (a few grams) of each explosive was used in these tests so that safety could be maintained in the laboratory. In each case for the results to be presented, the 90°-90° (phase = 90°) dual-pulse sequence was used. The results are presented as photographs of the oscilloscope display of the detected transient NMR signals. Each
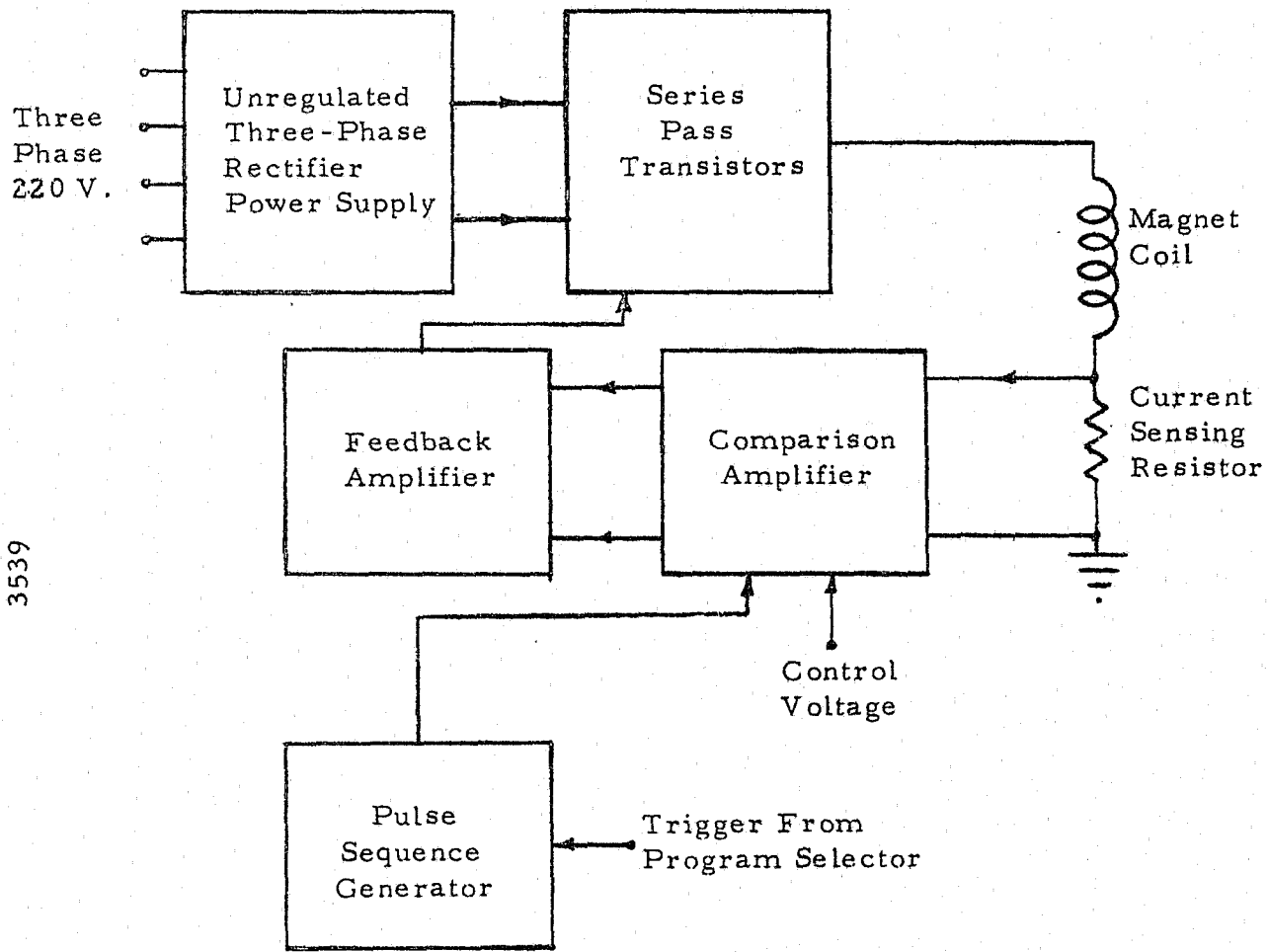
26

3539

FIGURE 15. BLOCK DIAGRAM OF THE REGULATED AND PULSED
POWER SUPPLY FOR THE MAGNET

27

oscilloscope tracing is a real-time display of one pass through the signal. This is important to understand because the signal/noise of the signals as presented has not been improved by a repetition of many signals. Such a technique could be used to increase the coherent signals relative to the incoherent noise.

The hydrogen transient NMR signals will be presented from dynamite, smokeless powder, black powder and plastic explosive. Two types of plastic explosive were used, type C-4 which has a base of RDX and plasticized PETN or Detasheet.

The hydrogen transient NMR signals from a sample of Hercules Unigel Tamptite brand of dynamite are given in Figure 16. A two-component transient NMR signal was obtained from the hydrogen in this dynamite. The signal in Figure 16a shows most of both components. The rapidly decaying component, which lasts for less than 100 microseconds, as shown in Figure 16a, is from the hydrogen in the molecules which are in the essentially solid components of the dynamite. The slowly decaying component persists for 2000 microseconds and comes from the hydrogen in the molecules which are in the essentially liquid components absorbed onto the solid components. If the liquid components were not absorbed or in some way not attached to the solid components, then the slowly decaying component would persist for times 10 to 100 times longer than the 2 milliseconds shown in Figure 16b.

The transient NMR signal in Figure 16a has been repeated with repetition intervals varying from 1 to 30 seconds. This is the time between transmitted burst sequences. The amplitude of the slowly decaying component does not change indicating that the value of T_1 for this component is less than 1 second. Further tests showed that the value of T_1 for the liquid-like components was of the order of T_2 or around 2 milliseconds. The rapidly decaying component, however, increases with increasing repetition time intervals, reaching a maximum for repetition time values above 10 seconds. Therefore, the value of T_1 for this component is between 2 and 5 seconds, probably about 3 seconds. The summary of the results from the Hercules Unigel Tamptite dynamite is given in Table I. Remember that although T_1 and T_2 are

TABLE I

TRANSIENT NMR CHARACTERISTICS FROM HERCULES
UNIGEL TAMPTITE DYNAMITE

Component	T_2	T_1
Solid-like	30×10^{-6} sec.	3 sec.
Absorbed liquid	2×10^{-3} sec.	2×10^{-3} sec.

a.
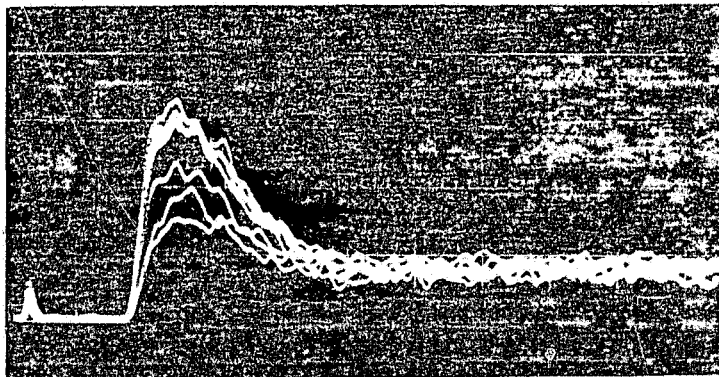
Vertical: 0.5 Volts/cm
Horizontal: 20 µ Sec/cm
Repetition Intervals: 1,2,5,10,
             15,20 and 30 seconds

b.
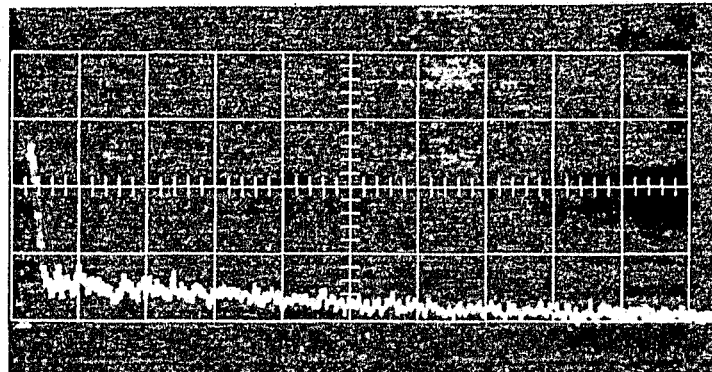
Vertical: 0.5 Volts/cm
Horizontal: 200 µ Sec/cm
Repetition Interval: 10 seconds

Dynamite: Hercules Unigel Tamptite
Frequency: 2.5 MHz

FIGURE 16.   HYDROGEN TRANSIENT NMR SIGNALS FROM HERCULES   UNIGEL
          TAMPTITE DYNAMITE TAKEN AT 2.5 MHz WITH A 90°-90° (Phase = 90°)
          DUAL PULSE SEQUENCE

listed as being the same, the value of T_1 is always longer than the value of T_2, or equal to it.

The hydrogen transient NMR signals from C-4 with an RDX base are given in Figure 17. The signal in Figure 17b shows clearly that RDX base C-4 has both a rapidly decaying component and a slowly decaying component. The slowly decaying component has a T_2 value of 2 milliseconds from Figure 17b. The rapidly decaying component, as shown in Figures 17a and 17b, does not appear clearly until the repetition time has reached a time longer than 10 minutes. The NMR characteristics found for RDX Base C-4 explosive are given in Table II.

TABLE II

NMR CHARACTERISTICS FOR RDX BASE C-4 EXPLOSIVE

Component	T_2	T_1
Rapidly Decaying	15×10^{-6} sec.	5 minutes
Slowly Decaying	2×10^{-3} sec.	2×10^{-3} sec.

The transient hydrogen NMR signals from C-4 with a PETN base are shown in Figure 18. In Figure 18b, both the slowly decaying and the rapidly decaying components are visible. In the signals in Figure 18a, the repetition time was varied from 10 seconds to 10 minutes to 30 minutes. The NMR characteristics for PETN Base C-4 explosive are listed in Table III.

TABLE III

NMR CHARACTERISTICS FOR PETN BASE C-4 EXPLOSIVE

Component	T_2	T_1
Rapidly Decaying	15×10^{-6} sec.	5 minutes
Slowly Decaying	2×10^{-3} sec.	2×10^{-3} sec.

The transient hydrogen NMR signals from black powder (DuPont FFg Superfine Rifle Powder) are shown in Figure 19a. The hydrogen transient NMR signals are from two sources in black powder. One source is water which has a concentration of less than one percent. The other source is the hydrogen in the incompletely pyrolyzed material called coke or charcoal. Since both of these sources are less than 1% in concentration, very small hydrogen NMR signals are expected and obtained as shown in Figure 19a. These signals indicate, as expected and predicted, that use of the hydrogen NMR technique is not a good method for detecting black powder.
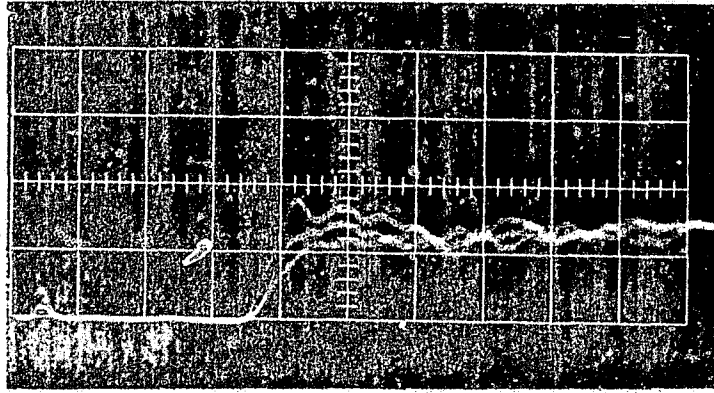
a. Vertical: 0.5 Volts/cm   Horizontal: 10 μ Sec/cm
Repetition Interval: 0.5, I, 2, 5 and 10 minutes
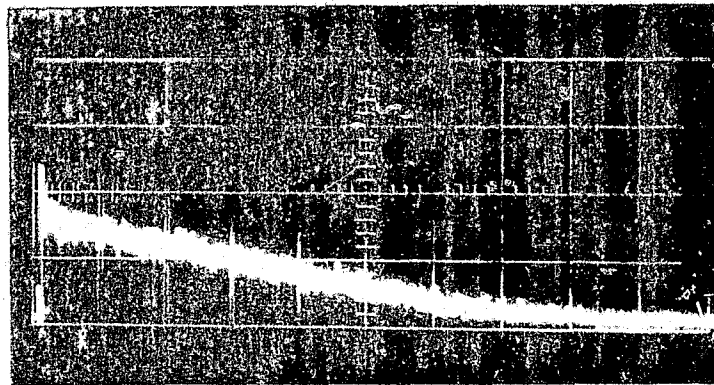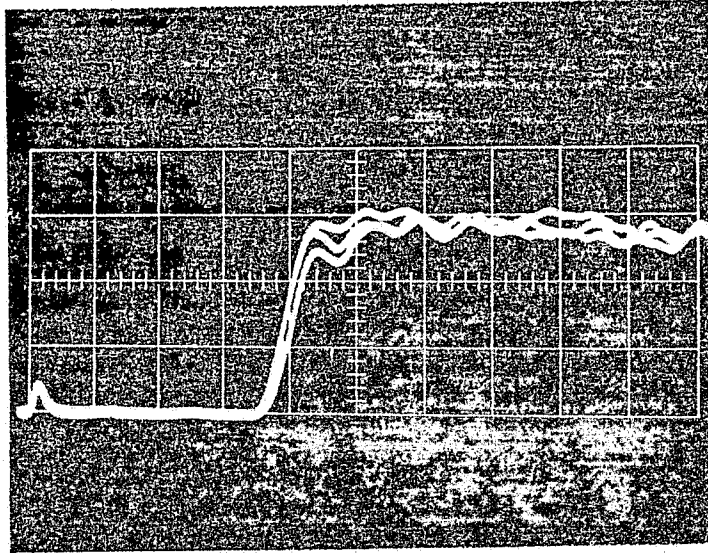

b. Vertical: 0.5 Volts/cm   Horizontal: 500 μ Sec/cm
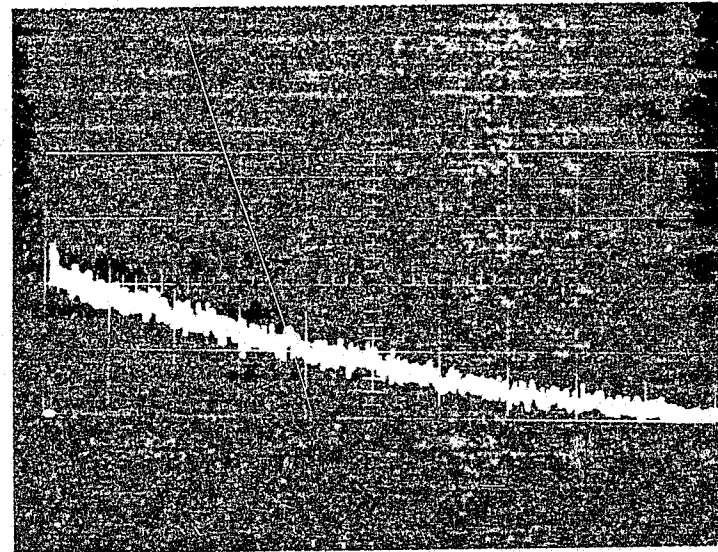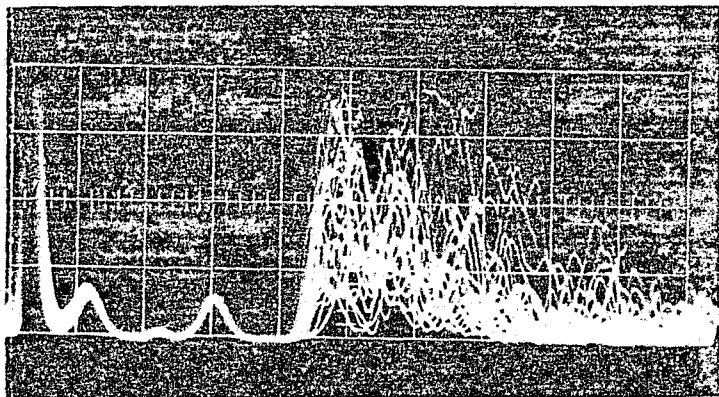Repetition Interval: 10 and 30 minutes
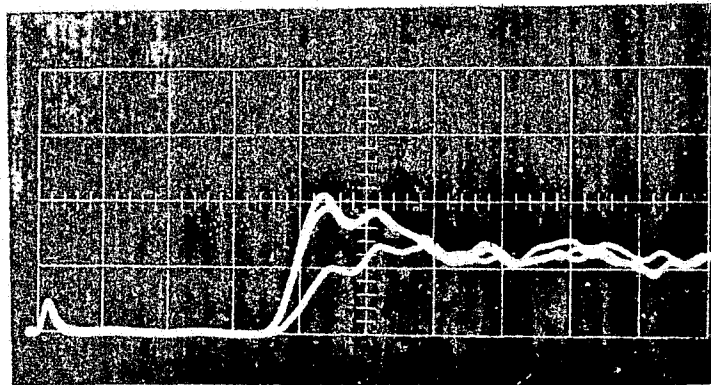
c. Vertical: 0.5 Volts/cm   Horizontal: 10 μ Sec/cm
Repetition Interval: 10 seconds, 10 and 30 minutes

FIGURE 17. HYDROGEN TRANSIENT NMR SIGNALS FROM RDX BASED
C-4 EXPLOSIVE TAKEN AT 2.5 MHz WITH A 90°-90°
(Phase = 90°) DUAL PULSE SEQUENCE

31

32

a.

Vertical:	0.5 volts/cm
Horizontal:	10 μ sec/cm
Repetition Intervals:	10 seconds, 10 and 30 minutes

Vertical:	0.5 volts/cm
Horizontal:	500 μ sec/cm
Repetition Intervals:	10 minutes

FIGURE 18. HYDROGEN TRANSIENT NMR SIGNALS FROM PETN BASED C-4 EXPLOSIVE TAKEN AT 2.5 MHz WITH A 90°-90° (Phase = 90°) DUAL PULSE SEQUENCE

a. Black Powder (Dupont FF$_g$ Superfine
   Black Rifle Powder)
   Vertical: 0.02 Volts/cm
   Horizontal: 10 µ Sec/cm
   Repetition Interval: 63 milliseconds
   Frequency: 2.5 MHz
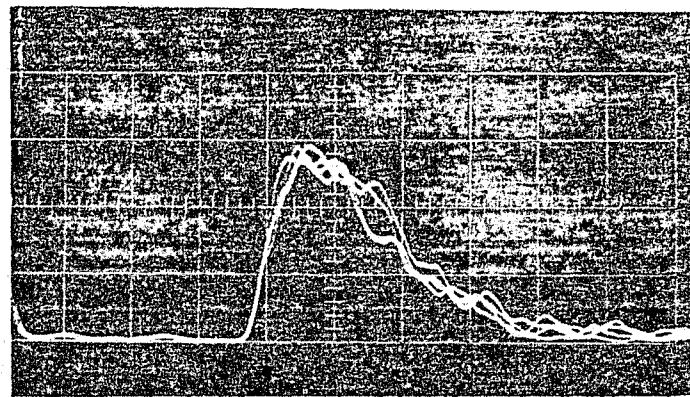
b. Smokeless Powder (Dupont IMR-
   3031)
   Vertical: 0.2 Volts/cm
   Horizontal: 10 µ Sec/cm
   Repetition Interval: 1 second
   Frequency: 2.5 MHz

33

FIGURE 19. HYDROGEN TRANSIENT NMR SIGNALS FROM BLACK POWDER (a) AND SMOKE-
           LESS POWDER (b) TAKEN AT 2.5 MHz WITH A 90°-90° (Phase = 90°) DUAL
           PULSE SEQUENCE

The transient hydrogen NMR signals from four smoke-less powders are shown in Figure 19b, 20a, 20b and 20c. The smokeless powder used for Figure 19b is DuPont IMR-3031. A total of 3 signals are given in the figure at a repetition interval of 1 second. Only one component is observable in the signal and it has a T_2 of around 20×10^{-6} seconds and a T_1 of much less than 1 second. The large magnet in Figure 4 was used for the signals in Figure 19b.

For the hydrogen transient NMR signals from the other three smokeless powders, a Helmholtz pair magnet was used to provide the magnetic bias field H_0. Also, a single 90° pulse was used to produce a FID (free induction decay) type transient NMR signal in-stead of the pulse echo obtained for the other materials. As may be seen the transient NMR signals from all the smokeless powders shown in Figures 19b, 20a, 20b and 20c are essentially the same in decay time but slightly different in amplitude. The decay times indicate that the source is a molecule in a solid.

5.   Results of Full Sample Tests

The electronic apparatus for the full-scale tests (Section II.A.3) was assembled with the full-sized magnet and coil of Figure 7. Initial tests were conducted with large samples to aid in achieving proper adjustment of the apparatus as well as to determine at what concentration hydrogen transient NMR signals could be obtained. A 5-gallon container of water (weight 41.7 lbs.) was inserted into the center of the detection coil and the FID signal in Figure 21 was obtained following a single transmitter pulse. The value of T_2^* from Figure 21 is is 40×10^{-6} seconds. Since the value of T_2 for water is much longer than T_2^*, the value of T_2^* represents the inhomogeneity of the magnet. The inhomogeneity equivalent to a T_2^* of 40 microseconds is 5.87 Gauss. This means that the inhomogeneity over the volume of the 5-gallon con-tainer is ± 5.87 Gauss. This is in agreement with the field measure-ments made and reported in Section II.A.3. The 5-gallon container was a cube which had dimensions of 10.5 inches at each corner. The magnet inhomogeneity then is equivalent to an average linear change in magnetic field over the sample of 5.87/10.5 or 0.559 Gauss per inch. As shown in Figure 11, the field varies in an oscillatory manner from side to side and top to bottom. The field variation front to back is parabolic in shape and gives the largest variation.
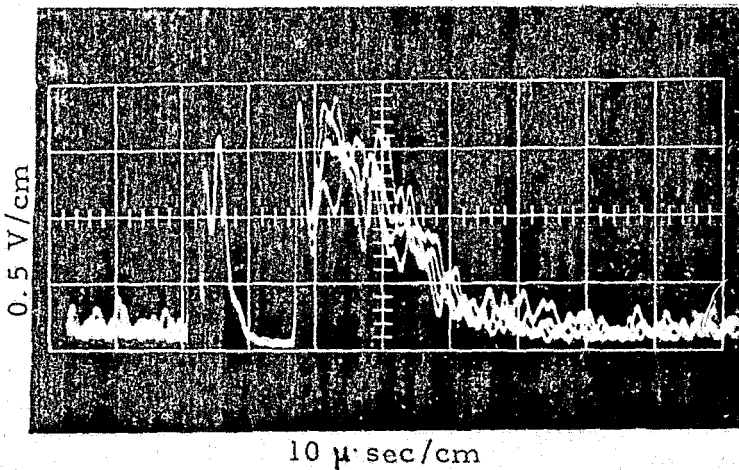
The hydrogen transient NMR signal from the water in Figure 21 was equivalent to a concentration of 1.33×10^{22} hydrogen nuclei per cm^3. This concentration is equivalent to 14.38 percent water mixture filling the complete volume of the RF coil.
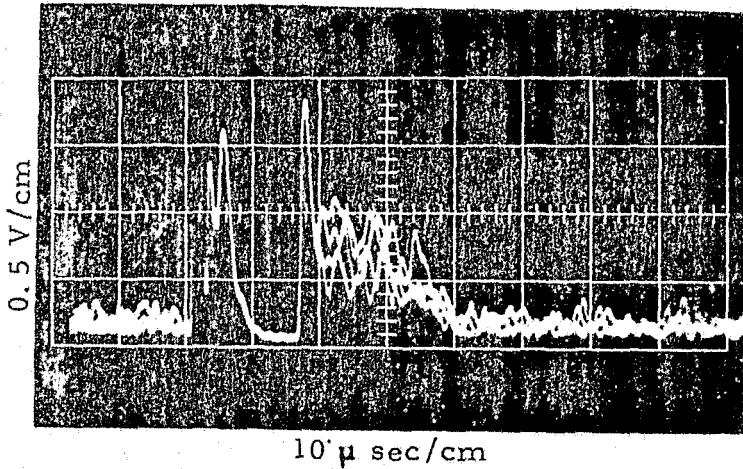
a. "Red Dot" Brand Smokeless Powder.
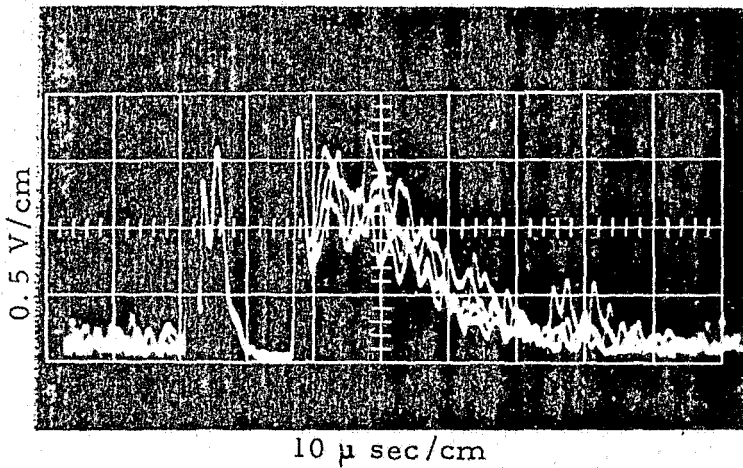
b. "Unique" Brand Smokeless Powder.

c. "2400" Brand Smokeless Powder.

FIGURE 20. HYDROGEN TRANSIENT NMR SIGNALS FROM THREE TYPES OF SMOKELESS POWDER TAKEN AT 2.5 MHz USING THE FREE INDUCTION DECAY OR SINGLE 90° PULSE RESPONSE
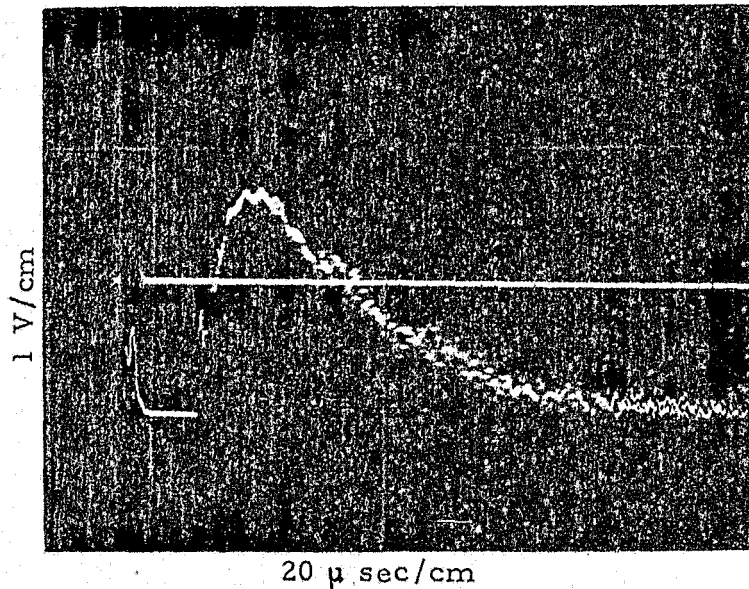
20 μ sec/cm

FIGURE 21. HYDROGEN TRANSIENT NMR SIGNAL FOLLOWING A
SINGLE 90° PULSE FROM FIVE GALLONS OF WATER
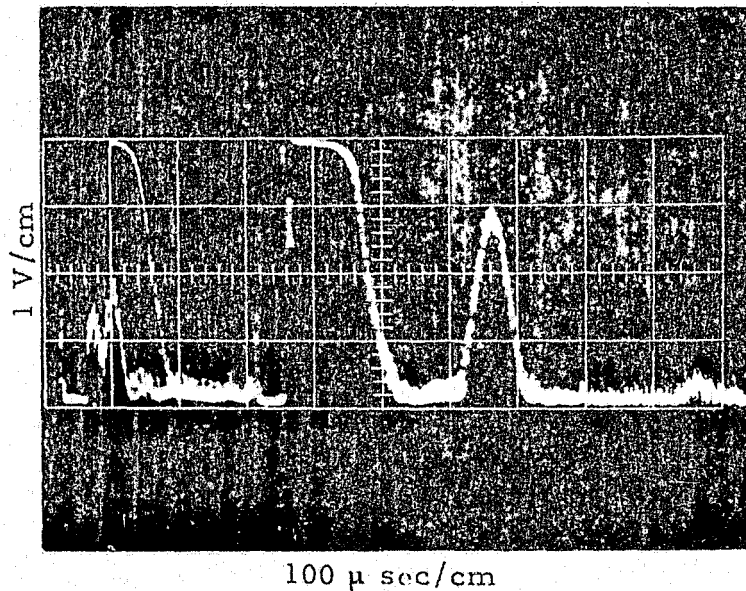IN THE FULL-SCALE MAGNET OF FIGURE 5.

3541

100 μ sec/cm

FIGURE 22. TRANSIENT HYDROGEN NMR ECHO SIGNAL FROM GLYCEROL
AND WATER SAMPLES EACH IN CYLINDERS 3.5" HIGH AND
6.5" IN DIAMETER.

After the above initial measurement of the hydrogen transient NMR signals from the full-scale magnet and coil setup, the detection apparatus was peaked in sensitivity until the hydrogen transient NMR echo signal in Figure 22 was obtained. Two samples, stacked one on top of the other, were used to give this signal, one of water and the other of glycerol. Each sample was in a plastic container which was a cylinder 3.5 inches high and 6.5 inches in diameter. These two containers were mounted, the glycerol on top and the water on the bottom, with the bottom of the water sample 2 inches above the bottom coil wires and symmetrical about the z axis in the magnet and coil arrangement shown in Figure 7. This sample is one-fifth of the amount of the 5-gallon sample used previously. Therefore, in this case, the signal is equivalent to a water concentration of about 3% distributed throughout the coil volume.

Further system modification and adjustment resulted in the signal in Figure 23 being obtained from the foregoing glycerol cylinder alone. This signal is equivalent to one from a distribution of 13.735×10^{20} hydrogen nuclei per cm^3 throughout all of the coil volume. A somewhat poorer signal was obtained with the cylinder filled with water as shown in Figure 24. The signal from the water is equivalent to 14.96×10^{20} hydrogen nuclei per cm^3 in the coil volume 14" x 24" x 12". These are very encouraging results since the theoretical sensitivity of the NMR spectrometer is a signal/noise ratio of 10/1 from 3×10^{20} hydrogen nuclei per cm^3 at a magnetic field intensity of 1000 Gauss. At 587 Gauss (2.5 MHz), where the signals in Figures 24b and 24c were made, the theoretical sensitivity would be a signal/noise of 10/1 at a concentration of 5.1×10^{20}. It should be noted that the signal/noise values in Figures 23 and 24 are not unity, although that of Figure 24 is very close, so that at least for glycerol, the concentration of 13.735×10^{20} must be increased by the ratio of the signal/noise ratios for comparison with the theoretical value.

Several measurements were made on representative types of baggage components to determine their potential to cause interference signals. To obtain a detection sensitivity more like that needed for the explosive detection (3 to 4 times the sensitivity shown by Figure 23), a second, smaller detection coil was fabricated. This coil was fabricated in a copper clad board enclosure and was similar in construction to that of the larger coil except the winding cross section was 6" x 14" and the seven turn winding extended over a length of 3 inches. The coil inductance measured 12.2 microhenries and the volume is 4129 cm^3. This medium-sized coil thus has a volume which is roughly 1/12 that of the full-sized coil.
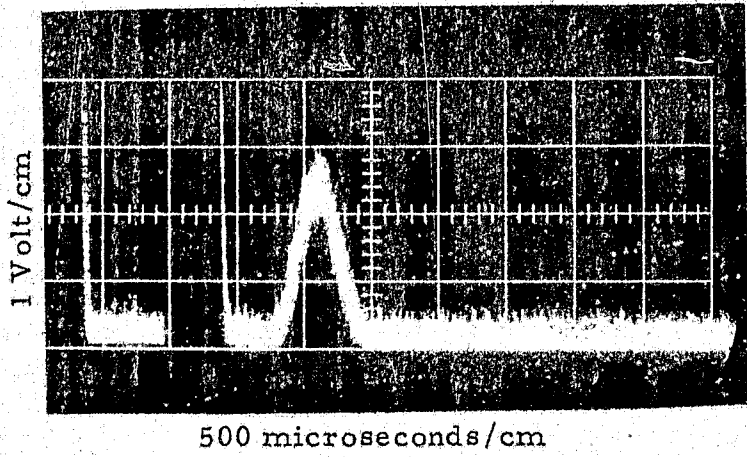
37

1 Volt/cm

500 microseconds/cm

FIGURE 23 . TRANSIENT HYDROGEN NMR ECHO SIGNAL
(90° - 180° pulse sequence) FROM THE 3.5" x
6.5" CYLINDER FILLED WITH GLYCEROL
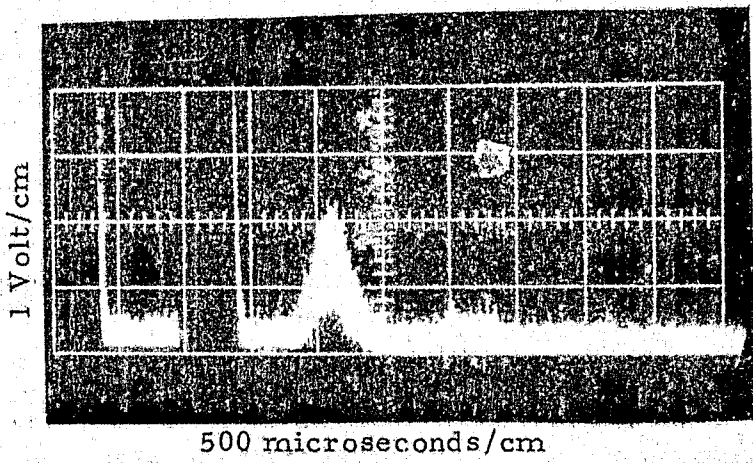
3542

1 Volt/cm

500 microseconds/cm

FIGURE 24 . TRANSIENT HYDROGEN NMR SIGNAL FROM
THE 3.5" x 6.5" CYLINDER FILLED WITH
WATER

With the medium-sized coil, the transient hydrogen NMR signal in Figure 25 was obtained from eight rods of phenolic plastic each 1" OD x 8" long. No similar signals were obtained from these rods in the full-sized coil. The sensitivity was further tested by using a sample of glycerol which was 3.5" OD and 0.75" high. The transient NMR signal from this smaller sample of glycerol was similar to that shown for the much larger sample (6.5" OD x 3.5" high) in Figure 25. Using the same receiver gain the amplitude of the signal from the smaller sample in the medium-sized coil was 4 volts while that from the larger sample in the larger coil was 2 volts. The smaller sample had a volume 9 times smaller than the larger sample. The two coils had a turn ratio of 7/5. Thus the expected comparison would be a sensitivity increase of 12 x 7/4 or 21 to 1. A sensitivity increase of 18 was measured. It is estimated that the difference is caused by the differences in the coil pickup and in the inductance values. That is, the inductance value for the full-scale coil is 4.5 microhenries while that of the medium-sized coil is 12.2 microhenries.

To further test the sensitivity of the medium-sized coil, a 10-milliliter sample of glycerol was used and a signal-plus-noise-to-noise ratio of 2 to 1 was measured. This 10 cm^3 sample was in a container 1" OD by 1.13" high. In this sample, there are 6.6 x 10^{23} hydrogen nuclei. In the coil volume, there is a concentration of 1.6 x 10^{20} hydrogen nuclei per cm^3 which compares very favorably with the theoretical sensitivity of 0.51 x 10^{20} hydrogen nuclei per cm^3 for a unity signal-to-noise ratio.

To test for interference signals, three briefcases were obtained and tested:

- Samsonite, 4-3/4 inches high
- Samsonite, 3 inches high
- Leather-covered wooden-frame, 5-1/8 inches high

The signals picked up by the detection coil following a single 90° pulse, 5 microseconds long, are shown in Figure 26. The signal in Figure 26a is that from the smaller Samsonite briefcase. The signal in Figure 26b is from the larger Samsonite briefcase. The signal from the leather-covered wooden-frame briefcase was much smaller than that from either of the other two and was of smaller duration.

The explosive in the briefcases was simulated with glycerol samples. One sample was the 6.5" OD x 3.5" high cylinder of glycerol previously mentioned and another was cylinders of glycerol
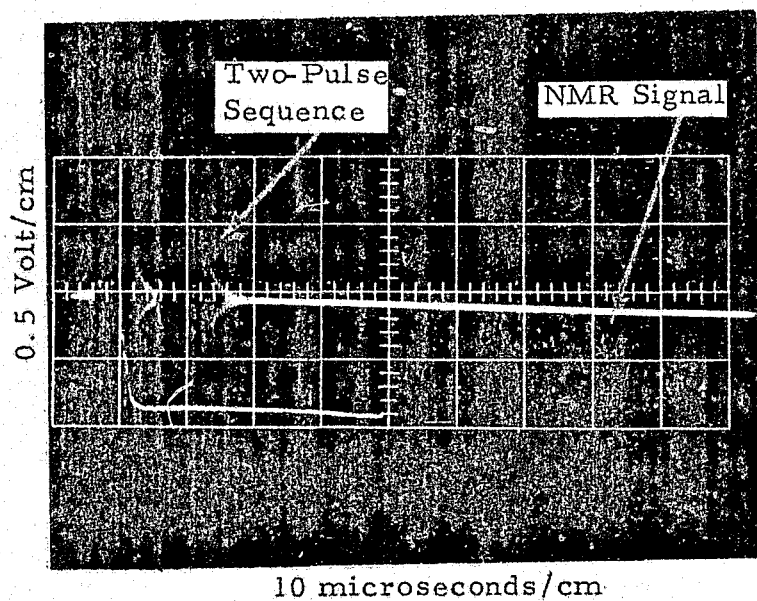
39

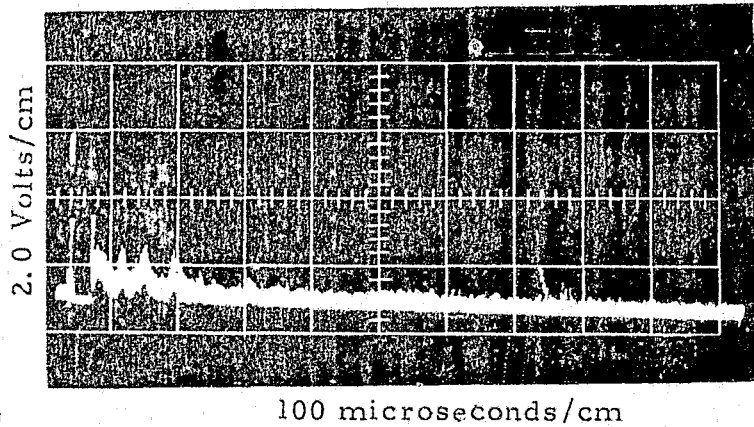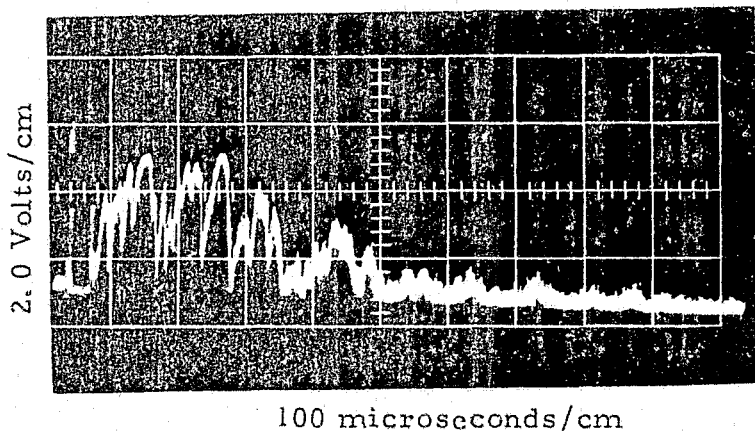3543

FIGURE 25. TRANSIENT HYDROGEN NMR SIGNAL FROM EIGHT
PHENOLIC RODS EACH 1" O.D. x 8" LONG IN
MEDIUM-SIZED COIL

a. 3" High Samsonite
   Briefcase
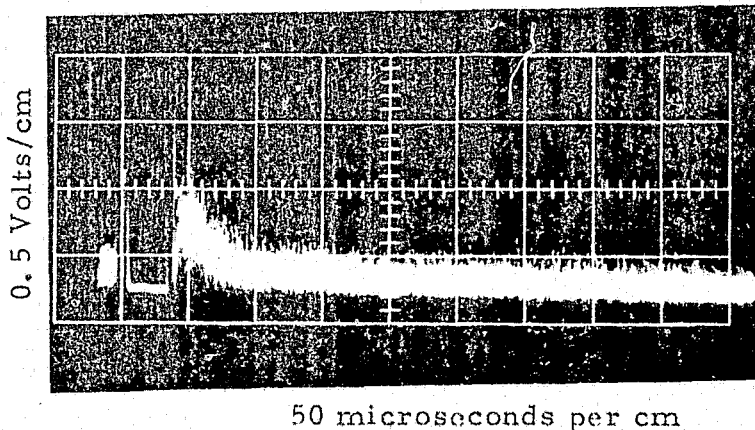
2.0 Volts/cm

100 microseconds/cm

3544

b. 4.75" High Samsonite
   Briefcase

2.0 Volts/cm

100 microseconds/cm

c. 5.125" High Leather-
   Covered Wooden-
   Frame Briefcase

0.5 Volts/cm

50 microseconds per cm

FIGURE 26. SIGNALS PICKED UP BY THE DETECTION COIL FOLLOWING
A 5 MICROSECOND 90° PULSE FOR THREE SAMPLES: (a)
3" Samsonite Briefcase, (b) 4.75" Samsonite Briefcase, and
(c) 5.125" Leather-Covered Wooden-Frame Briefcase.

41

1-1/16" ID x 7.25" long, used to simulate a stick of dynamite. When these samples were placed in the three briefcases, the signals in Figure 27 were obtained. The glycerol signal can be readily detected in each of the briefcases. When Figure 27a is compared with Figure 26a, the glycerol transient NMR signal is observed to be much larger than the potentially interfering signal. This conclusion can also be made when Figure 27b is compared with Figure 26b, and Figure 27c is compared with Figure 26c.

Other signal producing materials were packed in the 3" high Samsonite bag both with and without the two slender cylinders of glycerol. In Figure 28a, the signal from two laboratory coats in the 3" case is displayed. When the glycerol samples were inserted into the case along with the laboratory coats, the signal in Figure 28b was obtained. The glycerol signal is readily evident in the Figure. Other items were tested in the 3" case, both alone and with glycerol samples. Figure 28c is for the case with a hair dryer and one laboratory coat. Figure 28d is for the items in 28c but with glycerol added. Figures 28e and 28f are for the 3" case with one laboratory coat and five magazines but without glycerol in (e) and with glycerol in (f). In Figures 25g and 25h, some tools have been added, but still the glycerol signal is evident in Figure 28h. Liquid soap was added to the laboratory coat in Figures 28i and 28j, but still the glycerol signal is observable.

B. ESR Studies

1. Techniques

Certain materials can be detected using electron spin resonance (ESR) techniques. The occurrence of ESR depends on the presence of free electrons in the material being tested and is observed using method similar to those employed in NMR measurements. Some propellants such as black gunpowder contain a significant number of free electrons because of the broken bonds in the pyrolyzed materials used in their manufacture. Detection of such material is, therefore, possible with ESR techniques.
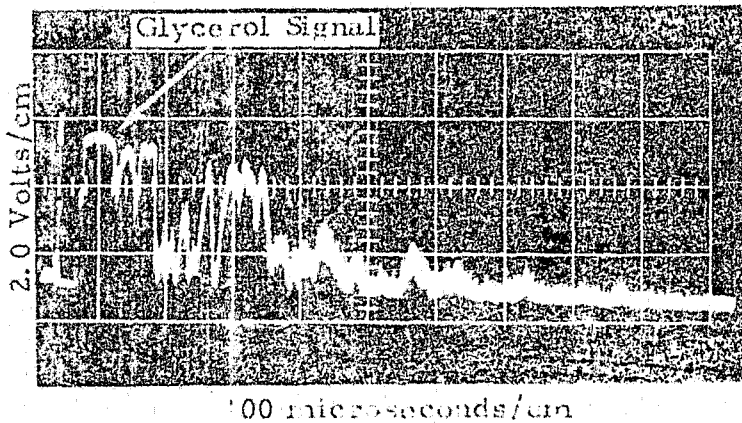
When electron spin resonance occurs, energy is exchanged between the applied fields and the free electrons that are involved. The resonance frequency, ν_o, is given by

$$\hbar \nu_o = g B H_o \tag{8}$$
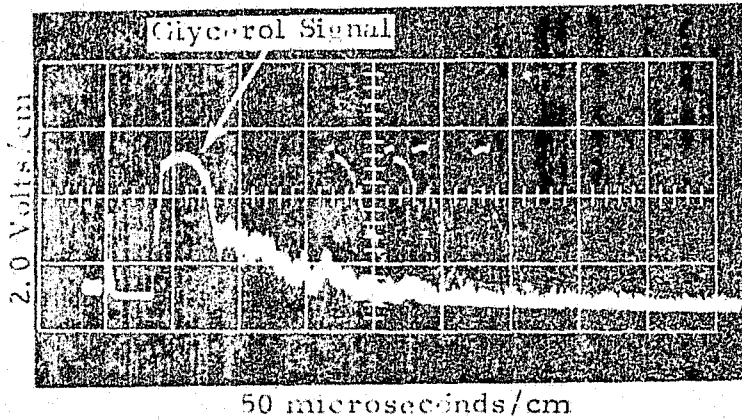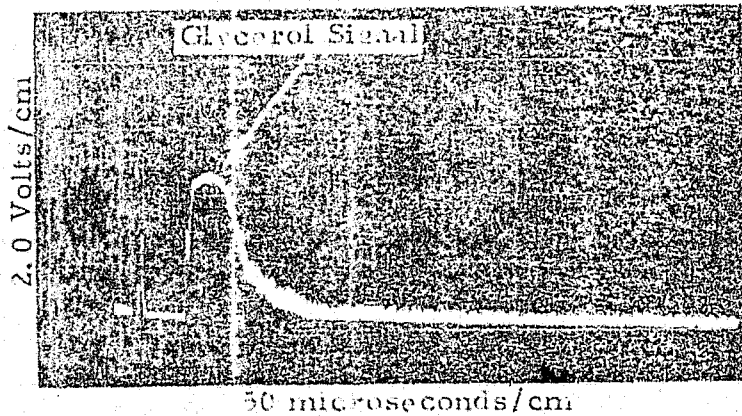
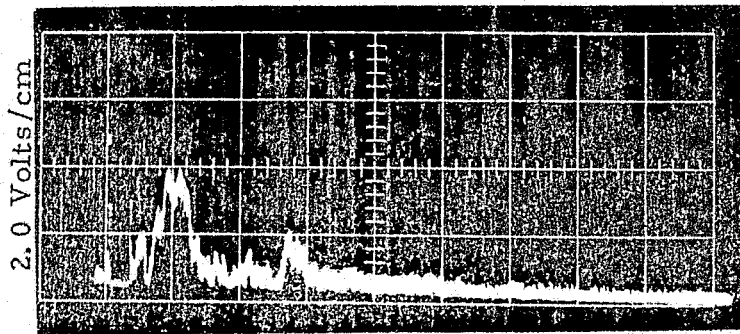a. 3" High Samsonite Case with Four of the Long Slender Cylinders of Glycerol

b. 4.75" High Samsonite Case with the 6.5" O.D. x 3.5" Cylinder of Glycerol

c. 5.125" High Leather-Covered Wooden-Frame Briefcase with Two of the Long Slender Cylinders of Glycerol

FIGURE 27. TRANSIENT NMR SIGNALS FROM GLYCEROL SAMPLES IN THE THREE BRIEFCASES. (a) 3" High Samsonite Case with Four of the Long Slender Cylinders of Glycerol, (b) The 4.75" High Briefcase with the 6.5" O.D. x 3.5" Glycerol sample, and (c) The 4.75" High Leather-Covered Wooden-Frame Brief-case with Two of the Long Slender Cylinders of Glycerol.
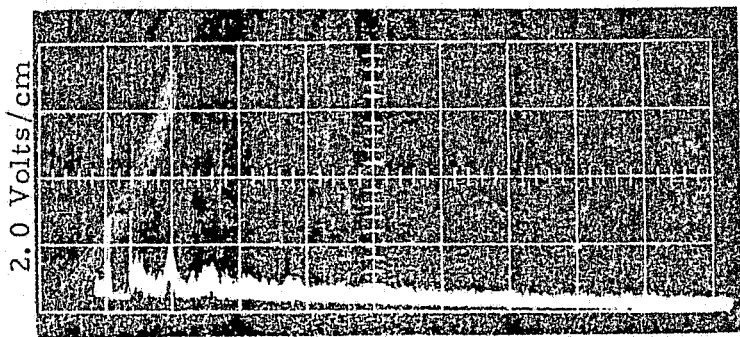
43

a. 3" High Samsonite Case with Two Laboratory Coats
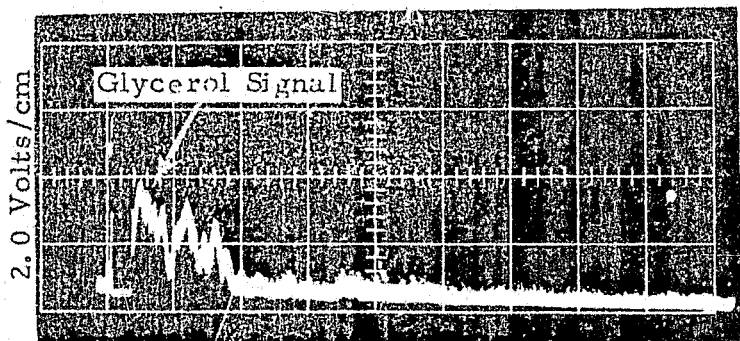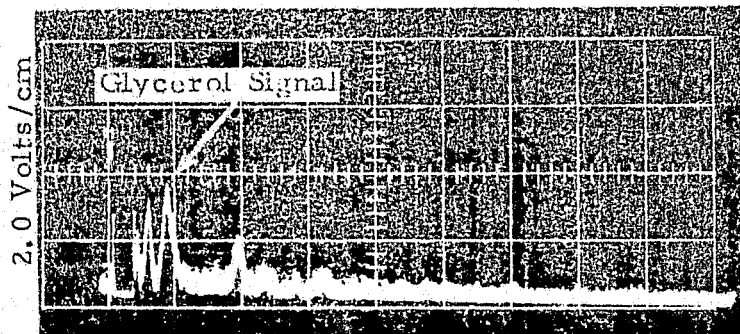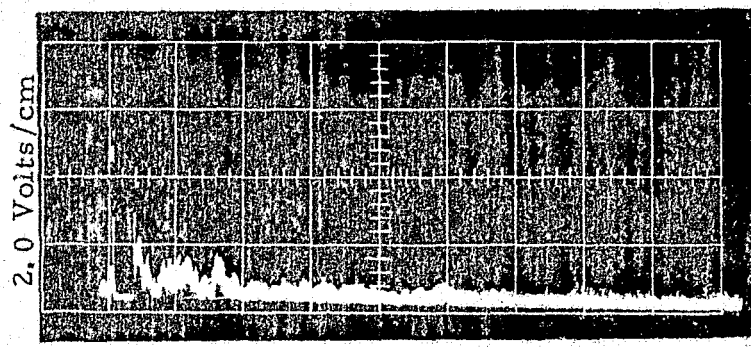
b. As in (a) but with Two of the Slender Cylinders of Glycerol Added

c. 3" High Samsonite Case with One Laboratory Coat and One Hair Dryer
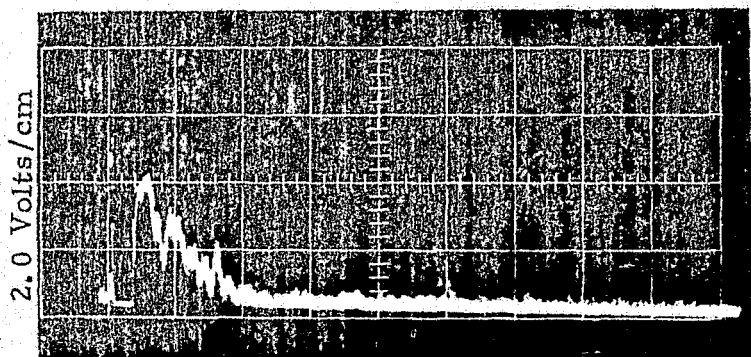
d. As in (c) above but with Two of the Slender Cylinders of Glycerol Added

FIGURE 28. THREE-INCH HIGH SAMSONITE CASE PACKED WITH SEVERAL TYPES OF MATERIAL, BOTH ALONE AND WITH TWO OF THE

2.0 Volts/cm

100 microseconds/cm

e. 3" High Samsonite Case
with One Laboratory Coat
and Five Magazines

2.0 Volts/cm

100 microseconds/cm

f. As in (e) above but with
Two of the Slender
Cylinders of Glycerol
Added

2.0 Volts/cm
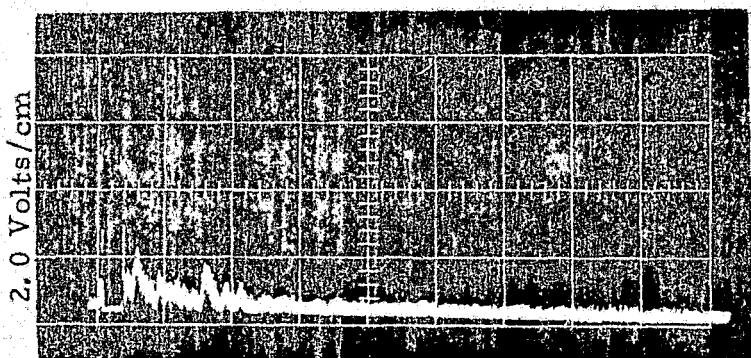
100 microseconds/cm

g. 3" High Briefcase with One
Lab Coat and Three Screw-
drivers and a Ball Pien
Hammer

2.0 Volts/cm
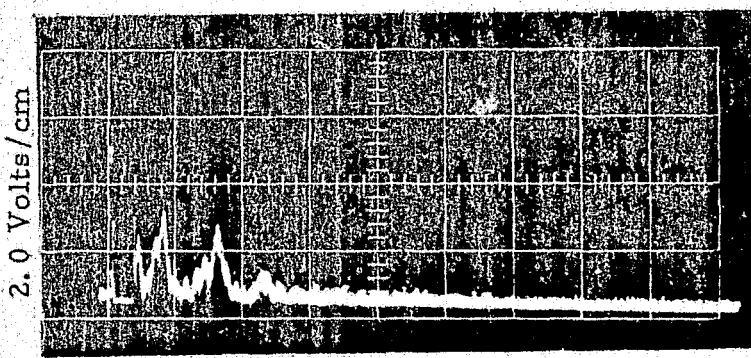
100 microseconds/cm

h. As in (g) above but with
Two of the Slender
Cylinders of Glycerol
Added

3546

FIGURE 28.(Cont'd)

45

2.0 Volts/cm

100 microseconds/cm

i. 3" High Samsonite Case with One Laboratory Coat and One Bottle of Joy Liquid Soap

3546

2.0 Volts/cm
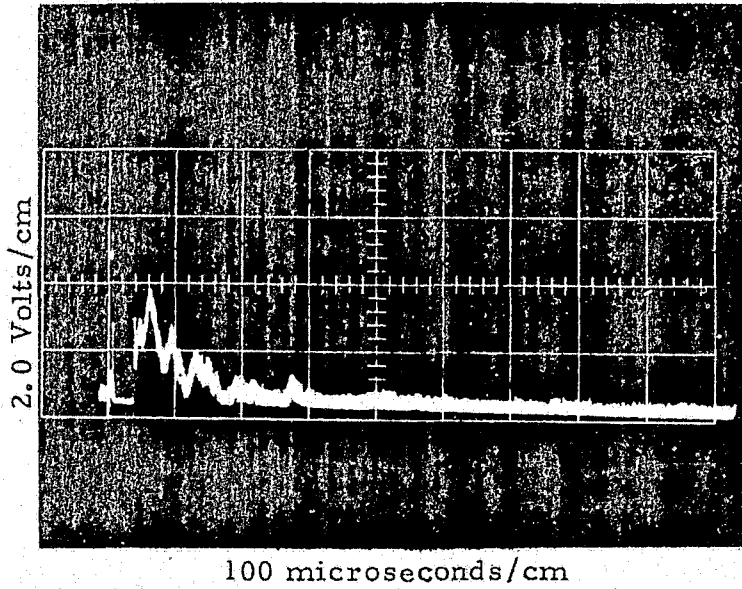
100 microseconds/cm
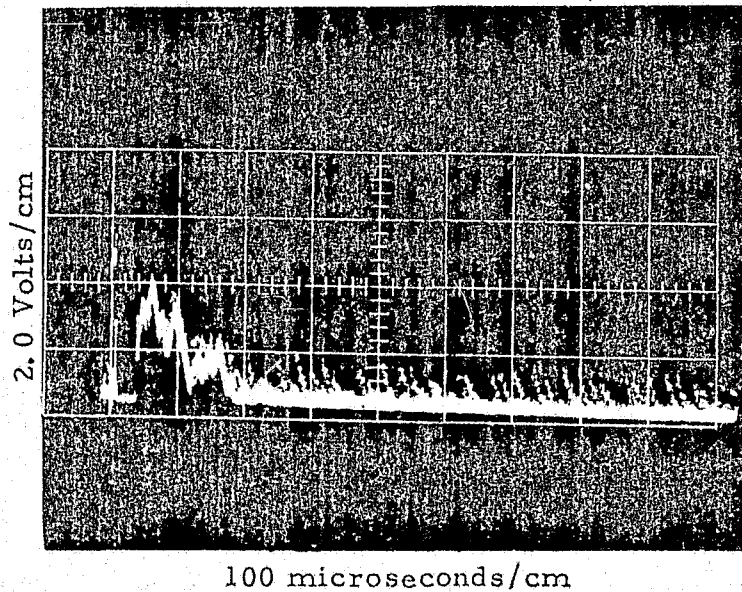
j. As in (i) above but with Two of the Slender Cylinders of Glycerol Added

FIGURE 28.(Cont'd)

46

where $\hbar$ is Planck's constant, g is the spectroscopic splitting factor (approximately 2.0 for most materials), B is the Bohr magneton, and H_O is the magnitude of the applied static magnetic field. In charcoal, g has a value of 2.003 which results in a value $\nu_O = 2.80 \times 10^6\ H_O$. Since H_O is in units of Gauss, $\nu_O = 2.80$ MHz/Gauss. Thus for a given magnetic field intensity ESR occurs at a much higher frequency (a ratio of 657:1) than does NMR. ESR studies are normally conducted at frequencies in the microwave range.

In the exchange of energy between the resonant electrons and the applied fields, there is a net loss of energy to the electrons. It is this absorption effect which allows the production of signals in most ESR spectrometers. Signal magnitude depends on the size of the sample, its concentration of free electrons, the type of apparatus used, and other factors. Since some of these factors may not be well known and since the primary interest in this case is the detection of a material rather than measuring its mass or volume, no attempt has been made to quantify the signals that may be produced. It should be stated, however, that if other factors remain equal, signals of greater amplitude are obtained when higher operating frequencies are used and is the primary reason for microwaves being commonly used for ESR studies.

2. Apparatus for Small Sample Tests

Commercially available ESR spectrometers typically operate on frequencies near 10 GHz and employ magnetic fields of approximately 3.6×10^3 Gauss. These instruments usually have a resonant microwave cavity which has a small chamber to accept a thin sample of the material to be studied. This approach results in much greater sensitivity than can be obtained with a non-resonant sample volume but the amount of material that can be accommodated is severely limited. An instrument of this type (Varian Type EM-500 ESR Spectrometer) was used during the program, however, to study the ESR response of the several different explosives and propellants of interest. This instrument sweeps the magnetic field and provides a chart recorder output which displays the detected signal as a function of the field intensity.

3. Apparatus for Full-Scale Tests

For possible use in baggage inspection it was necessary to investigate other spectrometer configurations which could allow much larger test volumes than is available in standard ESR spectrometers. After initial consideration, the spectrometer illustrated in Figure 29 was assembled. Sufficient room was allowed in the sample space to accommodate the baggage sizes of interest. With this
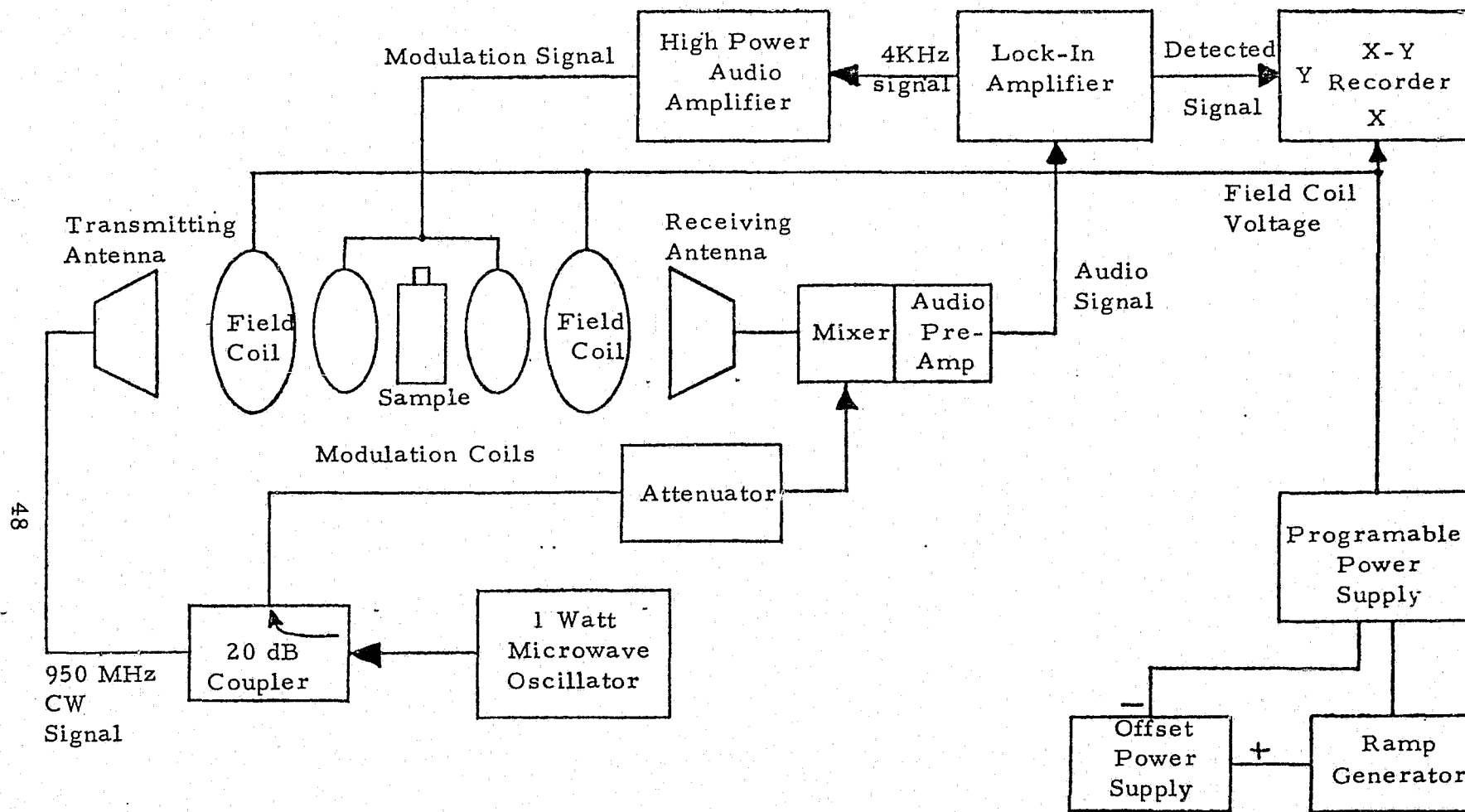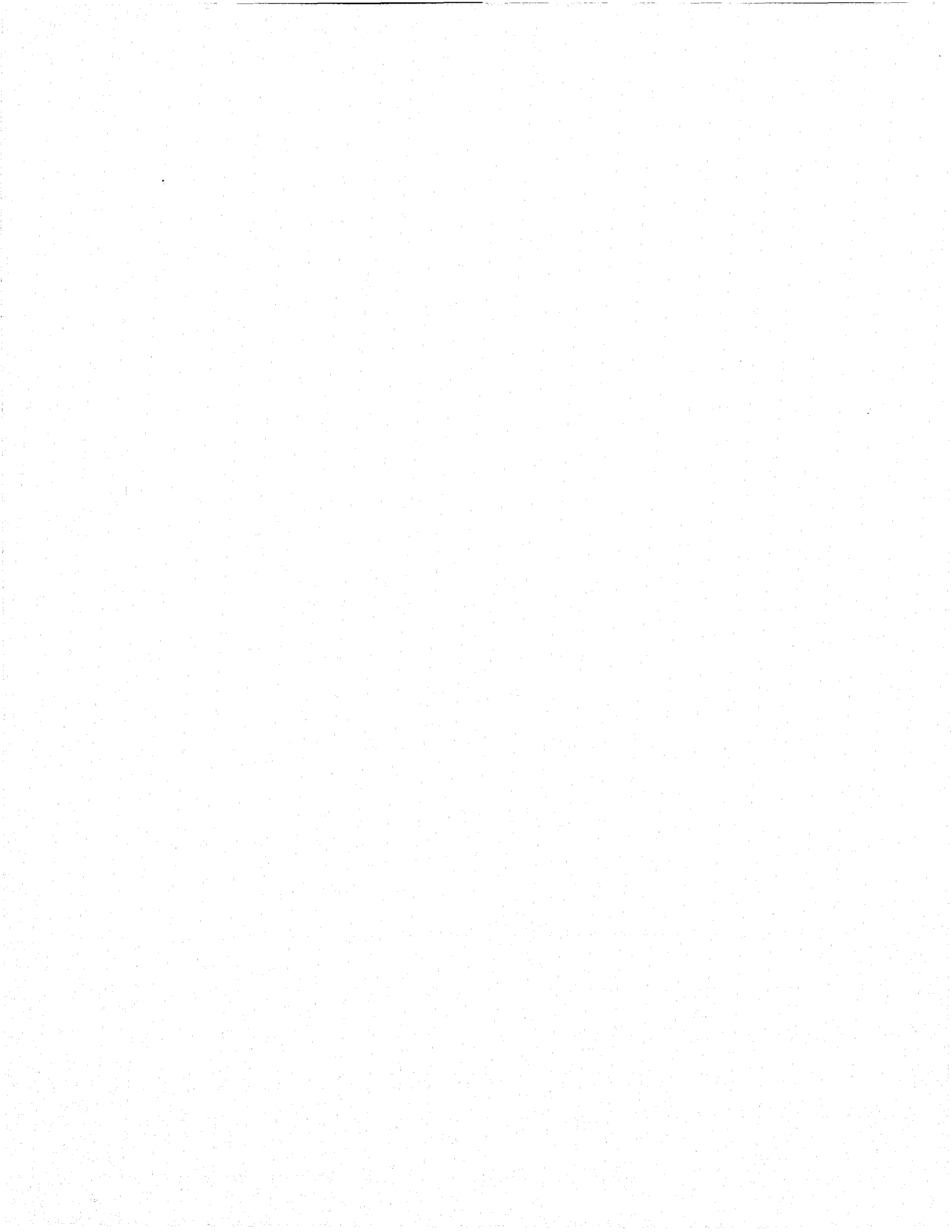
FIGURE 29.   HOMODYNE ESR SPECTROMETER USED IN FULL SCALE TESTS.

arrangement ESR responses from black powder and charcoal were successfully detected. The design and development of a baggage inspection unit using the same techniques appears to be quite feasible.

In use, the equipment was adjusted for operation at a frequency of about 950 MHz and H_0, the static magnetic field, was swept over the range of 280 to 360 Gauss. ESR signals were detected as the field passed through the expected resonance region of 335 to 340 Gauss. This is in close agreement with the field magnitude that would be predicted using the equation for ESR resonance.

The magnetic field was produced with a large Helmholtz coil pair which was constructed to allow the insertion of large sample containers. As indicated in Figure 29, the sample containers were placed in the center of the Helmholtz coil pair and two cross-polarized horn antennas were directed toward the center, on-axis with the coils. This arrangement was possible because of the holes at the center of the coils. The separation between the horn antennas was such that a clearance of 16" was available through which luggage could pass. The magnet construction, however, placed a lower limit on the available clearance space, but this is not significant to the results obtained.

The electronics portion of the equipment shown in Figure 29 includes a homodyne transmitter-receiver combination and a phase-sensitive detector unit. The transmitter output is approximately 1 watt on 950 MHz. Modulation for the magnetic field is provided by the 4 kHz oscillator output of the detector unit which is amplified and applied to a second set of coils, aligned concentric with the main Helmholtz pair. The main field, H_0, is also varied slowly using a programmable power supply driven by a ramp generator. An offset voltage is provided by a small power supply connected in series with the ramp generator. Signal data was obtained with an X-Y recorder which has its Y input connected to the output of the detector unit and its X input connected to a source of voltage that is proportional to the magnetic field magnitude.

Operation of the spectrometer depends on the generation of sidebands which occurs when ESR is obtained. These sidebands are generated by the resonance phenomena and are the result of interaction between the modulating field and the transmitted microwave signal in the sample. Detection of the sidebands is accomplished in the receiver portion of the homodyne arrangement. Since the receiver and transmitter antennas are directed toward each other, it is desirable to cross-polarize these units to reduce the level of direct signal applied to the receiver, and thereby aid in preventing detector saturation. This

49

does not, however, reduce the level of the desired sideband signals available at the receiver because the resonance phenomena produces a circularly polarized wave. Since the output of the receiver mixer consists of sum and difference frequency components, the sidebands are converted back to the modulating frequency when they are received. The output of the mixer is amplified and applied to the input of the phase sensitive detector unit where its phase is compared to that of the original modulating signal. Comparison of phase in this manner allows detection of much weaker signals than can be properly processed using simple amplitude comparison methods.

4. Results of Small Sample Tests

a. Dynamite (Hercules "Unigel Tamptite")

No detectable ESR response was obtained with this material.

b. Black Powder

An exceptionally strong ESR response was obtained with a very small sample (less than 1 milligram) of this material. A chart recording of the response is shown in Figure 30a.

c. Smokeless Powder (DuPont IMR-3031

A significant response was obtained with a sample containing 10 grains (pieces, not weight) of this material. Comparing the amplitude of the response to that of the black powder sample indicates that for the same amount of material the response from this smokeless powder is approximately 250 times less than that from the black powder. The smokeless powder response is shown in Figure 30b.

d. C-4 (RDX)

No detectable ESR response was obtained with this material.

e. C-4 (PETN)

No detectable ESR response.
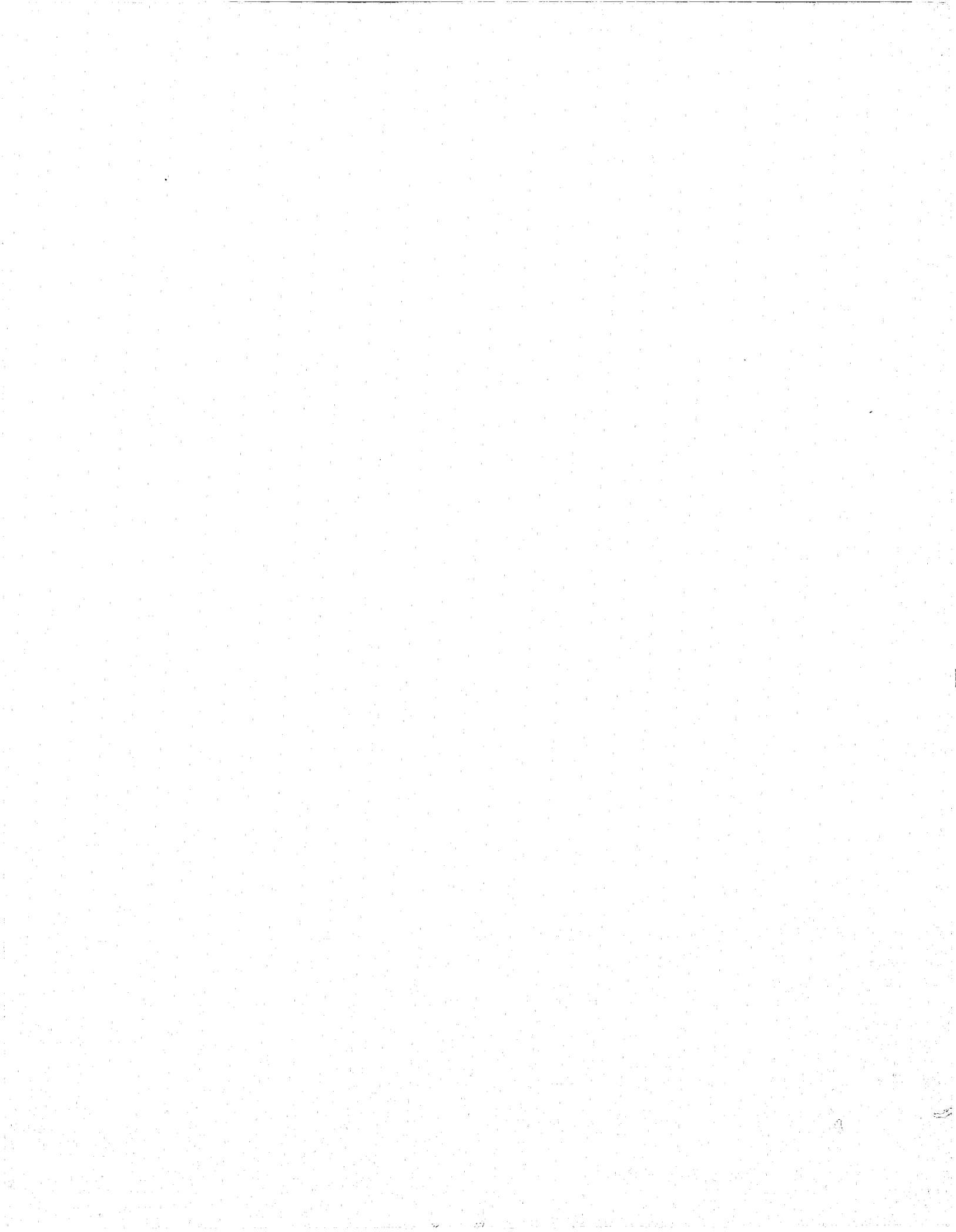
a. Black Powder (Dupont FF$_g$ Superfine Black Rifle Powder)

Quantity:	1 Flake
Gain:	X10
Frequency:	$\approx$ 10 GHz
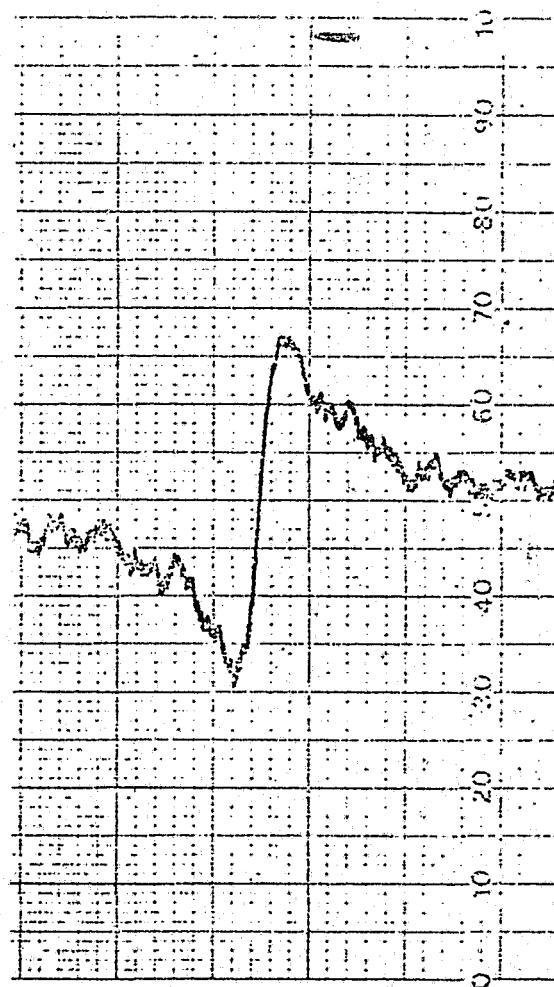
b. Smokeless Powder (Dupont IMR-3031)

Quantity:	10 grains
Gain:	X100
Frequency:	$\approx$ 10 GHz

FIGURE 30. ESR RESPONSE OF BLACK AND SMOKELESS POWDER

5.   Results of Full-Scale Tests

        The 950 MHz homodyne ESR spectrometer (described
previously in Section B. 3) was used to make tests on several materials.
Of the materials tested, black powder and charcoal produced strong
responses.   Charcoal was used as a reference material because it was
known to produce a large ESR response and was readily available in
large quantities. The black powder sample consisted of approximately
1-1/2 pounds of DuPont FFg Superfine Black Rifle Powder contained in
a plastic bottle and the charcoal sample consisted of a quart plastic
container filled with briquets.   The responses to these two samples are
shown in Figure 31 along with a reference scan that was made with no
sample present.   The same gain settings were used for each trace.

    C.   NQR Studies

        Parts of the descriptions and results of the studies involving
nuclear quadrupolar resonance are classified "Confidential" and their
release must be controlled on a need-to-know basis.   Because of this,
this section is separated from the rest of the report and bound separately
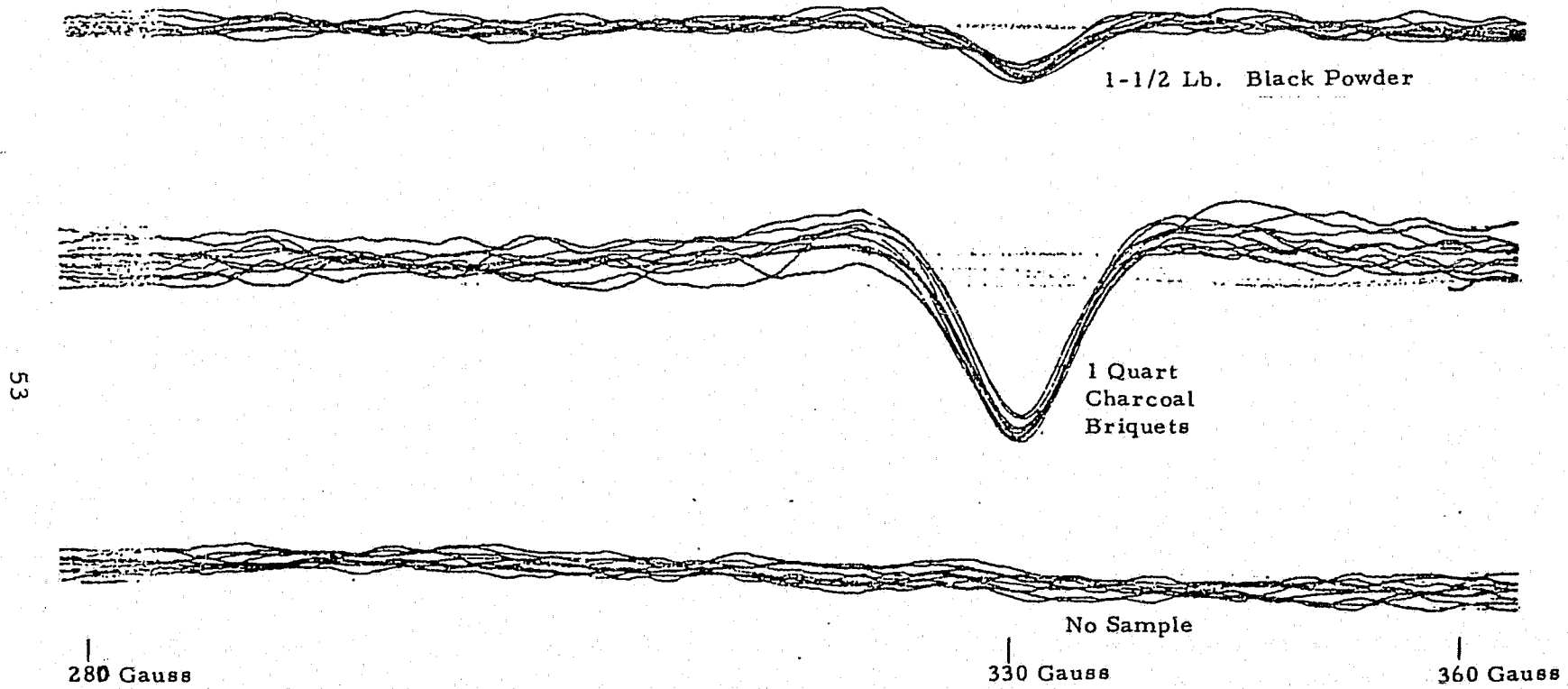as Volume 2.

1-1/2 Lb. Black Powder

1 Quart
Charcoal
Briquets

No Sample

280 Gauss   330 Gauss   360 Gauss

53
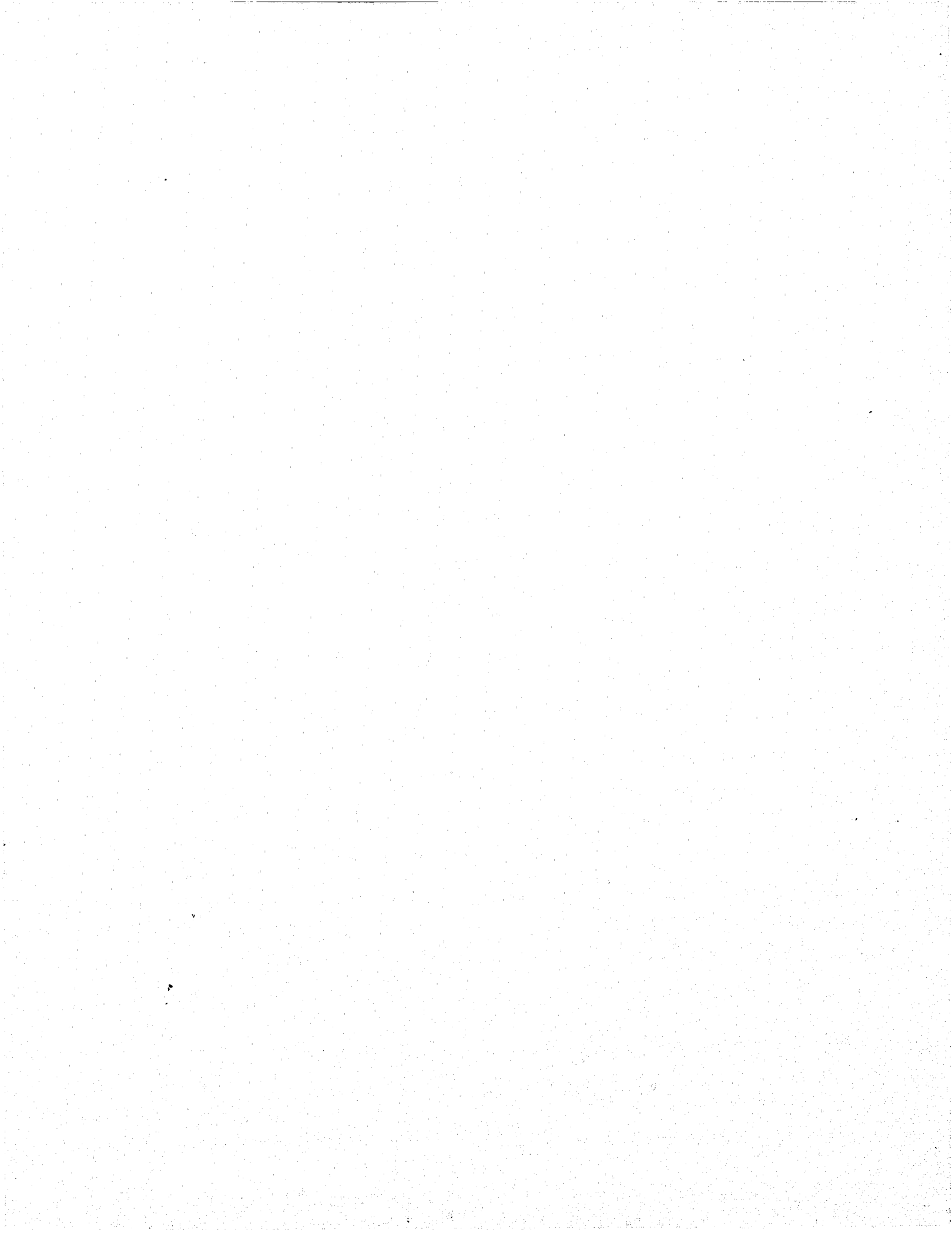
FIGURE 31.   ESR RESPONSES OBTAINED IN FULL SCALE TESTS

III.   ANALYSIS OF RESULTS

In each of the three parts of the second chapter, the results obtained from the apparatus and in sample evaluation were discussed. In the following paragraphs these results are analyzed and discussed in relation to the overall problem of using RRAS methods for detecting explosives in airline baggage. This analysis and discussion considers the apparatus requirements as well as the signal detection aspects of the problem.

A.   Apparatus for Full-Scale Tests

Several experimental items were constructed during the program to aid in evaluating the potential of RRAS methods for detecting explosives hidden in airline luggage. These items included: the large-volume magnet, three RF detection coils, and a high-power RF generator. The characteristics of these experimental units are summarized as follows:

1.   Large-Volume Magnet

A picture of the large-volume magnet is given in Figure 5. The characteristics of this magnet are as follows:

Overall Dimensions	22-1/2" high x 34" deep x 49.5" wide
Weight	2600 pounds
Coil Resistance at 22°C at 46°C	7.7 ohms 8.75 ohms
Field Intensity in Gap	587 Gauss at 13.3 Amperes 800 Gauss at 18.1 Amperes
Gap Dimensions for 17% homogeneity	17" high x 24" deep x 26" wide
Heat Rise to Equilibrium	24°C after 2 hrs of operation
Power Consumption - at 22°C at 46°C	1362 watts for 587 Gauss 1530 watts for 587 Gauss

The above characteristics meet or exceed the design goals and describe a magnet which makes practical the consideration of the use of hydrogen transient NMR techniques for the detection of explosives in baggage.
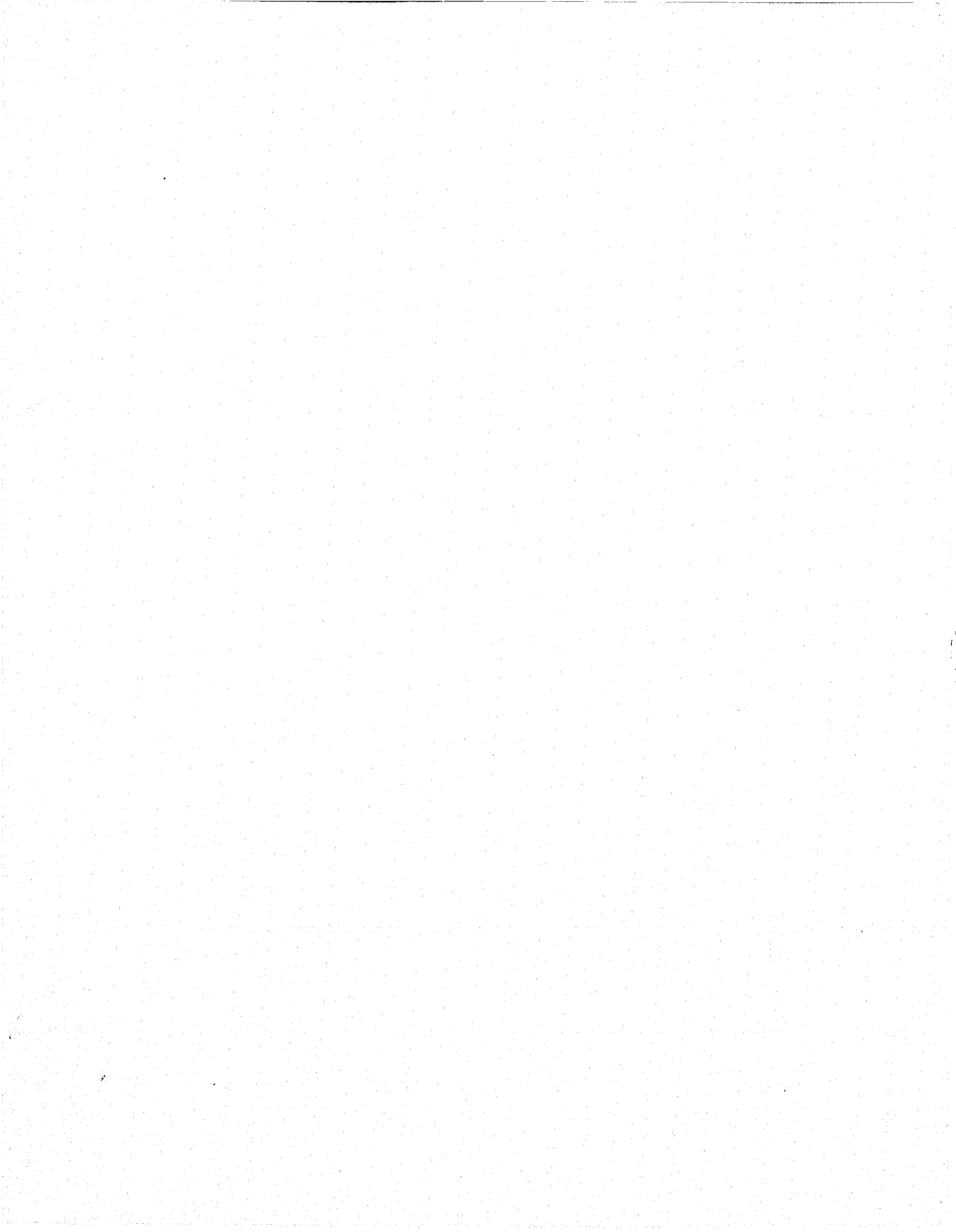
2. Radiofrequency Detection Coils

Three radiofrequency transient NMR detection coils were constructed and tested in the large-volume magnet. All used similar shielded construction but varied in size. The largest of the RF coils was full-sized to accommodate a bag with cross-sectional dimensions of 14" x 24". The medium-sized RF coil had cross-sectional dimensions of 6" x 14". The small-sized RF coil had cross-sectional dimensions of 3" x 5-1/2". In each of the above dimensions, the first is height and the second is width. Transient NMR signals were obtained with all three of these mounted one at a time in the large-volume magnet. The large-volume coil can be seen in Figure 6. The photograph in Figure 7 is of the large-volume RF coil mounted in the large-volume magnet. The characteristics of the large- and medium-volume radiofrequency coils are given in the next sections. The small coil was only used as a model for preliminary tests.

a. Large-Volume RF Coil Characteristics

The largest radiofrequency coil has the following physical and detection characteristics:

Detection Volume	14" x 24" x 9"
Number of Coils	Two in parallel
Number of Turns/Coil	4 turns in 4.5 inches
Inductance	4.5 microhenries
Shield Dimensions	17" x 26" x 24"
NMR Detection Sensitivity	A signal/noise of 5/1 from 13.7×10^{20} hydrogen nuclei/ cm^3 in glycerol
Peak RF Power per Pulse	1,186,000 watts for a 5 microsecond 90° pulse

CONTINUED

1 OF 2

b.   Medium-Volume RF Coil Characteristics

The medium-sized radiofrequency coil has the following physical and detection characteristics:

- Detection Volume

    6" x 14" x 3"

- Number of Coils

    1

- Turns/Coil

    7

- Inductance

    12.2 microhenries

- Shield Dimensions

    8" x 16" x 18"

- NMR Detection Sensitivity

    A signal/noise of unity from 1.6×10^{20} hydrogen nuclei per cm^3 in glycerol

- Peak RF Power per Pulse

    98,800 watts for a 5 microsecond 90° pulse

The theoretical sensitivity has been estimated at 0.51×10^{20} hydrogen nuclei per cm^3 for a signal/noise ratio of unity. It is therefore estimated that the noise figure of the transient NMR detection system used is three times that of an equivalent resistor. For the transient NMR signal, the 90° pulse had a width of 5 microseconds which meant that a peak radiofrequency field of 29.35 Gauss was generated at the sample. To give this RF field, a peak power of 98,800 watts is needed. To give the same conditions (a 5 microsecond 90° pulse) a peak RF power of 1,186,000 watts would be needed in the full-sized or large-volume coil. This nearly 1.2 megawatts peak pulse power could not be generated by medium-sized laboratory radiofrequency power amplifier and therefore a wider pulse of around 100 microseconds was used for the determination of the detection sensitivity in the full-sized coil listed above.

Although transient NMR signals were obtained with the smaller-sized RF coil in the large-volume magnet, these measurements are not summarized here because they add no more to the conclusions.

The results listed above do show that it is practical to consider the use of the large-volume magnet and the large-volume radiofrequency coil for the detection of explosives in a volume

56

having dimensions as large as 14" x 24" x 9" with a radiofrequency peak pulse power of 1.186 megawatts for a 5 microsecond 90° pulse. It should be noted that the average radiofrequency power would only be about 10 watts even in this case.

3. Radiofrequency Pulsed Power Generators

To give the results listed previously, three radio-frequency power generators were used. They will be described as low-powered, medium-powered and high-powered. The peak pulse power available from each of the three generators are listed in Table IV. When the results in Table IV are compared with the power needed for a 5 microsecond 90° pulse by the medium- and large-sized coils, then it

TABLE IV

COMPARISON OF RADIOFREQUENCY POWER GENERATORS

Unit	Peak Voltage Across 50 Ohms	Peak Pulse Power
Small	1000 volts	10,000 watts
Medium	4000 volts	160,000 watts
Large	12,000 volts	1,440,000 watts

is evident that only 2/3 of the output power from the power amplifiers is being applied to the radiofrequency detection coils by the matching network in each case. Therefore, unless additional efficiencies are obtained in the matching network, a transmitter output peak power level of nearly 1,800,000 watts will be required to obtain a 5 microsecond wide 90° pulse in the large-sized RF detection coil. This appears feasible using conventional vacuum tube techniques; however, other approaches to more simply obtaining such high peaks are desirable. The capacitor discharge approach such as used for the large power generator could, with refinement, provide these advantages.

B. Hydrogen NMR Test Results

1. Small Sample Tests

In small volumes, the hydrogen transient NMR signals from all of the explosives except black powder gave sufficient signals for detection in baggage by the transient hydrogen NMR method. The signals obtained indicated further that, with one possible exception, the explosive would give a transient NMR signal which could be distinctive enough to permit acceptance of the explosive signal while rejecting the non-explosive hydrogen transient NMR signals from non-explosive materials.

The exception may be smokeless powder though the results are not con-
clusive and further study is needed to determine a means for discrimi-
nation that would be useable with this material.

2.   Large Sample Tests

Most of the large sample measurements, which were
made with the two coils in the full-sized magnet, used glycerol or phenolic
rods as samples. These measurements also provided an insight into the
apparatus requirements that would be needed to give the required signals
from an explosive sample having 0.5×10^{20} hydrogen nuclei per cm^3.
It was also determined, from using the medium-sized RF coil, that
hydrogen transient NMR signals can be obtained from eight phenolic rods
each 1" OD by 8" long. While it is difficult to determine the concentra-
tion of hydrogen nuclei in these phenolic rods, it has been determined
previously that the signals from these rods closely represent the signal
levels obtained from explosives.

The potential interfering hydrogen transient NMR
signals from luggage and several types of luggage contents were also
made using attache cases in the medium-sized coil. In each case, the
signal could be readily observed from two slender cylinders of glycerol
placed in the luggage. In each case also, the hydrogen transient NMR
signals from the slender cylinders of glycerol were larger than those
from the briefcase and contents.

C.   ESR Test Results

1.   Small Sample Tests

The test results are listed in Table V according to
the types of sample used.

TABLE V

RESULTS FROM ESR TESTS WITH SMALL SAMPLES

Sample	ESR Response
Dynamite, Nitroglycerine Gel Type	None
Black Powder	Very Strong
Smokeless Powder (IMR-3031)	Weak
RDX Type C-4	None
Plasticized PETN or Detasheet	None

2.   Large Scale Tests

        Two types of samples were used for the large-scale
tests: black powder (DuPont FFg Superfine) and charcoal briquets of
the type sold for home barbecuing.   The black powder sample weighed
1. 5 pounds.   The charcoal sample consisted of briquets packed as dense
as possible in a quart plastic container.   The ESR responses from these
two samples were as follows:

                .   1.5 lb. Black Powder   2/1 Signal/Noise Ratio

                .   1 quart of Charcoal   5/1 Signal/Noise Ratio

From these results it can be concluded that the technique of electron
spin resonance can be used to detect the presence of black powder (if the
sample is in a nonmetallic container) in airline luggage of the specified
size.

D.   Results from NQR Tests

        The results from the NQR tests are included in Volume 2
of this report.   These results indicate that with the exception of C-4
(RDX) the NQR technique is not useable for detecting the explosives of
interest and that even this material can be more sensitively detected
with NMR.

IV.   CONCLUSIONS

The work described in this report has successfully demonstrated the following:

1.   The utility of NMR in the detection of the explosives dynamite, smokeless powders, RDX and PETN.

2.   The utility of ESR for detection of black powder and smokeless powder.

3.   That the use of NQR is essentially limited to the detection of RDX.

4.   The feasibility of constructing a magnet providing a sufficient field intensity and homogeneity over an adequate volume for use of NMR and/or ESR in checked baggage inspection.

5.   The feasibility of detecting an NMR response from a reasonable quantity (under 4 pounds) of material with an RF coil 9" long through which baggage up to 14" x 24" in cross sectional area can be passed.

6.   The feasibility of detecting useful NMR response even in the presence of materials and items commonly found in checked baggage.

APPENDIX A

NMR FUNDAMENTALS
by
William L. Rollwitz
Institute Scientist, Southwest Research Institute

I.   INTRODUCTION

Nuclear Magnetic Resonance (NMR) depends on the fact that most nuclei have angular momentum in addition to a magnetic moment. As a result, in the presence of a steady magnetic field, H_o, these nuclei will undergo a precessional motion about H_o at a angular frequency $\omega_o = \gamma H_o$ where γ is a nuclear constant depending on the magnetic moment and angular momentum. Since each nucleus has a different γ factor, one can, theoretically, determine different nuclei by observing the precessional frequency in a given magnetic field. The interactions of nuclei when placed in matter lead to small changes in ω_o, and/or changes in the character of the precessional motion. Thus, NMR measurements are able to identify nuclei as well as give information about the environment of the nucleus, i.e., about the physical state of matter.

Consider an ensemble of nuclei, each surrounded by other nuclei in some atomic configuration. In the absence of an external steady magnetic field, the axes of the magnetic moments of the nuclei are distributed uniformly over all directions, so that the resultant magnetization, M, of the complete ensemble is zero. The application of a uniform, fixed magnetic field H_o (in, say, the Z direction) leads to a non-equilibrium condition described by the vector equation

$$\frac{d\vec{M}}{dt} = \gamma(\vec{M} \times \vec{H}) \tag{A1}$$

This state is equivalent to an equal occupation of all nuclear magnetic energy levels and consequently the nuclei are not in equilibrium with their surroundings. The equilibrium condition is established by the thermal modulation of the interactions between the nuclei and its surroundings. In this manner, a magnetization, M_z, is built up to an equilibrium value, M_o. The growth with time can be described by means of the "relaxation time" T_1 in the following form

$$M_z = M_o[1 - \exp(-t/T_1)] \tag{A2}$$

where M_o is the equilibrium magnetization at an infinitely long time. The value of M_o is given by the Langevin equation

$$M_o = N_o\left(\frac{\mu H_o}{kT}\right)\left(\frac{I + 1}{3I}\right) = \chi_o H_o \tag{A3}$$

where

N_o = the number of nuclear magnets per unit volume

μ = magnetic moment of the nuclei

H_o = the external fixed magnetic field intensity

k = Boltzmann's constant

T = absolute temperature

I = spin quantum number

X_o = static nuclear magnetic susceptibility.

The quantum number I has integer or half-integer values where $Ih/2\pi$ is the angular momentum and the magnetic moment.

Adding the relaxation term to equation (A1) yields

$$\frac{dM_z}{dt} = - (M_z - M_0)/T_1 + \gamma(M \times H)_z \tag{A4}$$

This is the equation of motion for M_z in the presence of relaxation effects and a applied field H. In general, H can be composed of a steady field and a time varying field.

The energy exchange between the nuclear spin system and its surroundings becomes even clearer if the concept of a temperature of the spin system T_s is introduced by

$$M_z = N_o\mu \left(\frac{\mu H_o}{kT_s} \right) \left(\frac{I+1}{3I} \right) \tag{A5}$$

Since, when the magnetic field H_o is first turned on, the "longitudinal magnetization" M_z is zero, the spin temperature T_s is infinitely large. As the nuclear spin and the lattice exchange energy, the spin temperature falls to that of the specimen, T, and M_z becomes equal to M_o. While the temperature equilibrium is being established, energy is transferred from the nuclear spin system to the surroundings.

If the specimen is subjected to a steady magnetic field in the z direction and a radiofrequency field H_1 (H_1 much less than H_o) oscillating perpendicular to H_o, then the macroscopic magnetization M, composed of all the magnetic fields, performs a spiral motion, and a rotating "transverse magnetization," having components, M_x and M_y, is produced. The effect is greatest (resonance) when the frequency of H_1 is the Larmor precession frequency. Since this

"transverse magnetization" is rotating, it can induce a voltage in a radio-frequency coil surrounding the specimen. Thus with this resonance condition, the nuclear magnetization can be detected.

The transverse magnetization also has relaxation mechanisms. All of these mechanisms are characterized by one relaxation time, T_2. Analogous to Equation (A4), T_2 is quantitatively introduced as follows

$$\frac{dM_x}{dt} = -\frac{M_x}{T_2} + \gamma(M \times H)x; \qquad \frac{dM_y}{dt} = -\frac{M_y}{T_2} + \gamma(M \times H)y \qquad (A6)$$

Equations (A4) and (A6) are known as the Bloch Equations.

For liquids, T_1 and T_2 are very nearly equal and are often of the order of seconds. In crystals or solids, on the other hand, T_2 may be very small (10^{-4} to 10^{-5} seconds) while T_1 can be of the order of seconds or even minutes.

II.   STEADY-STATE NMR THEORY

After the application of the oscillating magnetic field, H_1 in addition to the steady field H_0, the component of the nuclear magnetization along the x axis approaches a steady value. If the equations for the motion (Equation A6) are solved, under these conditions the equation for this magnetization is

$$M_x = 2\chi' H_1 \cos \omega t + 2\chi'' H_1 \sin \omega t \qquad (A7)$$

where

χ'' = absorption part of the nuclear susceptibility

χ' = dispersion part of the nuclear susceptibility

and

ω = frequency of applied rotating magnetic field.

The nuclear susceptibilities are found to be

$$\chi' = \frac{M_0}{2} \gamma T_2 \frac{(\omega_0 - \omega)T_2}{1 + (\omega_0 - \omega)^2 T_2^2 + \gamma^2 H_1^2 T_1 T_2} \qquad (A8)$$

and:

$$\chi'' = \frac{M_o}{2}\gamma T_2 \frac{1}{1 + (\omega_o - \omega)^2 T_2^2 + \gamma^2 H_1^2 T_1 T_2} \qquad (A9)$$

where

M_o = static nuclear magnetization

T_2 = transverse relaxation time

T_1 = longitudinal relaxation time

ω = frequency of the applied rotating field

γ = gyromagnetic ratio for the resonating nuclei

and

H_1 = strength of the rotating magnetic field.

The resonance condition is where $\omega = \omega_o$. Therefore, at resonance, χ' is zero and χ'' is

$$(\chi'')_{\omega = \omega_o} = \frac{M_o}{2}\gamma T_2 \frac{1}{1 + \gamma^2 H_2^2 T_1 T_2} \qquad (A10)$$

If the term $\gamma^2 H_1^2 T_1 T_2$, called the saturation term D, is $\ll 1$, i.e., $5 \simeq$ the absorption nuclear susceptibility is

$$(\chi'')_{\substack{\omega = \omega_o \\ D = 0}} = \frac{M_o}{2}\gamma T_2 \qquad (A11)$$

Thus, by measuring χ'' and determining the peak value at $\omega = \omega_o$, the value of M_o can be determined if γ and T_2 are known. By this means, from Equation (A3), the number of nuclei per unit volume can be measured. The value of χ'' would be linearly related to N_o only if T_2 was constant for all values of N_o. If the value of T_2 is also measured or known, N_o could still be determined.

When $D \ll 1$ the absorption susceptibility off resonance is

$$(\chi'')_{D = 0} = \frac{M_o}{2}\gamma T_2 \frac{1}{1 + (\omega_o - \omega)^2 T_2^2} \qquad (A12)$$

The absorption part of the nuclear magnetic resonance signal, S'' combining Equations (A7) and (A9), is:

A-4

$$S'' = K\omega M_o H_1 \gamma T_2 \frac{1}{1 + (\omega_o - \omega)^2 T_2^2} \qquad (A13)$$

where K is a constant combining all of the terms in the detection scheme. If the absorption signal is plotted as a function of $(\omega_o - \omega)$, the curve of Figure A1 is obtained. The maximum value occurs at resonance where $\omega = \omega_o$ and is

$$S_o'' = K\omega_o M_o H_1 \gamma T_2 \qquad (A14)$$

The width $\delta\nu$ of the absorption curve at one-half amplitude is

$$\delta\nu = 2/T_2 \qquad (A15)$$

Therefore, the width can be a measure of T_2 under these conditions.

Usually, however, reducing H_1 to a value sufficiently low so as to make the saturation term much much less than one also reduces the maximum value of the absorption curve as shown in Equation (A14). If Equation (A14) is differentiated with respect to H_1, it is found to have a maximum value where $D = 1$. Under these conditions the maximum signal is

$$(S'')_{D=1} = K\omega_o M_o \left(\frac{T_2}{T_1}\right)^{1/2} = K \frac{\chi_o}{\gamma} H_o^2 \left(\frac{T_2}{T_1}\right)^{1/2} \qquad (A16)$$
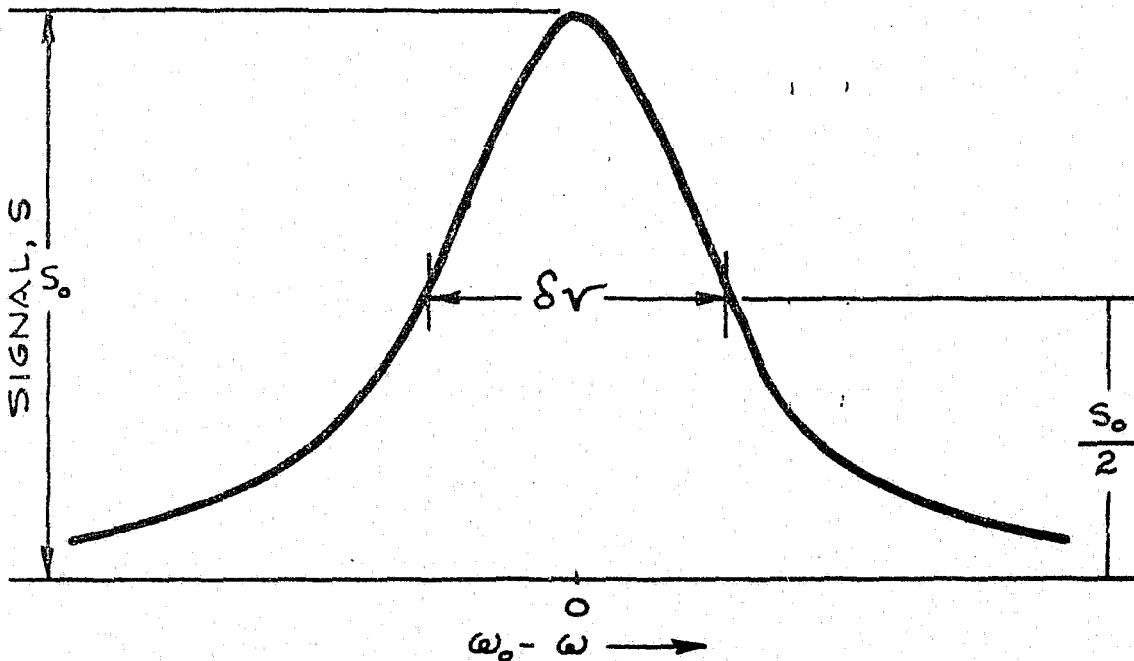

FIGURE A1. THE PLOT OF THE ABSORPTION TERM OF THE NUCLEAR MAGNETIC RESONANCE SIGNAL WHEN THE SATURATION TERM IS MUCH MUCH LESS THAN ONE

A-5

Although larger in amplitude, Equation (A16) shows that the amplitude is still proportional to T_2 in addition to now being proportional to T_1. If in the desired measurement both T_2 and T_1 are fixed, then quantitative measurements could be made, and it would be advantageous to operate at a r-f level, H, such that $D = 1$.

Also, note that the maximum signal is proportional to H_o^2 so that increased sensitivity can be obtained by increasing the operating field, H_o.

The effect of T_2 in the measurement can be eliminated by determining the area under the curve of Figure A1 or by integrating Equation (A9). The area, A'', is then proportional to:

$$A_o'' C \frac{M_o \gamma H_1}{(1 + D)^{1/2}} \tag{A17}$$

whereas the peak height is equal to

$$S_o'' = \frac{K \omega_o M_o \gamma H_1 T_2}{1 + D} \tag{A18}$$

If H_1 is such a value that $D << 1$, then the area is independent of T_1 and T_2, whereas the amplitude is dependent on T_2.

The dispersion signal of Equation (A8) has some interesting properties. It has a maximum value at

$$(\omega_o - \omega) = \pm \frac{(1 + D)^{1/2}}{T_2} \tag{A19}$$

The amplitude of the dispersion at that value of $(\omega_o - \omega)$ given by Equation (A19) is

$$S_o' = \frac{M_o \gamma \omega H_1 T_2}{2(1 + D)^{1/2}} \tag{A20}$$

A comparison of the amplitude of the absorption curve S_o'' with that of the dispersion curve S_o' shows that the absorption curve is twice the amplitude of the peak of the dispersion curve, and they are both a function of T_2 so that nothing is gained by using the amplitude of the dispersion curve. However, when the area is determined from zero to the maximum value, the area is independent of both T_1 and T_2, or:

$$A_{Peak}' = \gamma \omega M_o H_1 \tag{A21}$$

In addition, an inspection of Equation (8) shows that as H_1 increases, the value of χ' reaches a maximum value at H_1 infinite. Therefore, there are certain advantages to be gained by using the dispersion curve and integration up to the peak value only.

By these methods, then, it is possible to obtain a measure of M_0 from which can be determined the volume concentration N_0 of the nuclear species desired. In all of the amplitude measurements and in the absorption area measurement, the value determined is influenced by the values of T_1 and T_2 as well as H_1. The absorption area measurement can be made relatively independent of T_1 and T_2 if $D \ll 1$. Only in the partial integration of the dispersion curve is a value obtained which is independent of T_1 and T_2.

In any event, the actual value of N_0 is difficult to obtain unless all of the parameters are known. Since many parameters are difficult if not impossible to measure accurately, one usually constructs a standard calibration curve of signal strength or area as a function of known concentration in standard samples or a standard sample of the material to be measured.

III.   STEADY STATE TECHNIQUES

A.   Introduction

There are more than a dozen types of steady state nuclear magnetic resonance detectors which give a signal proportional to Equations (A8) and (A9) or combinations of them. All of these techniques can be considered in one of two categories: (1) nuclear magnetic resonance absorption, or (2) nuclear magnetic resonance induction. The basic concepts of these two categories will be considered. In the absorption techniques, the radiofrequency rotating magnetic field H_1 is supplied by the same coil from which the signal is taken. Therefore, they are sometimes labeled the "single-coil" systems. The induction techniques utilize two coils. One supplies the radiofrequency rotating field H_1, say along the x axis. The other is placed in quadrature with field of the first coil and the steady magnetic field, then along the y axis. The two-coil system is sometimes called the crossed-coil system.

B.   Nuclear Magnetic Resonance Absorption

The fields and directions for this technique are shown in Figure A2. If the material in the coil has a susceptibility, the inductance is changed from its value without the material, L_0, to the value

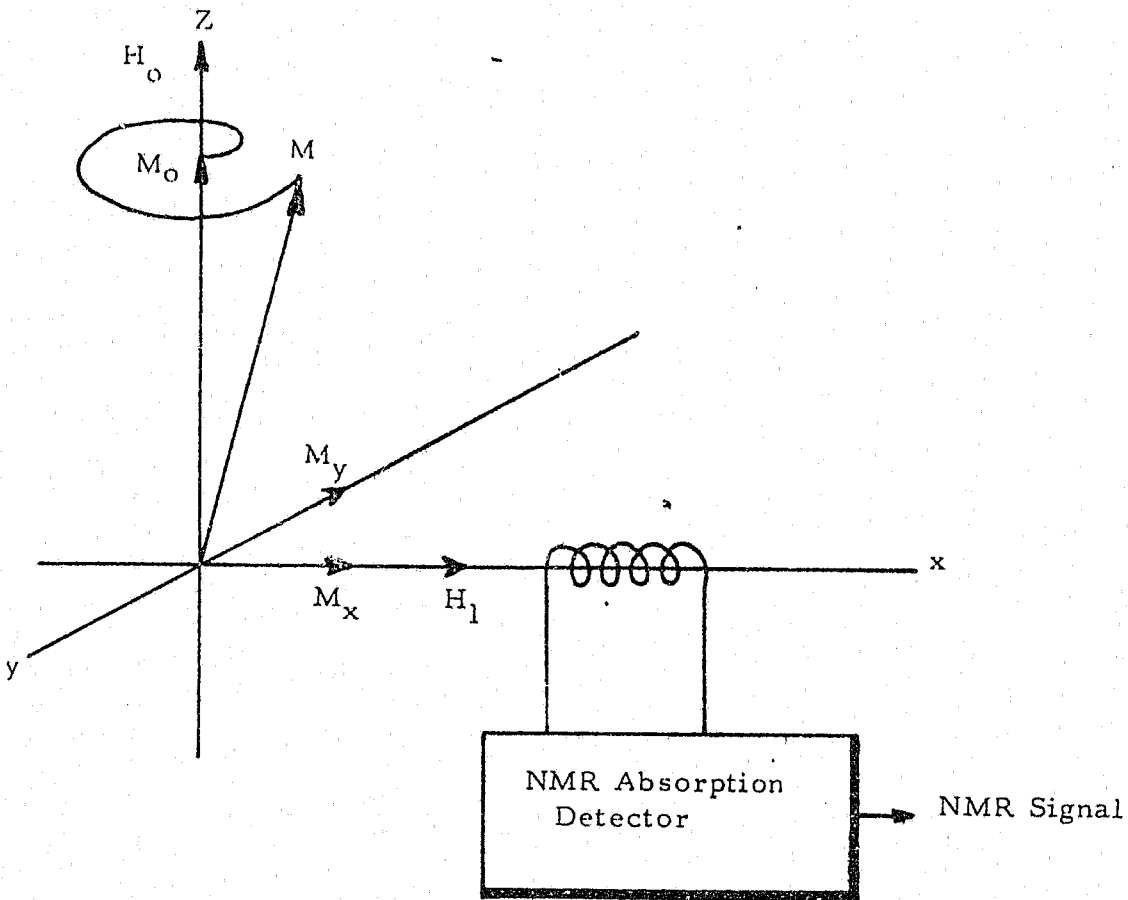$$L = L_0(1 + 4\pi\chi) \tag{A22}$$

FIGURE A2. THE DIRECTIONS OF THE COIL AND THE MAGNETIC
FIELDS FOR NUCLEAR MAGNETIC RESONANCE ABSORPTION

where χ represents the susceptibility. From Equation (A7), the coil will see two values of susceptibility in quadrature. Therefore, the total susceptibility is

$$\chi = \chi' - i\chi'' \tag{A23}$$

It will also be necessary to consider a filling factor F which represents how well the sample fills the magnetic field of the coil.

Therefore, the impedance of the coil can be written as

$$Z = iL_0\omega(1 + 4\pi F\chi') + R_0 + 4\pi\omega L_0 F\chi'' \tag{A24}$$

where R_0 is the AC resistance of the coil. The real part (dispersion) of the susceptibility changes the inductance, and the imaginary part (absorption) changes the losses in coil. The fractional change in resistance is

$$\frac{\Delta R}{R_0} = \frac{L_0\omega}{R_0} 4\pi F\chi'' = 4\pi F\chi''Q \tag{A25}$$

A-8

Using Equation (A25), the amount of absorbed energy can be obtained. If V is the volume of the coil, and i_0 is the peak current in the coil, then from energy considerations

$$\frac{1}{2} L_0 i_0^2 = \frac{1}{2\pi} H_1^2 V \qquad (A26)$$

The average power, P, absorbed by the nuclei is

$$P = \frac{1}{2} i_0^2 \Delta R \qquad (A27)$$

Therefore, by combining Equations (34), (35), and (36), the power absorbed by the nuclei is

$$P = 2\omega H_1^2 F\chi''V \qquad (A28)$$

If the coil is a part of a resonant circuit, whose impedance with no absorption is $Z_0 = L_0 C_0 R$ (where C_0 is the resonating capacitance), then the change in impedance caused by the power absorbed by the nuclei is

$$\Delta Z = Z_0 \frac{4\pi QP}{\omega_0 H_1^2} \qquad (A29)$$

The voltage across the tuned circuit will be

$$\Delta V = \frac{dV}{dZ} \Delta Z = \frac{dV}{dZ} \left(Z_0 \frac{4\pi QP}{\omega_0 H_1^2} \right) \qquad (A30)$$

and there will result a voltage change proportional to the impedance change which is in turn proportional to the susceptibility which is proportional to the number of nuclei and the relaxation times by Equation (A9). Thus, a single coil can be used both to obtain a signal proportional to the number of nuclei and their relaxation times and to supply the rotating magnetic field required by the resonance phenomenon.

As is shown by Equation (A24), the inductance is also changed by nuclear magnetic resonance absorption signal, or more specifically, by the dispersion term. Therefore, unless means are taken to exclude the effect of the dispersion component, the voltage across the tuned circuit will be a function of both the absorption and dispersion terms. The means most often used is to make the rate of change (dV/dZ) of the voltage with impedance being very small for the inductive part and very large for the resistive part. Systems used are the bridge systems and the marginal oscillator systems. In the bridge systems, the bridge is inductively balanced and resistively unbalanced to obtain the different rates of change. The bridge system can also be resistively balanced

A-9

and inductively unbalanced to display the dispersion signal. In the marginal oscillator systems, the tuned circuit, containing the inductance which is filled with the sample, is the frequency controlling element of a weakly oscillating oscillator. In this circuit, the oscillator voltage change with conductance change is very large, whereas, the voltage change with frequency is very small. By this means then, the marginal oscillator displays only the absorption curve if the output is peak detected. The dispersion curve can be obtained if the output is detected by a frequency discriminator.

C. Nuclear Magnetic Resonance Induction

If two coils are used as shown in Figure A3, one can perform an induction measurement. The voltage induced into L_2 as M precesses is

$$v = - k \frac{dM_y}{dt} \tag{A31}$$

where k is a constant which includes the coil geometry variables and the filling factor. The value of the magnetization in the $\dot{y}$ direction is

$$M_y = 2H_1(X'' \cos \omega t - X' \sin \omega t) \tag{A32}$$

The induced voltage in L_2 is

$$v = 2k\omega H (X'' \sin \omega t + X' \cos \omega t) \tag{A33}$$

Thus, the output of coil L_2 is a mixture of both X'' and X' as it was in the single-coil system. In the induction system the separation is accomplished in the amplifier-detector system.

The most straightforward method is the use of a radiofrequency phase detector in which a part of the voltage fed to L_1 is fed to the phase detector in the output of the radiofrequency amplifier for use as a reference. When the phase angle between the reference and the signal is zero degrees, the output is proportional to X''. Conversely, when the phase angle is 90 degree: the output is proportional to X'.

A straight detector will also give a separation if another voltage is directly added to the system. This voltage is obtained from the leakage between coils L_1 and L_2 by adjusting their geometry. When the leakage is $V_L \sin \omega t$, the output of the detector will be

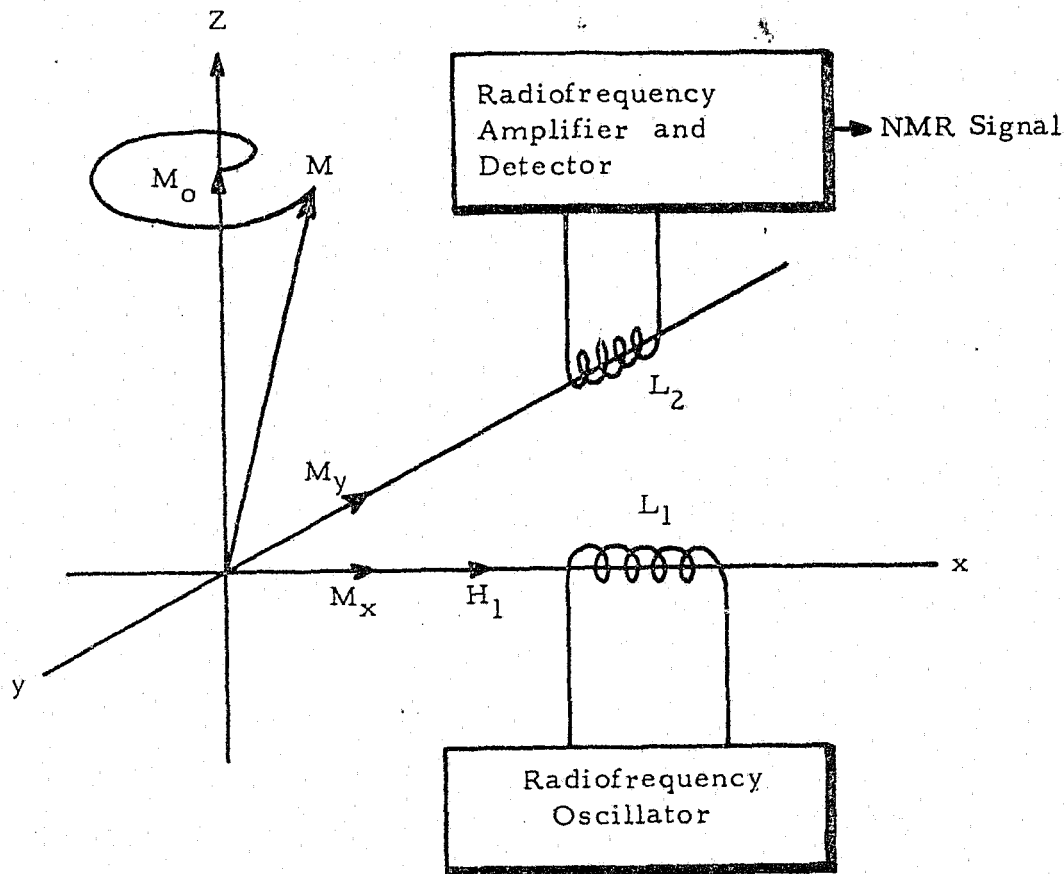$$v_o'' = [(V_L + 2k\omega H_1 X'')^2 + (2k\omega H_1 X')^2]^{1/2} \tag{A34}$$

A-10

FIGURE A3. THE DIRECTIONS OF THE COILS AND FIELDS
FOR NUCLEAR MAGNETIC RESONANCE INDUCTION

If v_L is much larger than either of the signal voltages, the output is

$$v_o'' \approx V_L + 2k\omega H_1 \chi''.$$ (A35)

If the leakage is adjusted to be $V_L \cos \omega t$, the output will be

$$v_o' \approx V_L + 2k\omega H_1 \chi''$$ (A36)

Each of the Equations (A35) and (A36) are approximate because the other term
is not completely excluded.

IV.   TRANSIENT NMR THEORY

The transient NMR theory considers the behavior of the spin system
(or magnetization) in two situations: (1) during a rf pulse and (2) after a rf
pulse. Once this behavior is known, it can be applied to multiple pulse sequences

to produce signals yielding the particular desired information as will be discussed below.

During the rf pulse, one assumes that the r-f pulse width t_w is much less than T_1 or T_2. This is equivalent to considering the spin system as being free, i.e., no relaxation effects as described by Equation (A1). Rewriting Equation (A1) in a coordinate frame rotating with the r-f field $\hat{H}_1$ at angular frequency, $\vec{\omega}$, one has,

$$\frac{d\vec{M}}{dt} = \frac{d}{dt} \vec{M} \bigg)_{Rot} + \vec{\omega} \times \vec{M} = \gamma(\vec{M} \times \vec{H}) \tag{A37}$$

where $\vec{H} = \vec{H}_o + \vec{H}_1$. Solving for the time derivative in the rotating frame,

$$\frac{d}{dt} \vec{M} \bigg)_{Rot} = \gamma \left[\vec{M} \times \left(\vec{H} - \frac{\vec{\omega}}{\gamma} \right) \right] \tag{A38}$$

In the rotating frame, the vector $\vec{H}$ is a constant vector. If the magnetic field and rf frequency are adjusted to the Larmor precession frequency then $\vec{H}_o = \frac{\omega}{\gamma}$ so that $\vec{H} = \vec{H}_1$, only. Thus Equation (A38) becomes

$$\frac{d}{dt} \vec{M} \bigg)_{Rot} = \gamma \vec{M} \times \vec{H} \tag{A39}$$

This equation shows that the magnetization $\vec{M}$ simply precesses about $\vec{H}_1$ at a angular rate γH_1 in the rotating frame as shown in Figure A4.

If the r-f pulse width, t_w, is adjusted so that

$$\gamma H_1 t_w = \frac{\pi}{2} \tag{A40}$$

$\vec{M}$ will rotate through an angle of 90°. This pulse is termed a 90° pulse. Similarly, a 180° pulse is formed by a pulse whose width satisfies $\gamma H_1 t_w = \pi$.

V.   TRANSIENT TECHNIQUES

A.   Introduction

The transient method of measurement affords a convenient means of measuring the equilibrium magnetization M_o as well as separately measuring the two relaxation times T_1 and T_2. While steady-state methods of measuring relaxation times are possible, the required homogeneity of the static magnetic field and saturation effects have made it difficult to make direct quantitative
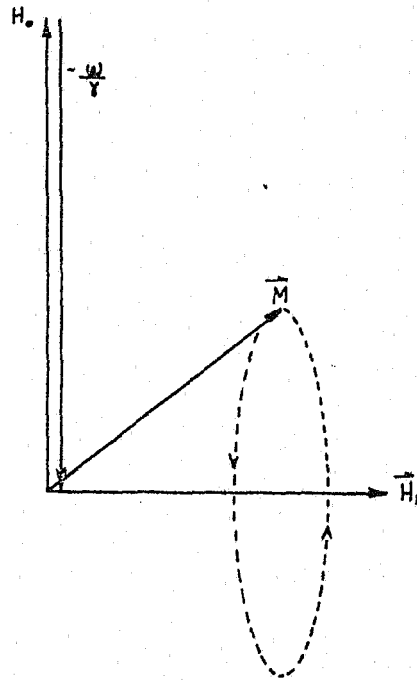
FIGURE A4.   GRAPHICAL PRESENTATION OF THE VECTORS
IN EQUATION (A38)

measurements of T_1 and T_2.   The lack of a direct measurement would
seriously limit the study of moisture in hygroscopic materials.   It is
characteristic of the transient method that it permits a direct measure of
T_1 and T_2 with no nuclear saturation problems.   The free precession technique
of measuring relaxation times may be utilized even in the presence of a
magnetic field with an inhomogeneity ΔH_o which is large compared to NMR
linewidths.   In fact, an inhomogeneous field is usually required for relaxation
time measurements.

When nuclei have been in a fixed magnetic field H_o for a time
much longer than the relaxation times, thermal equilibrium has been
established between the nuclei and their surroundings.   This equilibrium
results in a net nuclear magnetization M_o along the direction of the magnetic
field.   When a radiofrequency magnetic field, of magnitude H_1 and of frequency
$\omega = \gamma H_o$, is applied perpendicular to the fixed magnetic field, the nuclear
magnetization vector M_o begins to tip over perpendicular to the plane enclosing
M_o and H_1.   The rate of tipping, ω_t, is

$$\omega_t = \gamma H_1 \tag{A41}$$

Since ω_t is so many radians per second, the angle θ_t through which the nuclear
magnetization tips in a time, t, is:

A-13

$$\theta_t = \omega_t \, t = \gamma H_1 t \qquad \text{—} \qquad (A42)$$

When the nuclear magnetization is tipped away from its equilibrium condition by an angle, θ_t, it is then not in thermal equilibrium and it precesses around the direction of the magnetic field. It will then lose energy by the two relaxation methods at a rate proportional to: the cosine of the tipping angle times T_1 plus the sine of the tipping angle times T_2. Therefore, if the tipping angle is any odd multiple of $\pi/2$, only T_2 will be effective since the cosine will be zero and the sine unity. If the tipping angle is an even multiple of $\pi/2$, only T_1 will be effective. Thus, it is possible to selectively measure either T_1 or T_2 separately and distinctly by employing radiofrequency pulses of the proper duration to give the proper tipping angle as defined by Equation (A42).

Usually, either 90 degree ($\pi/2$) or 180 degree (π) pulses are used. These pulses are used either singly or in combinations to give an echo effect. When a single 90 degree pulse is applied, a signal is generated in the receiver coil as shown by the first pulse in Figure A5. This means that after a 90 degree pulse, the M_0 vector is in the x, y plane and two things happen to it. First, since it is composed of many individual vectors and they are now precessing freely, each will precess at its own rate. In time this rate difference will cause the component vectors of the vector to disperse to the condition that no voltage is induced into the receiver coil. This decay is called the free induction decay. Secondly, the magnitude of the individual magnetization vectors
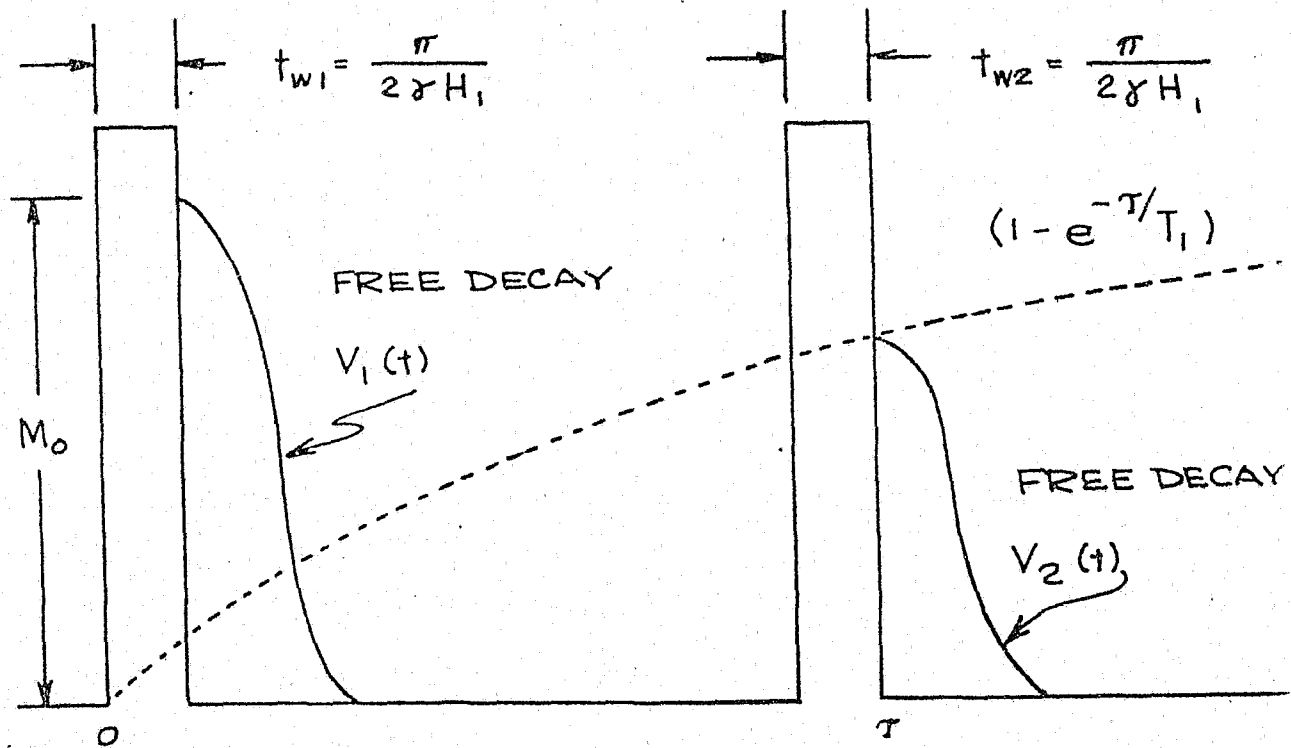

FIGURE A5. 90°-90° METHOD OF T_1 MEASUREMENT

A-14

comprising M_o will decrease as the nuclei lose energy by the T_2 relaxation mechanism. Thus, there is both a spreading and a weakening of the magnetization vector following a 90 degree pulse. Following a 180 degree pulse there should be no signal because the magnetization vector does not couple to the receiver coil. For all spin-echo measurements on paper, a single 90 degree pulse, or a combination of 90 degree and/or 180 degree pulses has been used. With these two pulses, the value of M_o can be measured, the value of T_2 can be measured, and the value of T_1 can be measured.

B.   Measurement of M_o

In order to measure the total equilibrium magnetization M_o, it is only necessary to apply a single r-f pulse and observe the maximum amplitude of the free induction decay signal. The voltage induced in the receiver coil due to the free induction decay signal following a single r-f pulse is

$$V(t) = M_o \sin (\gamma H_1 t_w) \exp - (t/T_2 + t^2/T_2^{*2}) \qquad (A43)$$

where

M_o = the z component of the magnetic moment at equilibrium

γ = the gyromagnetic ratio of the nucleus

H_1 = the magnitude of one component of the rotating magnetic radiofrequency field at the nucleus

t_w = the duration of the r-f pulse

and

$T_2^* = \sqrt{2}/\gamma \delta$ is the linewidth.

The zero of the time scale is the beginning of the r-f pulse. Diffusion effects are neglected.

The expression $(\gamma H_1 t_w)$ is the tipping angle of Equation (A42). The magnitude of the r-f pulse and its duration are chosen so as to make the angle equal to $\pi/2$. The amplitude is also chosen such that $\gamma H_1 >> 1/T_2^*$. When $\theta = \pi/2$, a 90 degree pulse is obtained as indicated in Equation (A42). The sine of an angle of $\pi/2$ radians is equal to one, and thus, Equation (A43) becomes

$$V(t) = M_o \exp - (t/T_2 + t^2/T_2^{*2}) \qquad (A44)$$

Equation (A44) shows how the free induction signal may be studied as a function of time and how M_o is measured. If the measurement is made at a time just greater than t_w (right after the 90 degree pulse) then $V(t)$ very nearly

equals M_o. The shorter the 90 degree pulse, the greater the accuracy. For all of the reported measurements, the pulse length was much less than the free precession decay time, and the measurements were accurate to within 2 percent.

If the value of T_2^* of Equation (A44) is made very large by decreasing the magnet inhomogeneity, then the free induction decay will be controlled by T_2, and the free induction decay can be used to measure T_2.

C. Measurement of T_1

As has been briefly described previously, a combination of pulses of the proper length and height can be used to measure T_1. Three distinct methods can be used: (1) the 90 degree - 90 degree double pulse sequence, (2) the 180 degree - 90 degree or null method, and (3) the 90 degree - 90 degree - 90 degree triple pulse system.

(1) The 90° - 90° Method

When two pulses are applied as shown in Figure 1a, the free decay following the first pulse is

$$V_1(t) = M_o \sin (\gamma H_1 t_{w1}) \exp - (t/T_2 + t^2/T_2^{*2}) \qquad (A45)$$

The free decay following the second pulse a time τ after the first pulse is

$$V_2(t) = M_o \sin (\gamma H_1 t_{w2}) \left\{ 1 + [\cos (\gamma H_1 t_{w1}) - 1] \right.$$

$$\left. \exp (-\tau/T_1) \right\} \exp [-(t-\tau)/T_2] \exp[t-\tau)^2/T_2^{*2}]$$

$$- 1/2 \, M_o \sin (\gamma H_1 t_{w1})[\cos (\gamma H_1 t_{w2}) + 1]$$

$$\exp (-t/T_2) \exp (-t^2/T_2^{*2}) \qquad (A46)$$

In both Equations (A45) and (A46), diffusion effects have been neglected.

When both t_{w1} and t_{w2}, the width of the first and second pulse, respectively, are made of the proper length to make

$$\gamma H_1 t_{w1} = \gamma H_1 t_{w2} = \pi/2 \qquad , \qquad \text{then } V_1(t)$$

and $V_2(t)$ are

$$V_1(t)_{90} = M_o \exp - \left(\frac{t}{T_2} + \frac{t^2}{T_2^{*2}} \right) \qquad (A47)$$

and

$$V_2(t)_{90} = M_0 [1 - \exp(-\tau/T_1)] \exp - \frac{(t-\tau)}{T_2} \exp - \frac{(t-\tau)^2}{T_2^{*2}}$$

$$- 1/2 M_0 \exp - \frac{t}{T_2} \exp (-t^2/T_2^{*2}) \qquad \text{(A48)}$$

With the proper choice of the value of T_2^* in Equations (A47) and (A48), the decay voltages can be made to be

$$V_1(t)_{90} \approx M_0 \exp(-t/T_2) \qquad \text{(A49)}$$

and

$$V_2(t) \approx M_0 [1 - \exp(\tau/T_1)] \exp \left[-\frac{(t-\tau)}{T_2} \right] \exp \left[-\frac{(t-\tau)^2}{T_2^{*2}} \right] \qquad \text{(A50)}$$

At the time τ, if $\tau \gg T_2$, the decay voltages are

$$V_1(\tau)_{90} = 0 \qquad \text{(A51)}$$

and

$$V_2(\tau)_{90} \approx M_0 [1 - \exp(-\tau/T_1)] \qquad \text{(A52)}$$

Therefore, the decay signal following the second 90 degree pulse has an amplitude which is proportional to the time constant T_1. If the amplitude of the decay signal following the second pulse is plotted as a function of τ, the value of T_1 can be obtained. The more useful plot is that of $[V_1(0) - V_2(\tau)]$ as a function of τ. In either case, the slope is T_1 within the accuracy with which the second term of Equation (A48) is negligible relative to the first term. The pulse sequence and the two free-decay signals are shown in Figure 5.

(2)   The 180° - 90° Method

When the first pulse width t_{w1} is made to be equivalent to 180 degrees and the second pulse width t_{w2} is made to be equivalent to 90 degrees, as shown in Figure A6, then

$$V_1(t)_{180} = 0 \qquad \text{(A53)}$$

and

$$V_2(t)_{90} = M_0 [1 - 2 \exp(-\tau/T_1)] \exp - \left[\frac{(t-\tau)}{T_2} + \frac{(t-\tau)^2}{T_2^{*2}} \right] \qquad \text{(A54)}$$
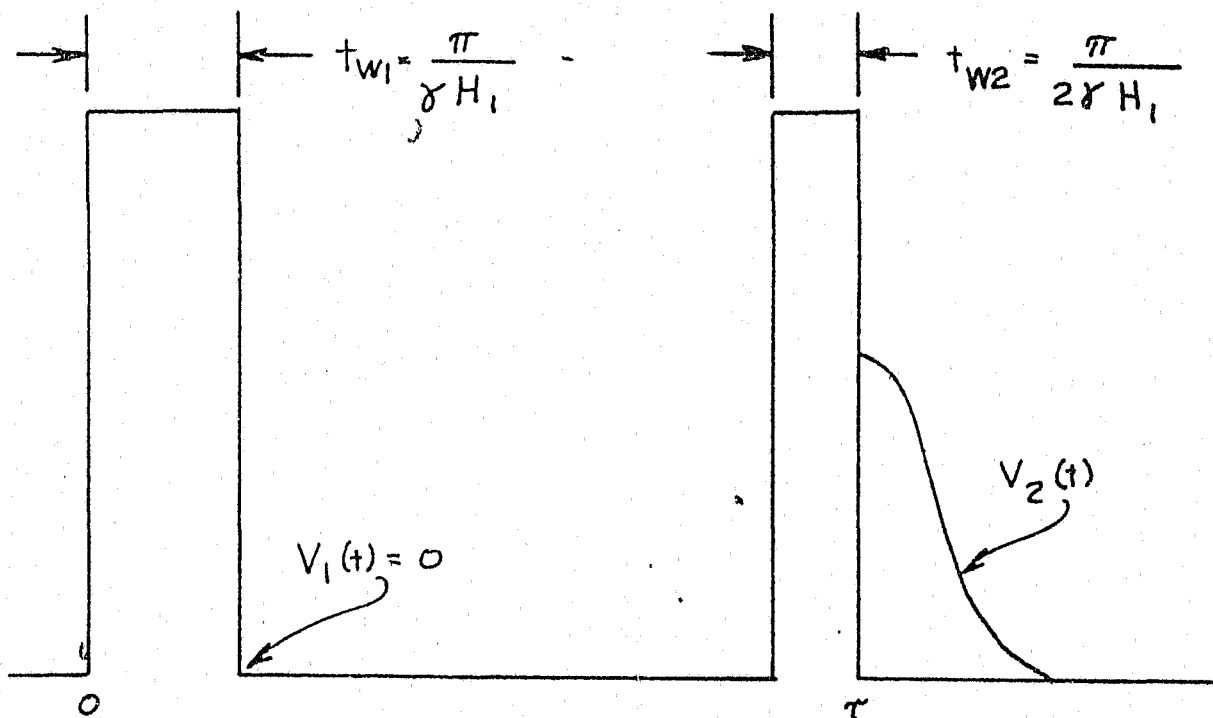
A-17

FIGURE A6. 180° - 90° OR NULL METHOD OF
T_1 MEASUREMENT

At the end of the second pulse, or at $t = \tau$, the free-decay signal following
the second pulse is

$$V_2(\tau)_{90} = M_o[1 - 2 \exp(-\tau/T_1)] \tag{A55}$$

When the value of τ is adjusted such that $V_2(\tau_n)_{90} = 0$, then the value of T_1
can be calculated from $T_1 = \tau_n/\ell n_2$, where τ_n is the value of the pulse
separation to make the free decay after the second pulse equal to zero. This
method does not depend upon the approximation of the 90 degree - 90 degree
method, but it does have a diffusion effect.

(3)   The 90° - 90° - 90° Measurement of T_1

When three 90 degree pulses are applied as shown in
Figure A7, there will be free decays following each pulse and there will be
echoes at times of $2\tau_1$, $(\tau_2 + \tau_1)$, $(2\tau_2 - 2\tau_1)$, $(2\tau_2 - \tau_1)$, and $2\tau_2$. The
echoes at $2\tau_1$ and $(\tau_2 + \tau_1)$ are the most important. The echo at $2\tau_1$ is called
the primary echo. The echo at $(\tau_2 + \tau_1)$ is called the stimulated echo.
Table A1 shows the amplitudes of the various echoes of Figure A7 with diffusion
being neglected. If τ_1 is kept constant and τ_2 is varied, the amplitude of the
stimulated echo at $\tau_2 + \tau_1$ can be plotted as a function of τ_2 to give the time
constant T_1. As will be seen later, the primary echo can be used as a measure
of T_2 as τ_1 is varied.

TABLE A1

ECHO AMPLITUDES

	Echo	Position	Echo Amplitudes	
			Trig. Part	Exponential Part
1.	Primary	$2\tau_1$	$\sin\theta_1 \sin^2\theta_2/2$	$\exp - (2\tau_1/T_2)$
2.	Stimulated	$\tau_2 + \tau_1$	$1/2 \sin\theta_1 \sin\theta_2 \sin\theta_3$	$\exp\left[-\dfrac{(\tau_2 - \tau_1)}{T_1} - \dfrac{2\tau_1}{T_2}\right]$
3.	-	$2\tau_2$	$\sin\theta_1 \cos^2\theta_2/2 \sin^2\theta_3/2$	$\exp(-2\tau_2/T_2)$
4.	-	$2\tau_2 - \tau_1$	$\sin\theta_2 \sin^2\theta_3/2$	$\exp - [(2\tau_2 - 2\tau_1)/T_2]$
5.	-	$2\tau_2 - 2\tau_1$	$-\sin\theta_1 \sin^2\theta_2/2 \sin^2\theta_3/2$	$\exp - [(2\tau_2 - 2\tau_1)/T_2]$

In Table A1, $\theta_1 = \gamma H_1 t_{w1}$, $\theta_2 = \gamma H_1 t_{w2}$, and $\theta_3 = \gamma H_1 t_{w3}$
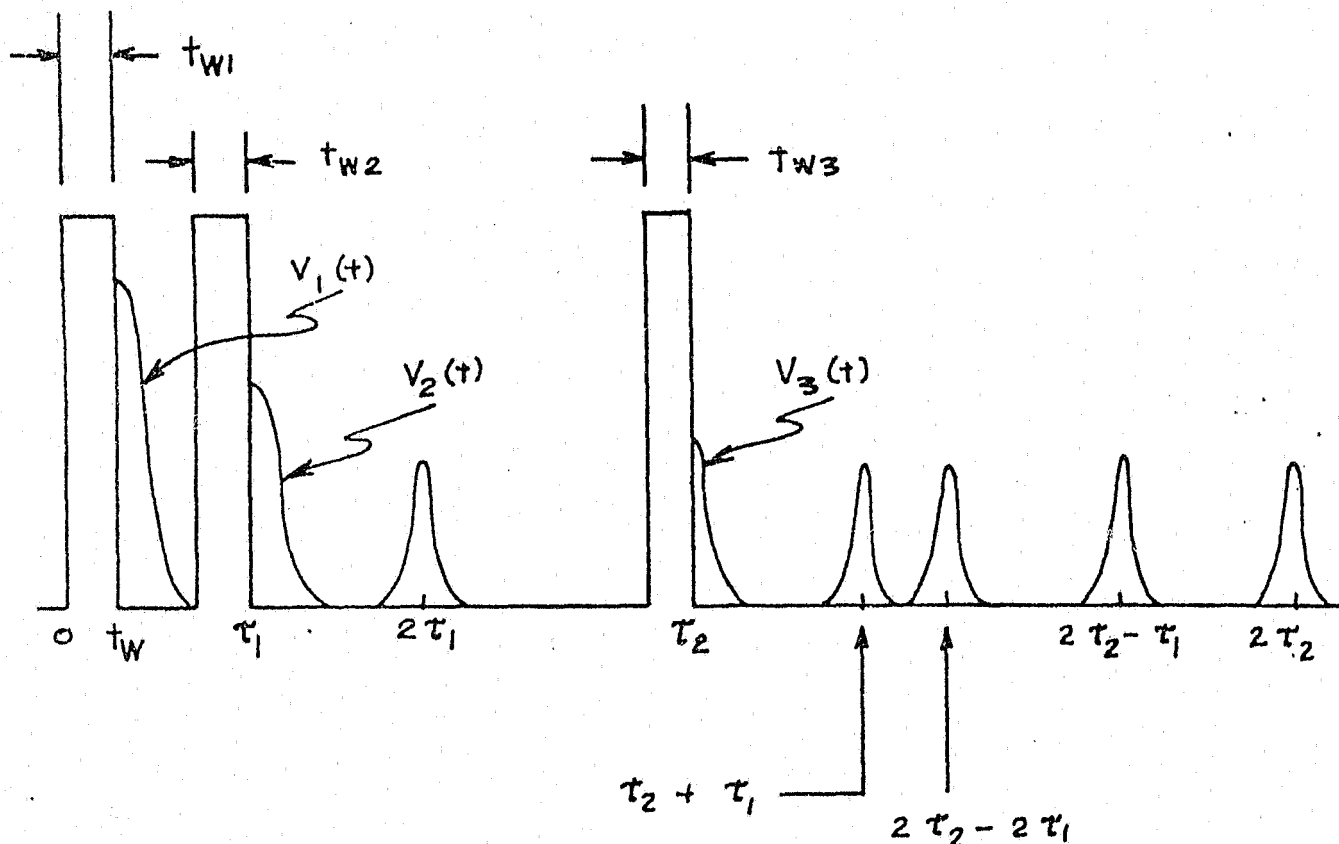
FIGURE A7. 90°-90°-90° METHOD OF T_1 MEASUREMENT

D. Measurement of T_2

(1) The Hahn or 90° - 180° Method

The essentials of the Hahn method are shown in Figure A8, and in Table A1. In Table I it is seen that if $\theta_1 = \pi/2$, $\theta_2 = \pi$, and $\theta_3 = 0$ (no third pulse), then there is only a single echo at $2\tau_1$. The echo amplitude decreases exponentially with increasing pulse spacing τ_1. Therefore, if the echo amplitude is plotted as a function of τ_1 for successive applications of the two pulses, allowing equilibrium to be established between the pulses, the echoes of Figure A8 will be obtained. When the various echoes are plotted as a multiple exposure, the exponential decay is readily observed. This method requires that the equilibrium condition be established between each echo amplitude measurement for each different pulse spacing τ. Therefore, the time between measurements must be at least 10 times the value of T_1. If there is any diffusion effect, then the effect will be enhanced because of this long time. To decrease the effect of diffusion on the T_2 measurement, the Carr-Purcell method can be used.
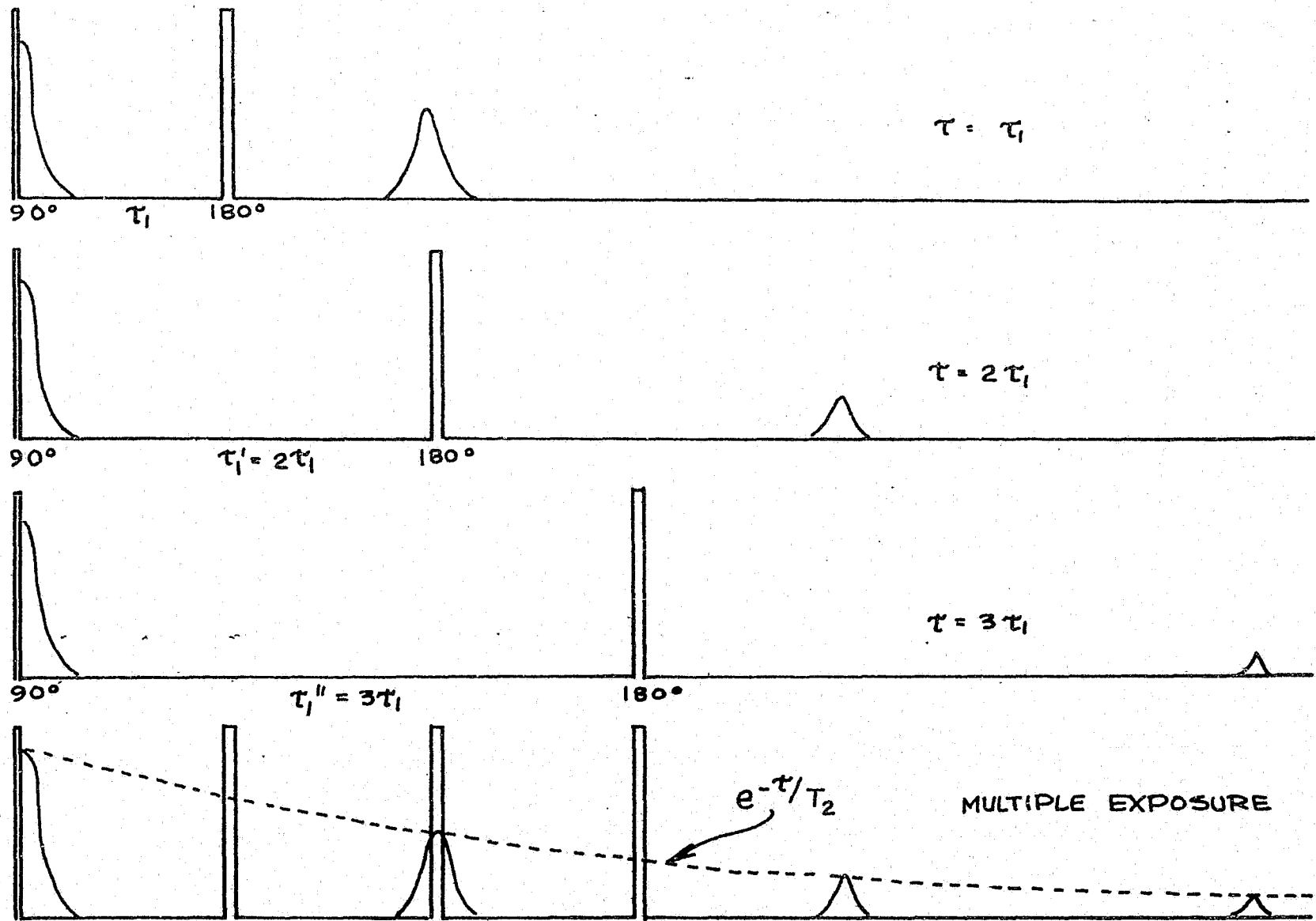
A-20

$\tau = \tau_1$

$90°$ τ_1 $180°$

$\tau = 2\tau_1$

$90°$ $\tau_1' = 2\tau_1$ $180°$

$\tau = 3\tau_1$

$90°$ $\tau_1'' = 3\tau_1$ $180°$

$e^{-\tau/T_2}$ MULTIPLE EXPOSURE

FIGURE A8.   HAHN METHOD OF MEASURING T_2

(2)   The Carr-Purcell Method

An inspection of Table A 1 shows that for three pulses, if the first is a 90 degree pulse and the other two are 180 degree pulses, and if the second pulse if τ_1 away from the first pulse and the third pulse is $3\tau_1$ from the first pulse, then there will be a primary echo at $2\tau_1$ and a stimulated echo at $4\tau_1$. The amplitude of the pulse at $2\tau_1$ is $M_o e^{-2\tau 1/T_2}$. The amplitude of the pulse at $4\tau_1$ is $M_o e^{-4\tau 1/T_2}$. A further analysis would show that another 180 degree pulse added at $5\tau_1$ will produce another stimulated echo at $6\tau_1$. As more 180 degree pulses are added at odd multiples of τ_1, there are more stimulated echoes at even multiples of τ_1. The case for one 90° pulse and three 180° pulses is shown in Figure A9. This measurement is made from one equilibrium condition and is completed in less than a time equal to $10T_2$. Therefore, the effect of diffusion is reduced.

(3)   The Free-Decay Method

As stated previously in Equations (A43) and (A44), the free induction decay can be used to measure the value of T_2 for very short T_2 values where T_2^* can be made very long. The lower limit is approximately 20 microseconds. This limit is set by the limitations on the value of H_1 required for a very short 90 degree pulse length of a few microseconds. The upper limit is about 500 microseconds which is determined by the lower limit of the magnet inhomogeneity.

F.   Regenerated Free-Decay

The essential idea of the pulse regeneration system is shown in Figure A10. Figure A10 shows that the decay following a single 90 degree
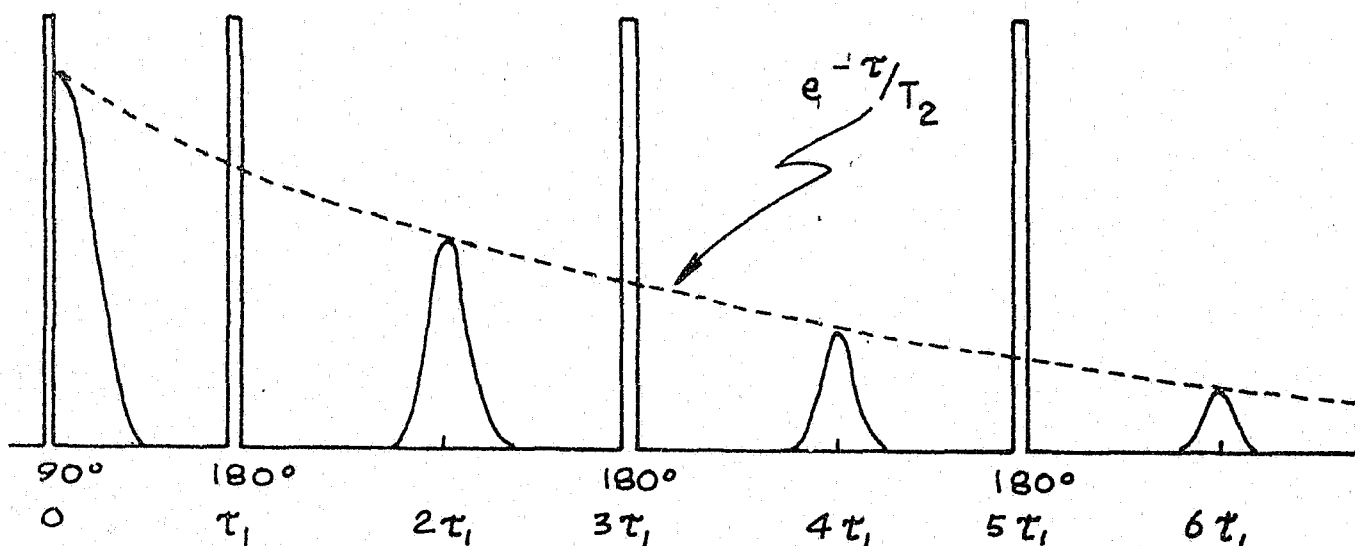

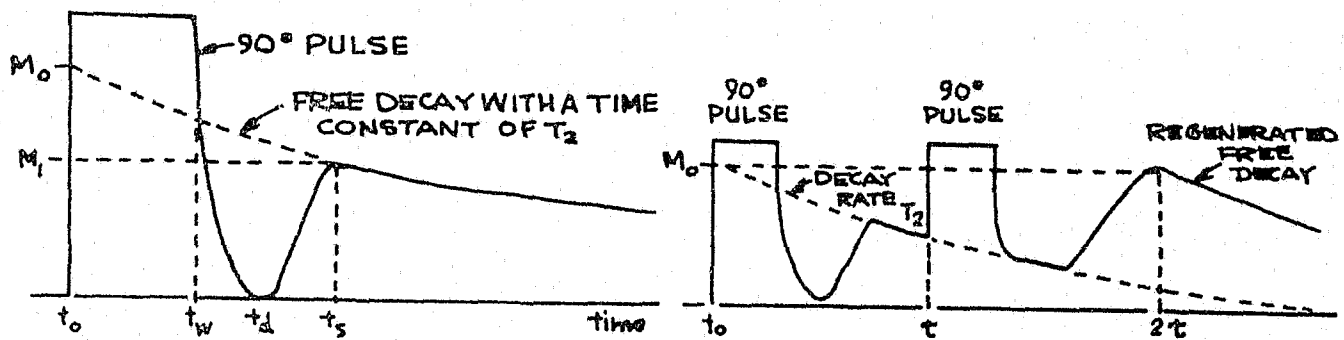FIGURE A9.   CARR-PURCELL METHOD OF MEASURING T_2

FIGURE A10. DIAGRAMMATIC REPRESENTATION OF THE
REGENERATED FREE DECAY

pulse is a value M_1 which is less than the value M_0 at time equal to zero. The delay is caused by the decay during the pulse and the dead time of the receiver following the large overload from the leakage of the 90 degree pulse. (The exact scale has not been used to obtain clarity.) The dashed line shows how the decay has proceeded up to the time when the decay signal can be observed. Between t_w and t_d, the receiver has been saturated and has given no signal output. Between t_d and t_s, the receiver is coming out of saturation and is giving back the signal. The value of the decay signal, M_1, at t_s is much less than the amplitude, M_0, required to be measured.

However, if another 90 degree pulse is inserted a time, τ $(T_2 < \tau > t_d)$, after the start of the first pulse, and the radiofrequency within the pulse is phase-shifted by 90 degrees relative to the first pulse, then the regenerated decay of Figure 10b will be obtained. The regeneration will start at the end of second pulse as shown and the peak will occur at 2. If the dead time after the second pulse permits the regenerated signal to come to the maximum, then the value of M_0 can be measured. This then makes an exact measurement of M_0 possible for values of the relaxation time which are nearly equal to the pulse width plus the dead time. For instance, if the pulse width is 4 microseconds and the dead time is 2 microseconds, then M_0 can be measured for T_2 values as low as 7 microseconds. The regeneration scheme will not work if there is motion narrowing of the linewidth or for T_2 values above 50 microseconds. Therefore, it is effective for T_2 values of between a few microseconds to 50 microseconds.
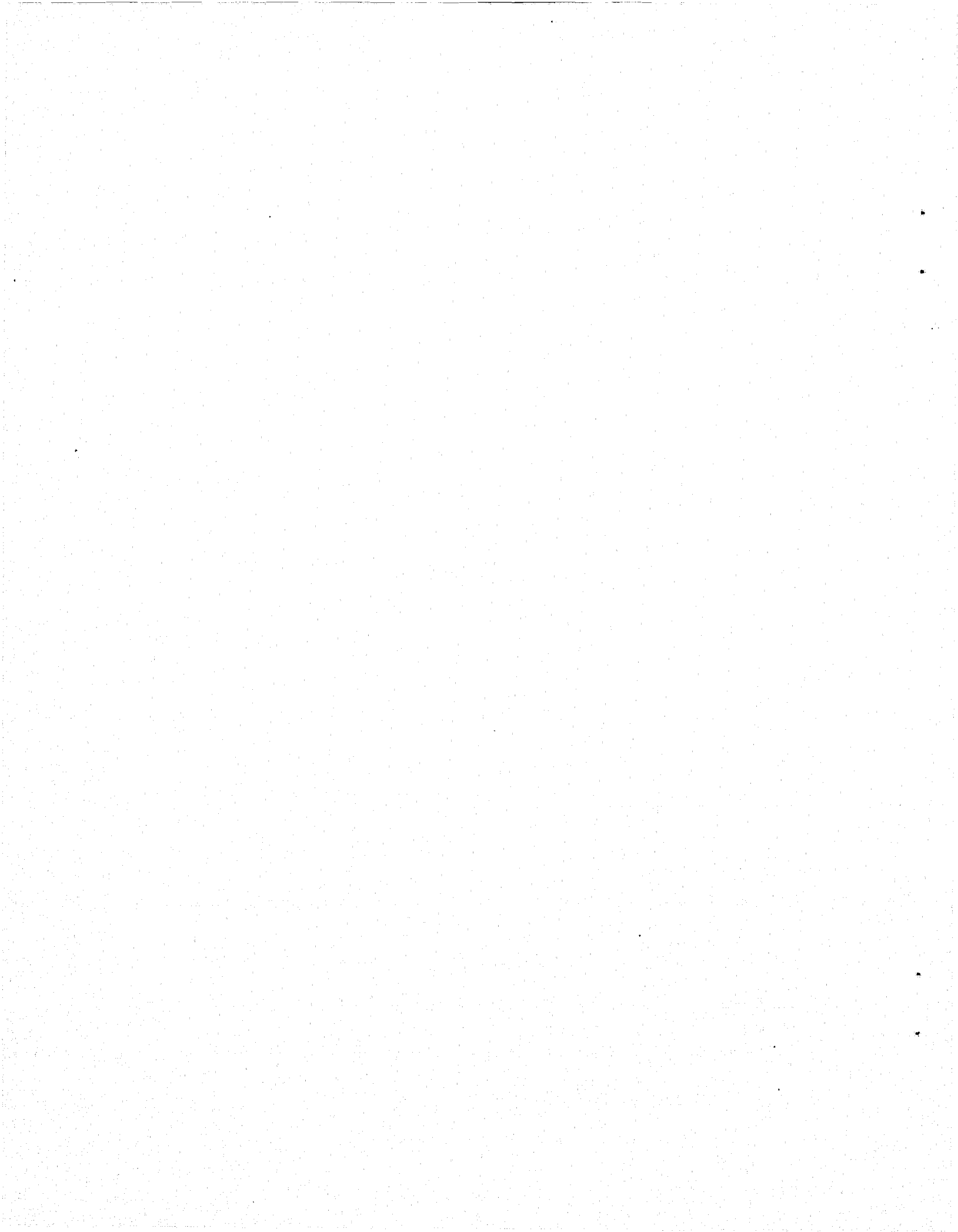
APPENDIX B

HIGH POWER RF PULSE
GENERATION TECHNIQUE

During this program, previously considered means for simply generating the high peak RF power required for transient NMR detection in large sample volume were evaluated. The approach utilized was a capacitor discharge into a resonant LC circuit which resulted in a free ringing signal centered on the circuit frequency. This investigation is described in this Appendix.

The basic diagram of gated, freely oscillating or ringing circuit is given in Figure B-1. When the switch is open, capacitor, C, charges to the voltage of the high voltage supply, V_S. When the switch is closed, the ringing circuit is "gated on". The capacitor, C, then discharges through the switch and the detection coil L. Since L and C now comprise a series resonant circuit, the voltage across the detection coil will be a voltage oscillating at the frequency

$$\omega^2 = 1/LC \tag{B-1}$$

and decaying in amplitude according to the relation

$$v = V_S \exp \frac{-t}{2RC} \cos \omega t. \tag{B-2}$$

In the time $T = 2L/R$, or one time constant, the amplitude of oscillation will decrease from a peak value of V_S at $t = 0$ to $0.37 V_S$. The time constant, T, therefore, is

$$T = \frac{2L}{R} = \frac{2Q}{\omega} \tag{B-3}$$

If $Q = 100$, and $\omega = 2\pi \times 2.5 \times 10^6$ radians, then

$$T = \frac{2 \times 100}{6.28 \times 2.5 \times 10^6} = 12.7 \times 10^{-6} \text{ seconds.} \tag{B-4}$$

If a 5-microsecond wide pulse is desired, the switch could be turned on for only 5 microseconds and then turned off. When the switch is turned off, the oscillation will stop and capacitor C will be recharged through the charging resistance to V_S. The voltage thus produced is as drawn in Figure B-2. In the 5-microsecond time, the peak value of the oscillating voltage has decayed from V_S to $0.675 V_S$.
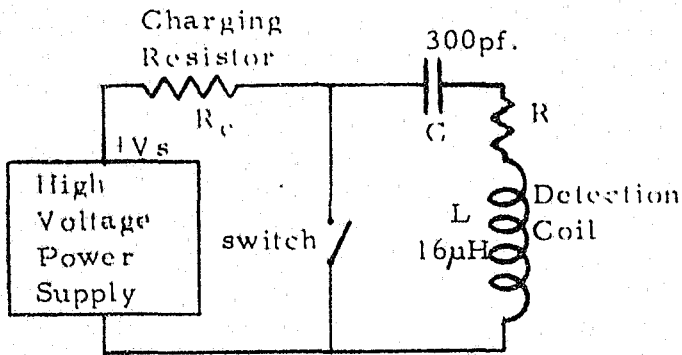
Charging
Resistor

300pf.

R_c

C

R

V_s

High
Voltage
Power
Supply

switch

Detection
Coil

L
16 μH

FIGURE B-1. BASIC DIAGRAM
OF THE GATED, FREELY-
OSCILLATING CIRCUIT FOR
TRANSIENT NMR

V_s

Recharge
of C

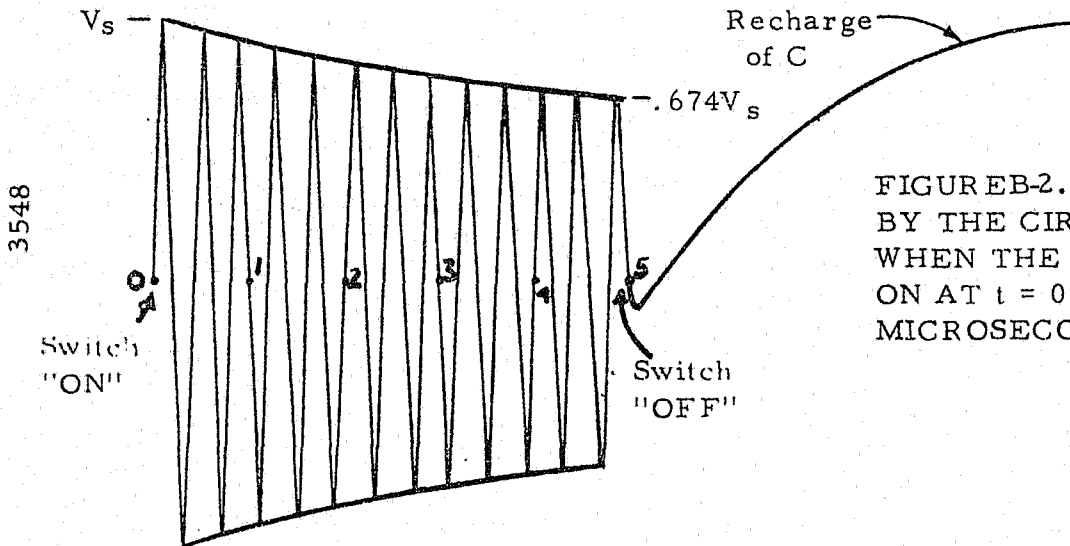$.674 V_s$

3548

0

1

2

3

4

5

Switch
"ON"

Switch
"OFF"

FIGURE B-2. PULSE GENERATED
BY THE CIRCUIT IN FIGURE 5
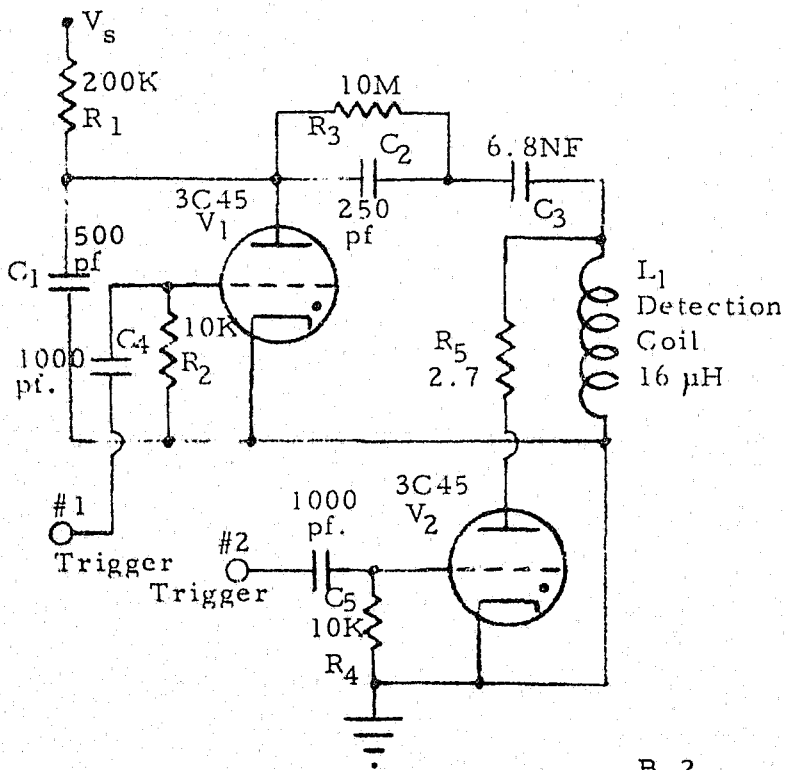WHEN THE SWITCH IS TURNED
ON AT t = 0 AND OFF AT t = 5
MICROSECONDS

V_s

200K
R_1

10M

R_3

C_2

6.8NF

C_3

3C45
V_1

250
pf

500
pf

C_1

L_1
Detection
Coil
16 μH

1000
pf.

C_4

10K
R_2

R_5
2.7

#1

Trigger

#2
Trigger

1000
pf.

C_5

10K

R_4

3C45
V_2

FIGURE B-3. GATED SELF-
OSCILLATING OR RINGING
CIRCUIT WHEREIN THE
HYDROGEN THYRATRON V_1
IS USED AS THE START
SWITCH AND V_2 IS USED AS
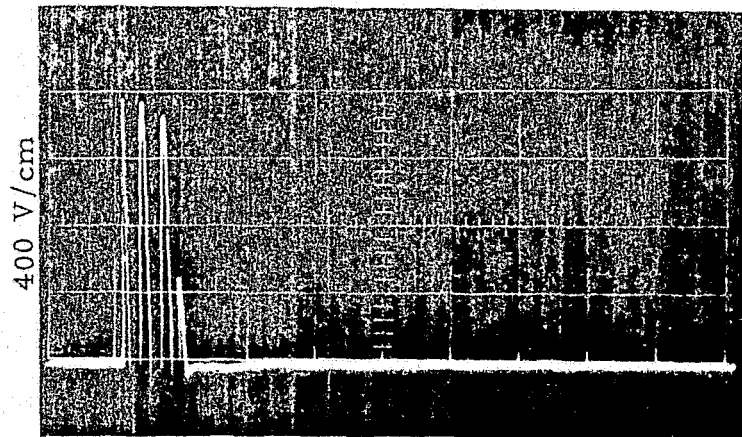THE DAMPER TO TURN OFF
THE RINGING OR SELF
OSCILLATION

B-2
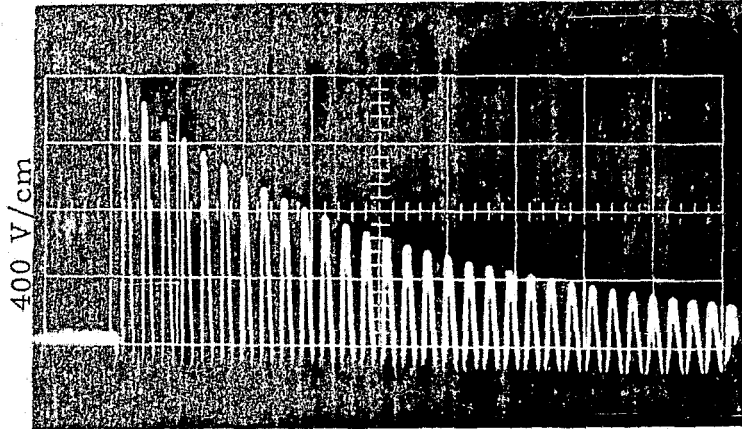
a. Damper Tube V_2 not used.

10^{-6} sec/cm

3549
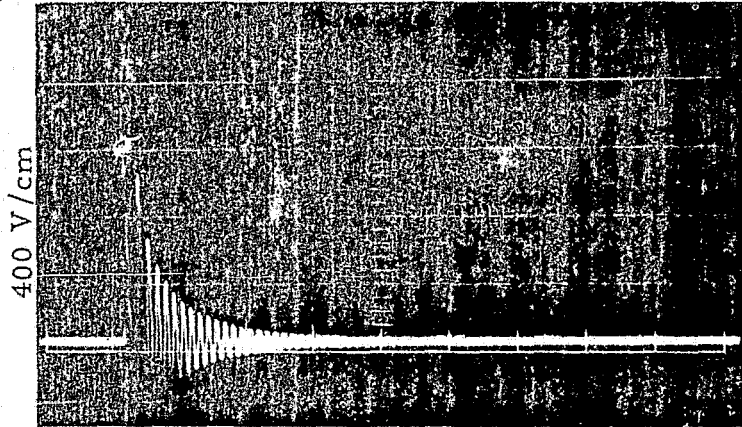
b. Damper Tube V_2 and C_1 not used.

10^{-6} sec/cm

c. Damper tube and C_1 both used.

10^{-6} sec/cm

FIGURE B-4. OSCILLATING VOLTAGE ACROSS L_1 IN FIGURE 7 FOR THREE CONDITIONS

After much experimentation it was found that high current hydrogen Thyratrons should make a usable switch for supply voltages, V_S, up to 25,000 volts except that other means of "turn-off" would be required. To test these "switches", the circuit in Figure B-3 was constructed and tested. The test results from the use of Figure B-3 are given in the oscilloscope photographs in Figure B-4. The oscilloscope pictures are of the voltage across L_1 in Figure B-3, the NMR detection coil when the circuit is used as a transient NMR detector. The time-constant for the ringing with no damping, Figure B-4a, is approximately 4.5 microseconds. This ringing time means that the circuit Q is about 35. When the 500 pf capacitor C_1 in Figure B-3 was removed, the decay without damping was reduced to less than one microsecond, indicating that the self-oscillating Q of the circuit had been reduced to about 8.

When the circuit of Figure B-3 was used with C_1 and with the damper V_2, the RF pulse given in Figure B-4c was obtained. Such a pulse is more like the ones used previously with the driven oscillator system.

In the past, the matching circuit in Figure 2 used a series resonant circuit for the detection coil and an L-network to match the input to the RF signal amplifier. In these circuits, as used previously, the ring-down time, after the driving RF pulse had been removed, was controlled by selecting the value of the Q of the series resonant circuit. When the gated, self-oscillating generator was adapted for use with the series resonant detection circuit, the circuit in Figure B-5 resulted. In Figure B-5, the capacitance C_1 charges to the power supply voltage V_S when the Thyratron V_1 is "off". When the Thyratron is turned "on" by a trigger pulse on the grid, capacitor C_1 discharges through the resistor R_1 and through D_1, C_3, L_1, etc. The resultant voltage across R_1 is given by the oscilloscope picture reproduced in Figure B-6a. With a voltage V_S of 1450 volts, the negative 500-volt pulse in Figure B-6a was obtained. There is a self-oscillating voltage across the detection coil L_1 as is given in Figure B-6b. About 0.50 microseconds after the start of the pulse of the first trigger, another trigger pulse is seen in Figure B-6a to again turn "on" the Thyratron V_1. This second trigger was unwanted and caused by feedthrough or feedback to the trigger generator causing another trigger pulse in an undesired position.

In spite of the retriggering (which was subsequently corrected), when the detection coil (L_1 in Figure B-5) was inserted into the large magnet (Figure 4), transient NMR signals were obtained with samples of glycerol and phenolic rod. The peak of the NMR signal occurred at 35 microseconds after the start of the pulse and the signal amplitudes were
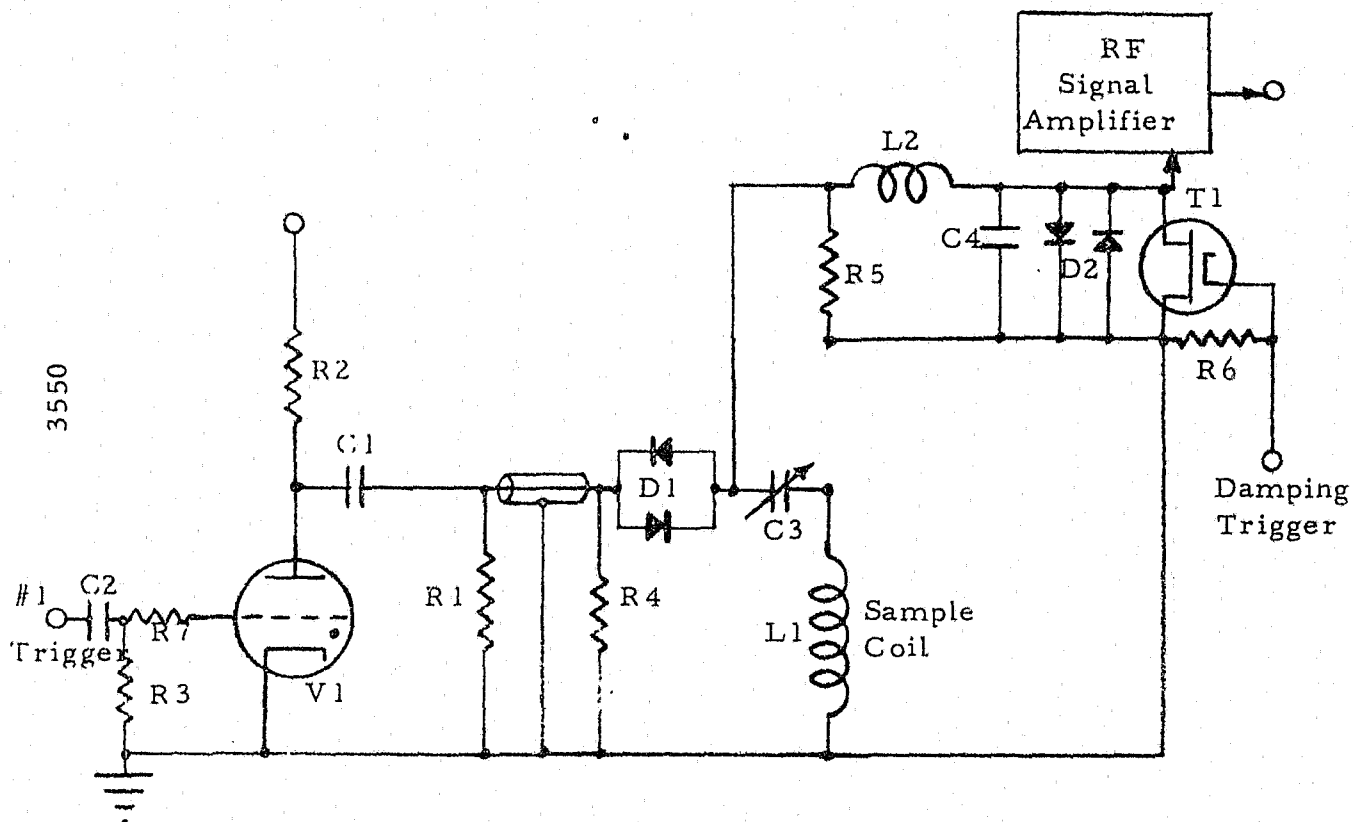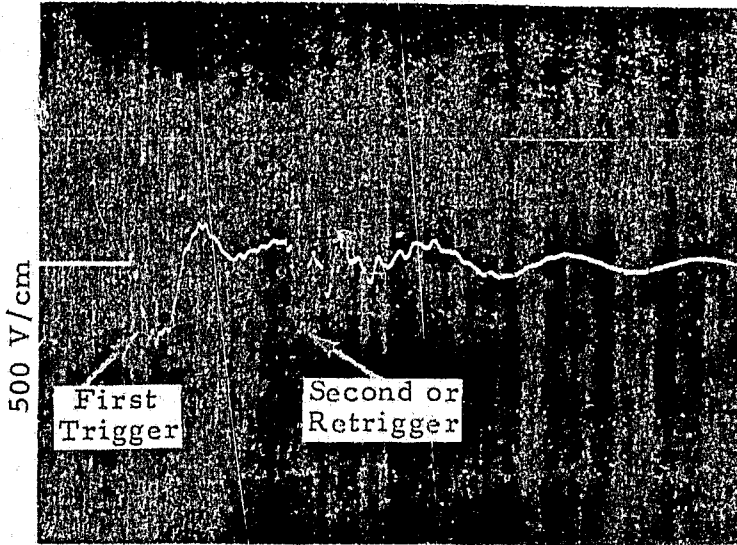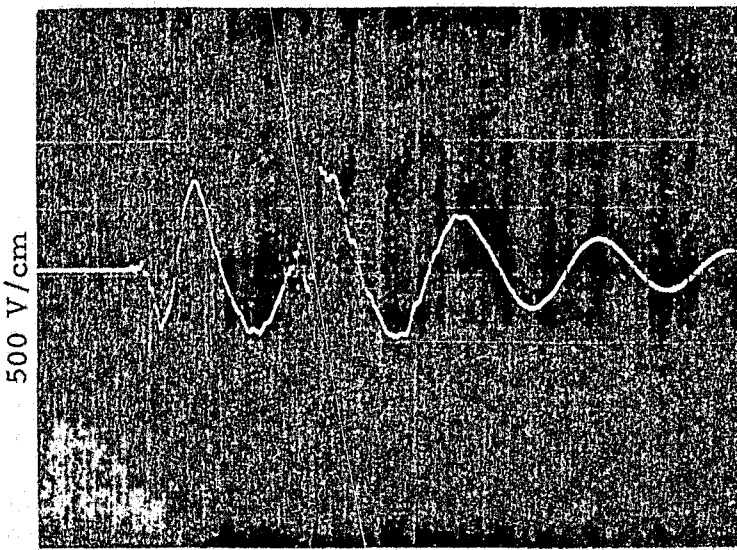
B-4

FIGURE B-5. TRANSIENT NMR DETECTION CIRCUIT WITH A SELF-
OSCILLATING RF PULSE GENERATOR COMPOSED OF
ALL COMPONENTS TO THE LEFT OF R_4

500 V/cm

First Trigger   Second or Retrigger

0.2 x 10^{-6} sec/cm

a. Voltage Across R_1 in Figure 9 with C_1 = 1000 pf.

3551

500 V/cm

0.2 x 10^{-6} sec/cm

b. Voltage Across L_1 in Figure 9.

FIGURE B-6. VOLTAGES ACROSS R_1 AND L_1 IN FIGURE 9 WITH C_1 = 1000 pf.

. 0. 6 volts for the phenolic rod, and

. 3. 5 volts for the glycerol sample.

The detection coil was the one shown in Figure 4, having an inside diameter of one inch.

To determine how large the RF pulses could be made across the detection coil with the circuit in Figure B-5, the part of the circuit to the receiver was disconnected and the voltage measured across the detection coil. For these tests, C_1 was chosen to be 5000 pf, R_2 was increased to 3 megohms, and R_1 was raised to 107 ohms. The RF pulses in Figure B-7 were obtained with $V_S = 10,000$ volts. In Figure B-6a, no capacitance was added from the plate of V_1 to the ground. In Figure B-7b, a high-voltage capacitance of 510 pf was added across V_1, in Figure B-7c, 1020 pf was added, and in Figure B-8d 1530 pf was used. The peak pulse amplitude was 10,000 volts and the pulse duration was one microsecond in Figures B-7a and B-7b. The pulse duration was longer in Figures B-7c and B-7d with the much larger capacitances shunted across the Thyratron V_1.

A comparison was made of the frequency spectrum of the RF pulses from the gated, freely oscillating pulse generator and the driven oscillator. No large differences were noted. However, only the spectra of amplitude were recorded. The equipment could not display phase differences if any existed. It was noted in a paper by J. D. Ellett, et al in Vol. 5 of "Advances in Magnetic Resonance", Vol. 5, edited by J. S. Waugh, (1971), that phase changes had been noted during the rise and fall times in driven oscillation pulses. These phase changes were rather large and caused by the presence of a quadrature component only during the times of changing amplitude. Therefore, we could expect a phase change during all of the time with a free-oscillation pulse because it is always falling in amplitude after the initiating pulse.

To determine if there were differences between the signals detected with the driven- and free-oscillation pulses, experiments were made using comparable pulses of both types. The same circuit as drawn in Figure 4 was used for the gated, free oscillation circuit. For the driven oscillation condition, the output of the gated power amplifier was fed into the 5000 pf condenser C_1, with the Thyratron turned off. The results obtained are displayed in Figure B-8. In both cases in Figure B-8, the pulse conditions were adjusted for the maximum signal. The peak value of the free-oscillation pulse in Figure B-8b is 7500 volts and its decay has a time constant of 9 microseconds. The free-oscillation pulse of Figure B-8b produced the free induction decay NMR

a. No Capacitance from Plate to Ground of Thyratron

b. 510 pf from Plate to Ground of Thyratron

c. 1020 pf from Plate to Ground of Thyratron

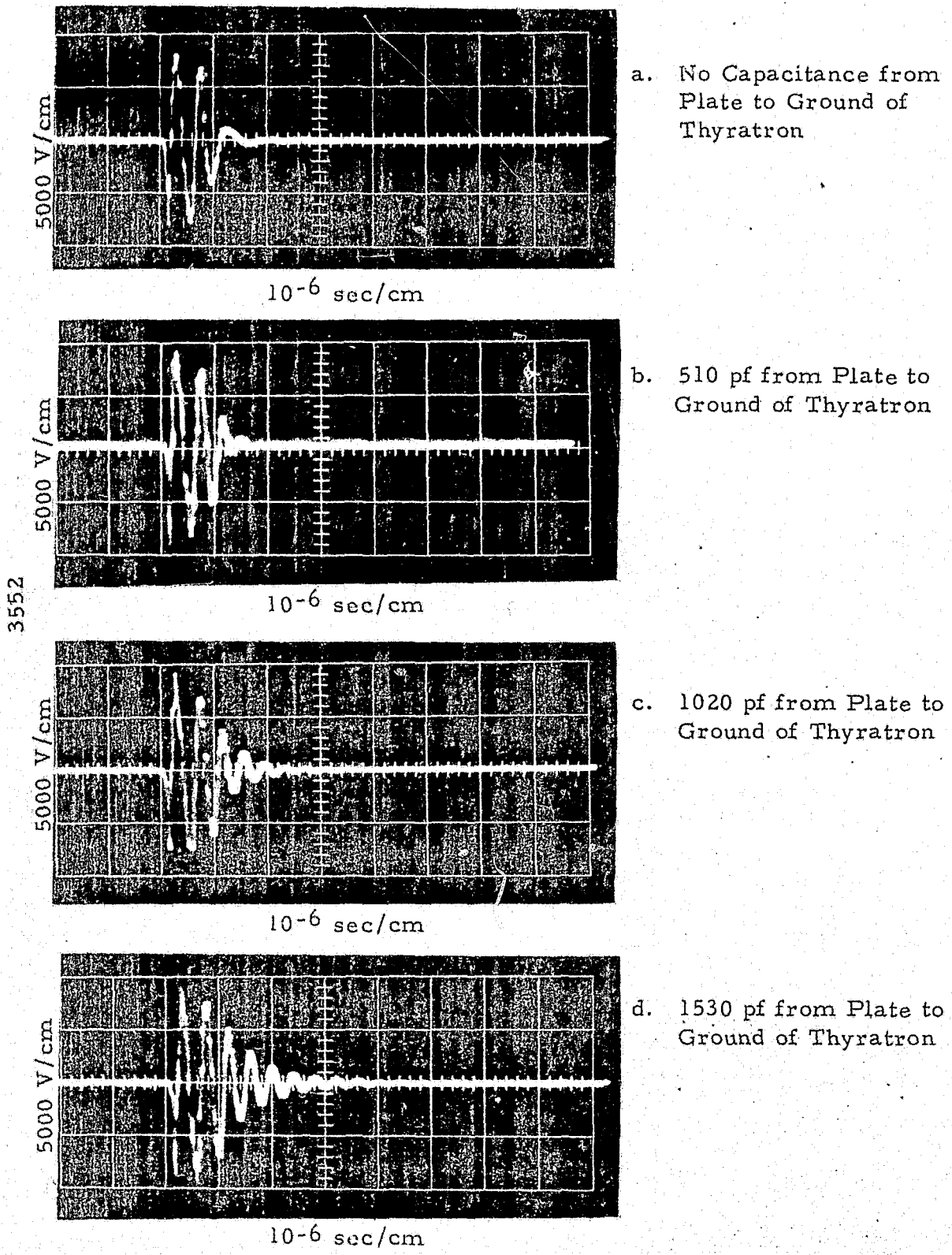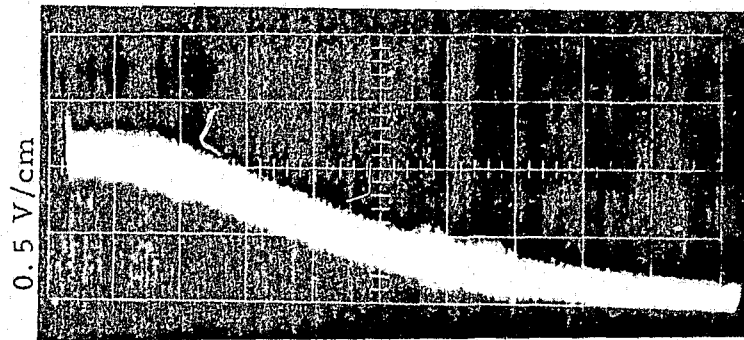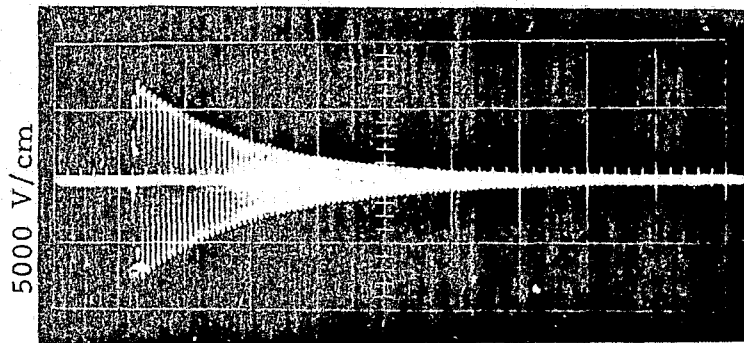d. 1530 pf from Plate to Ground of Thyratron

FIGURE B-7. PULSES GENERATED ACROSS THE DETECTION COIL WITH THE CIRCUIT OF FIGURE 9 UNDER FOUR DIFFERENT CONDITIONS

a. FID Type NMR Signal with Free Oscillation Pulse.
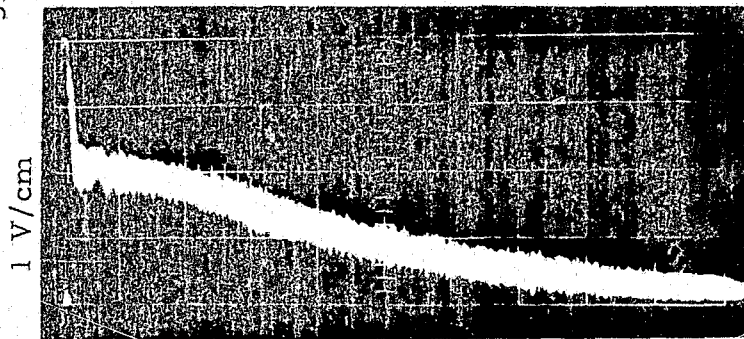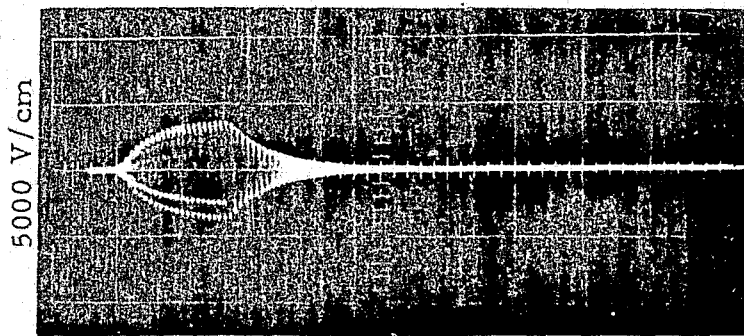
0.5 V/cm

0.5 x 10⁻³ sec/cm

b. Free Oscillation Pulse.

5000 V/cm

5 x 10⁻⁶ sec/cm

3553

c. FID Type NMR Signal with Driven Oscillation Pulse.
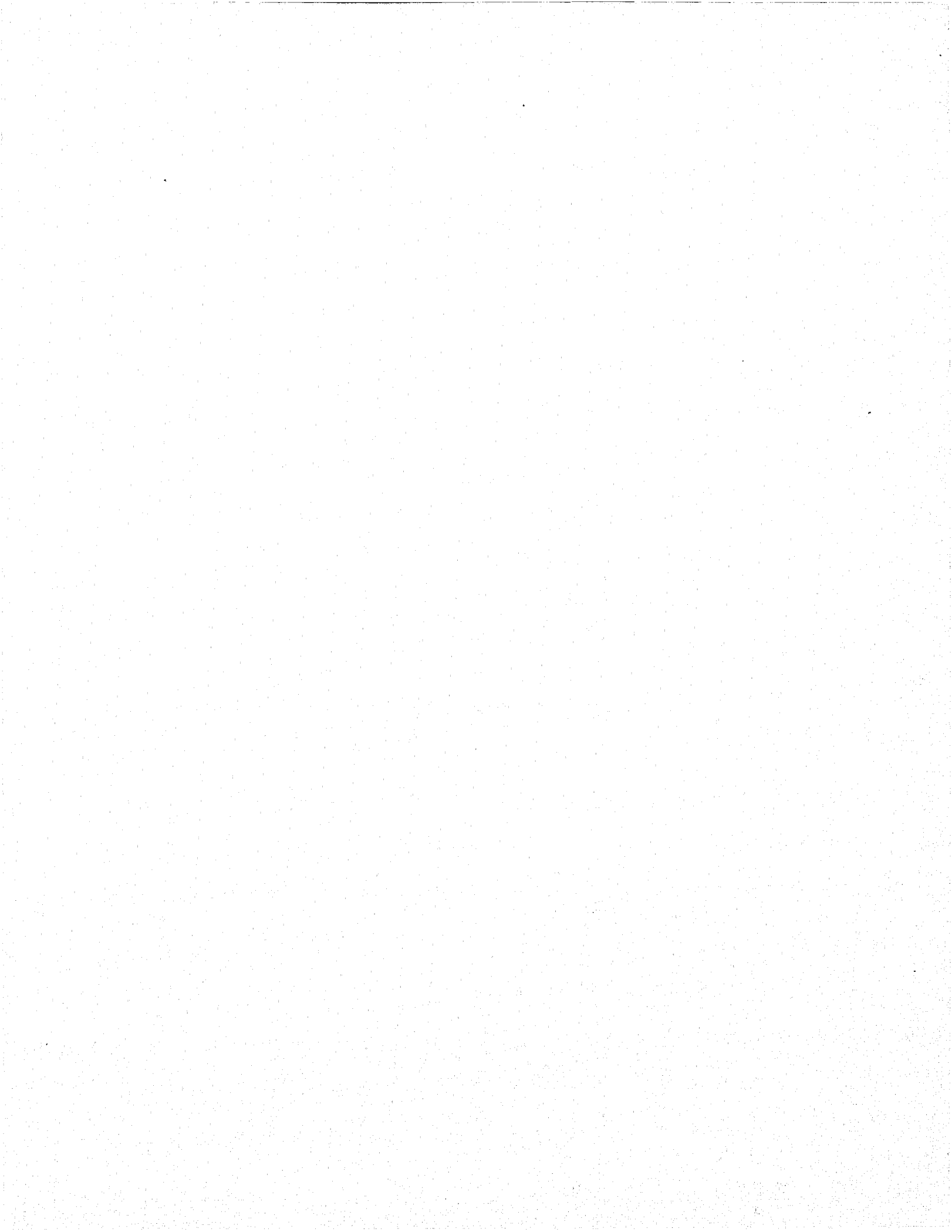
1 V/cm

0.5 x 10⁻³ sec/cm

d. Driven Oscillation Pulse.

5000 V/cm

5 x 10⁻⁶ sec/cm

FIGURE B-8. COMPARISON OF FID, NMR SIGNALS WITH DRIVEN AND
FREE OSCILLATION PULSES

signal of Figure B-8a. The peak amplitude was 1 volt.

The peak value of the driven oscillation pulse in Figure B-8d is only 4000 volts and its length from the 10% rising value to the 10% falling value is 13 microseconds. The width of the pulse at its 90% points is 5 microseconds. The signal produced by the driven oscillation pulse is 2 volts peak as shown in Figure B-8c. Thus with a much smaller pulse, the driven oscillation pulse produced twice as much transient NMR signal amplitude as did the free oscillation pulse. The reasons for this difference are not fully known and understanding requires further investigation. Such further investigation of this technique was not possible within the limited scope of the present program.

END